DEVELOPMENT OF INNOVATIVE THERANOSTIC PLATFORMS FOR BIOMEDICAL APPLICATIONS

by

MIN KYUNG KHANG

Presented to the Faculty of the Graduate School of

The University of Texas at Arlington in Partial Fulfillment

of the Requirements

for the Degree of

DOCTOR OF PHILOSOPHY

THE UNIVERSITY OF TEXAS AT ARLINGTON

August 2019

Abstract

Min Kyung Khang, PhD

The University of Texas at Arlington, 2019

Supervising Professor: Dr. Liping Tang

Modern technologies have been successfully identifying patient's disease-related genetic information and developing effective drugs continuously. The discovery of molecular biomarkers paves new roads for potential individualized therapeutic applications; thus far, the call for a more development of advanced targeting/delivery platforms is highly required in the bioengineering field. Unfortunately, bioengineered targeting platforms for drug delivery at the right place, right dosage and right time have still remained in the developmental stages. To develop innovative nanosystems for various biomedical applications, polymer chemistry and click chemistry are needed to improve the function of the nanosystems. My dissertation research is based upon a unique mingling of chemistry and bioengineering. The developed platforms are the perfect examples of interdisciplinary research (IDR) and what modern technologies really needs. I believe that the new nanoplatforms and hydrogel scaffolds made here can be used, not only for specific targeting and diagnosis, but also for drug delivery and treatment of various diseases, including cancer, inflammatory disease and cardiovascular disease.

Acknowledgements

Above all, I would like to thank Jesus for giving me the strength to persevere through this journey.

I sincerely thank you all. To my committee members, Dr. Subhrangsu S Mandal, Dr. Junha Jeon and Dr. Kayunta Johnson-Winters for your time and advice. To Dr. Robin Macaluso and Dr. Kytai Truong Nguyen and Dr. Jun Zhou for your warm-hearted support. I would like to extend my appreciation to Dr. Liping Tang for all your patience, encouragement and tremendous support. I would have never completed this journey without you, my academic father. To the department of Chemistry and Biochemistry as well as the department of Bioengineering for giving me the opportunity to have this unique research experience. Lastly, I give my appreciation to my loving family and friends.

Table of Contents

Chapter 1

Introduction

1.1 Background

1.1.1 Bioengineering

The call for further development of innovative targeting/delivery platforms is highly required in bioengineering field.[1] Development of the optimal platforms for targeting/delivery has been accelerated based on the idea of combining targeting ligands and imaging/therapeutic agents into a platform. There are various biomaterials offer new opportunities to develop those platforms for various diseases theragnosis. Especially multifunctional nanoparticles (NPs), including targeting, imaging and therapy, have been broadly studied.[2,3] Surface modifications of the NPs may be easily introduced for providing the multiple functions through conjugation with targeting moieties, such as small molecules or proteins, as well as fluorescence dyes or drugs. A variety of physical and chemical approaches has been used to conjugate targeting ligands, imaging fluorescence or therapeutic drugs onto NPs' surfaces. These methods can be categorized as conventional bioconjugation strategies; direct conjugation, linker chemistry, physical interaction, or click chemistry.[3–5] Conjugation of the targeted ligands on surfaces of NPs without losing its stability and functionality is the main goal in designing and preparing multifunctional NPs. Also conjugated therapeutic drugs must be released from the nanoplatform system after

targeting in order to show therapeutic effects. In the following sections, three different nanoplatform systems were designed and prepared using different conventional bioconjugation strategies. And then those platforms were applied to different diseases in order to prove their functionalities.

1.2 Background and Aims of This Dissertation

1.2.1 Polymer Chemistry

Hydrogels are a class of high-water content polymers based on their physical or chemical crosslinking.[2–6] Crosslinking gives stabilization in polymeric chains which result a strong network structure. Three-dimensional (3D) injectable hydrogel scaffolds composed of polymeric chains have been widely studied and used in cell therapy and tissue regeneration. They have various unique characteristics, including controlled porosity, high water content, and mimicking of microenvironment of natural extracellular matrix.

In situ physical-crosslinking mechanisms in response to certain environmental changes such as pH, temperature, ion, solvents and light, have gained popularity. Among all *in situ* gelling systems, the thermally induced gelling mechanism is the most common method to produce in situ forming scaffolds. Typically, these gel systems can flow at room temperature but solidify immediately and form 3D scaffolds when brought to body temperature (37 ^{o}C).[5–8] I fabricated a series of new injectable *in situ* gelling hydrogel (**Figure 1.1**) with three monomers, di(ethylene glycol) methacrylate (MEO_2MA), OEGMA (mw = 300 g/mol), and acrylic acid

(AAc). Additionally, the capability of this new thermally induced gelling system to release proteins and recruit circulating cancer cells was assessed *in vivo.*

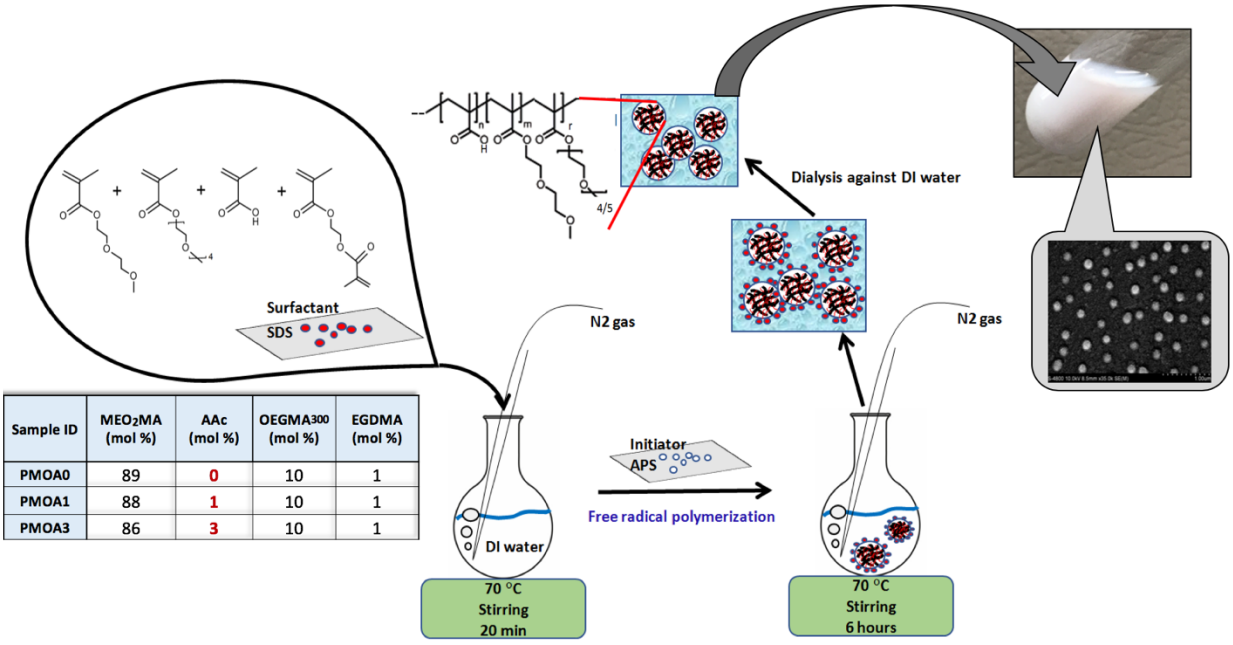

Sample ID	MEO_2MA (mol %)	AAc (mol %)	$OEGMA_{300}$ (mol %)	EGDMA (mol %)
PMOA0	89	0	10	1
PMOA1	88	1	10	1
PMOA3	86	3	10	1

Figure 1.1 Preparation of a new *in situ* injectable nanoparticle based hydrogel via physical polymerization.

1.2.2 Ligand-receptor Interaction

A larger number of pre-targeting platforms have been reported especially for theranostic cancer treatment in the literature thus far. Two separated processes were typically employed in those platforms.[9] Briefly, the first step is to pre-target at the disease site and then, the second step is to deliver therapeutic agents to the diseased site by interacting with the pre-targeting agent.

Non-covalent affinity interactions are the most common chemical reaction which are applied for the pre-targeting strategy. Amongst non-covalent binding systems, avidin/biotin system has been widely used for biomedical applications due to the multiple biotin binding sites of avidin as well as the avidin protein has the strongest non-covalent interaction with biotin (dissociation constant:10^{-15} M).[9–11] In fact, the avidin/biotin system has been extensively utilized in biochemical assays and affinity purification due to its unique advantages, including signal amplification, high specificity and robust stability. I proposed a pre-targeting "sandwich" platform (**Figure 1.2**) to amplify inflammation theragnosis via neutravidin-biotin system. I then assess the capability of the "sandwich" platform to reduce inflammatory responses both *in vitro* and *in vivo*.

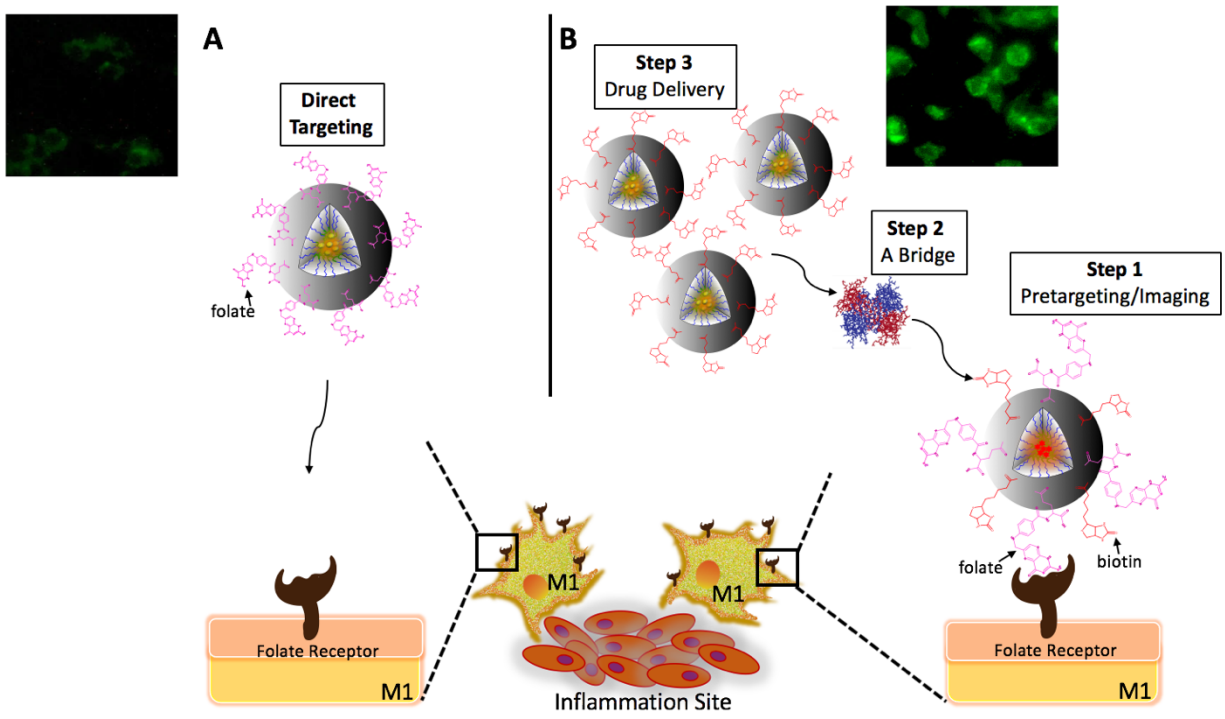

Figure 2.2 A schematic of A) the traditional direct targeting strategy of drug delivery for inflammation treatment and B) the new "Sandwich" pre-targeting strategy of amplified drug delivery for inflammation treatment as well as diagnosis (imaging). It should be noted that, by using neutravidin as the bridge which has multiple biotin-binding sites, the drug delivery efficacy can be amplified as depicted on this scheme.

1.2.3 Click Chemistry

Bioorthogonal click chemistry was recently introduced to develop biomedical nanoplatforms or cell adhesion to cell/tissue.[12–14] because of its advantages; (1) covalent bonds between click chemistry are more stable than biologically physical bonds; (2) conjugation of these small chemicals can be maximized on the cell surface; (3) the reaction rates between click chemistry are very fast; (4) there are no toxic byproducts.[15–19]

I developed and optimized a novel multifunctional engineered nanoparticles (NP) for targeting thrombosis by conjugating both a ligand and click chemistry on the surface of NPs.[20–22] The new NP is further expected to be applied stem cell therapies for cardiovascular diseases *in vivo* in the future. (**Figure 1.3**)

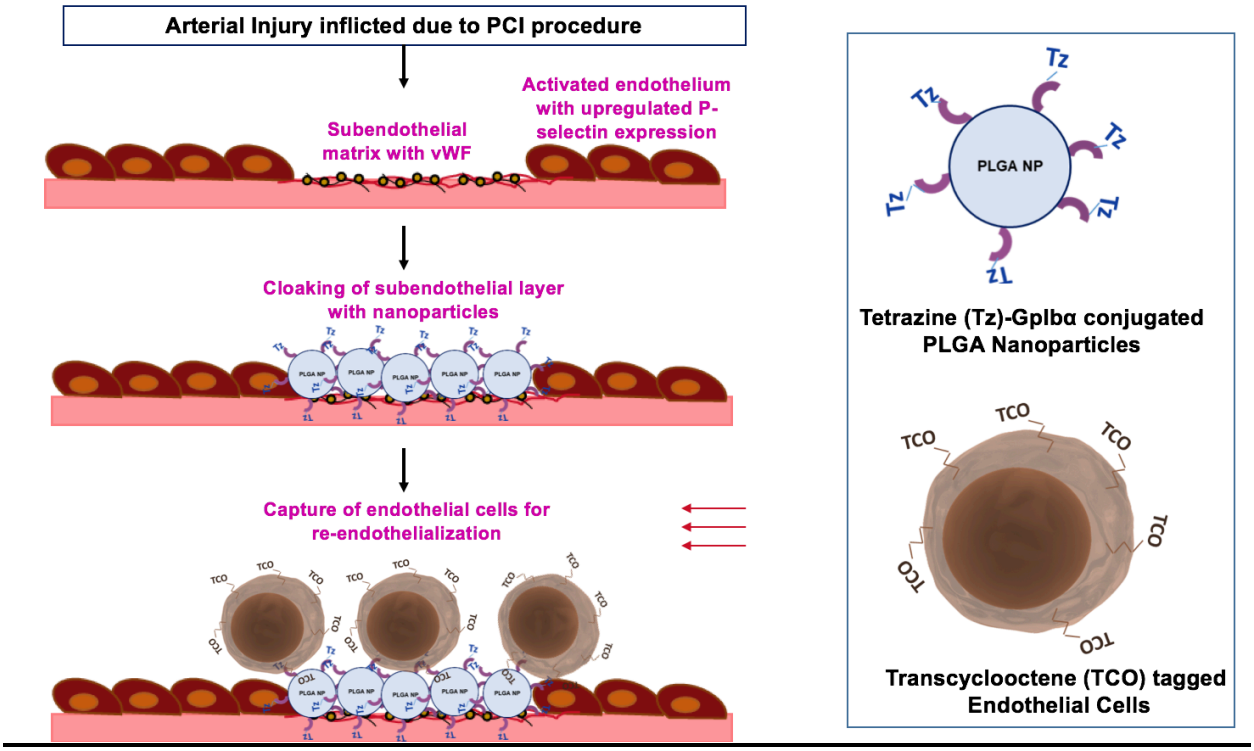

Figure 3.3 Design of an optimal multifunctional nanoparticle for accelerated endothelium regeneration of injured blood vessels.

CHAPTER 2

In situ-forming injectable temperature sensitive hydrogel scaffolds

2.1 Introduction

Three-dimensional (3D) injectable hydrogel scaffolds have been widely used in cell therapy and tissue regeneration based on their unique characteristics, including controlled porosity, high water content, and mimicking of microenvironment of natural extracellular matrix.[23,24] Although the 3D porous scaffolds can be either formed *in situ* or preformed, the injectable *in situ* forming scaffolds offer many advantages over preformed ones. Specifically, cells and bioactive molecules can be readily incorporated into the *in situ* forming matrix by simply mixing prior to solidification. Additionally, *in situ* forming gels can be implanted via a needle injection unlike implantation of preformed scaffolds that often require costly surgical procedures with risk of complications.[1] Last but not least, *in situ* forming scaffolds, but not preformed gel, can easily fill irregularly-shaped defects which are associated with different injuries and trauma.[1,2] Consequently, there has been an increasing focus on the development of injectable *in situ*-forming systems for biomedical applications in recent years. Based on their gelation mechanisms, *in situ* forming hydrogel scaffolds can be categorized into chemically- and

physically-crosslinked scaffolds.[3] Chemically-crosslinked hydrogel scaffolds can be formed by either *in situ* polymerization or crosslinking reactions between the components. However, the toxicity and reactive nature of chemical reagents used in scaffold fabrication may adversely affect the survival and bioactivity of seeded cells and bioactive molecules.[4] To overcome such shortcomings, *in situ* physical-crosslinking mechanisms in response to certain environmental change such as pH, temperature, ion, solvent and light, have gained in popularity.[5–7,25–27]

Among all *in situ* gelling systems, the thermally induced gelling mechanism is the most common method to produce *in situ* forming scaffolds. Typically, these gel systems can flow at room temperature but solidify immediately and form 3D scaffolds when brought to ambient temperature (37 ºC). There are two benefits of using thermally induced gel in biomedical applications. Firstly, toxic reagents and crosslinkers are not required for the production of many thermally induced gelling systems. Secondly, thermally induced gelling system can be made of a wide variety of biomaterials including natural polymers and their derivatives, synthetic polymers and polypeptides.[27–31] While many of these thermally induced gelling systems were composed of linear or branched polymers, thermosensitive nano-/micro-size polymer particles have recently been used as building blocks for *in situ* forming hydrogel scaffolds. Compared to these linear/ branched polymer-based thermogelling systems, the particle-based ones have several advantages including the reduced viscosity and improved mechanical properties at the same concentration. Furthermore, the building blocks (particles) can be employed as carriers of growth factors or bioactive molecules to deliver them in a controlled manner for guiding differentiation of stem cells.[28,32,33] Among these particle-based thermogelling systems, poly (N-isopropylacrylamide) (PNIPAM)-based microgels are the most studied and have been widely explored as *in situ* forming scaffolds for use in tissue engineering.[28,32,34–41] PNIPAM polymer has a lower critical

solution temperature (LCST) at near to physiological temperature therefore, PNIPAM-based microgels can be used for reversible cell adhesion or detachment and for triggered release of therapeutics.[39,40] However, there are limitations for long-term application in biotechnology.[42] The monomer of PNIPAM, N-isopropylacrylamide (NIPAM) is carcinogenic as well as the byproducts are neurotoxic, perhaps generated by hydrolysis of PNIPAM.[33] To overcome these concerns, a series of thermosensitive polymers or nanoparticles based on oligo(ethylene glycol) methacrylate (OEGMA) with different ethylene glycol chain lengths have been developed.[43–46] By copolymerization of OEGMA monomers with different length of ethylene glycol chain, the as-prepared nanoparticles have a wide range of LCST, similar to those of PNIPAM or PEG-based hydrogels.[43–46] For instance, a copolymer hydrogel based on di(ethylene glycol) methacrylate (MEO_2MA, n = 2) and $OEGMA_{475}$ (mw = 475 g/mol, n = 8,9) has a volume phase transition temperature (VPTT) between 23 ºC and 90 ºC.[47] These results support the overall hypothesis of this work that thermally induced gelling system can be made of OEGMA particles.

Herein, we fabricated a series of new injectable *in situ* gelling hydrogel with three monomers, di(ethylene glycol) methacrylate (MEO_2MA), OEGMA (mw = 300 g/mol), and acrylic acid (AAc). The P(MEO_2MA-co-$OEGMA_{300}$-co-AAc) (PMOA) hydrogel has physiochemical and biological properties similar to PNIPAM and PEG. (**Figure 2.1**) Specifically, we have synthesized three hydrogel nanoparticles with different content of acrylic acid (0, 1, and 3 mol % of AAc.) The physiochemical and biological properties of the three hydrogels were assessed *in vitro*. Finally, the capability of this new thermally induced gelling system to release proteins and recruit circulating cancer cells was assessed *in vivo.*

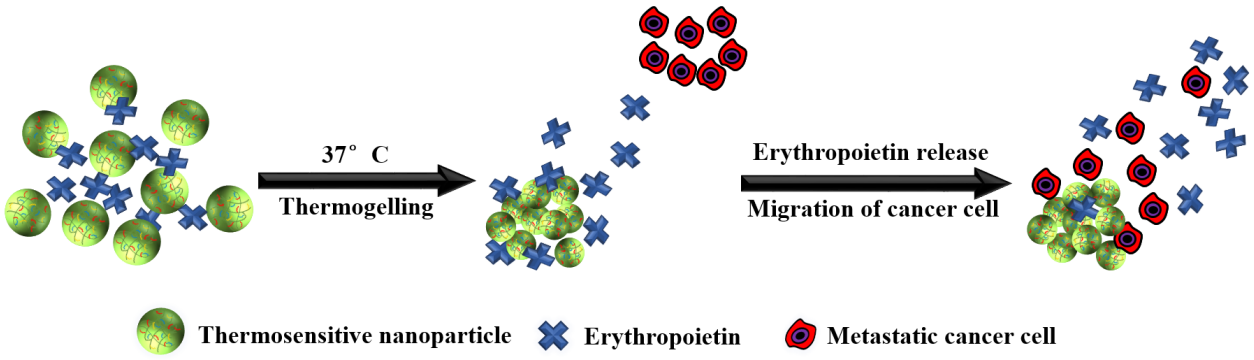

Figure 2.1 At body temperature, thermosensitive nanoparticles release erythropoietin to lure metastatic cancer cells.

2.2 Materials and methods

2.2.1 Materials

Di(ethylene glycol) methyl ether methacrylate (MEO_2MA), poly(ethylene glycol) methyl ether methacrylate (300 g/mol, $OEGMA_{300}$), acrylic acid (AAc), ethylene glycol dimethacrylate (EGDMA), and ammonium persulfate (APS) were purchased from Sigma-Aldrich (St Louis, Missouri). Sodium dodecyl sulfate (SDS) was obtained from Bio-Rad (Hercules, CA). Milli-Q grade deionized water was used through all experiments.

2.2.2 Synthesis of P(MEO_2MA-co-$OEGMA_{300}$-co-AAc) (PMOA) hydrogel nanoparticles

A series of hydrogel nanoparticles were synthesized via a free radical precipitation polymerization method.[33] In brief, MEO_2MA, $OEGMA_{300}$, AAc, SDS, EGDMA and DI water

were mixed in a 500 ml round bottle flask. The mixture was heated to 70 ^{o}C in a water bath under nitrogen purging. After 30 mins, APS solution was added to the mixture to initiate polymerization. The reaction was allowed to proceed for 6 hours with magnetic stirring at 70 ^{o}C under N_2 atmosphere. Here three batches of nanoparticles with different AAc contents (0, 1, and 3 mol %) were prepared (Table 1), and defined as PMOA0, PMOA1, and PMOA3, respectively. The above-prepared nanoparticle dispersions were purified with exhaustive dialysis (cutoff: 10 kDa) against deionized water for one week. The purified nanoparticles were concentrated and collected using a centrifuge, and then stored in a refrigerator for further use.

2.2.3 Size, polydispersity, zeta potential, and morphology of the particle

The size, polydispersity, and zeta potential of the hydrogel nanoparticles were determined using a ZetaPALS dynamic light scattering (DLS) detector (Brookhaven Instruments, Holtsville, NY).[48] The samples at a concentration of 1 mg/mL in DI water were prepared, and sizes of these nanoparticles were determined at 24 and 37 °C, respectively. Furthermore, to observe morphology of the nanoparticles, Scanning Electron Microscope (SEM) was employed as described earlier.[49] Briefly, a drop of the diluted particle dispersion was placed onto a glass slide cover adhered to a SEM specimen holder with the conductive tape, and then dried at ambient temperature. After sputter-coating with silver, SEM images were recorded by a Hitachi S-4800 II FE Scanning Electron Microscope.[49]

2.2.4 Conductivity measurement

Using a FP30 Conductivity meter (Mettle Toledo, Columbus, OH), carboxyl group content of the nanoparticles was determined quantitatively following a published method.[50] 1.0 mL of HCl solution (0.01 M) was added into a 20 mL of the nanoparticle dispersion (30 mg/mL), followed by stirring for 20 mins. Conductivity measurement was conducted using NaOH aqueous solution (0.01 M) as a titrant. The COOH contents of these nanoparticles were calculated based on the following formulation: COOH (μmole/mg) = C×V/W, where C and V are the concentration and used volume of NaOH solution, respectively. W is the solid content of the nanoparticles.

2.2.5 Turbidity test

To determine the phase transition temperature of the nanoparticles, the turbidity of the nanoparticles in DI water and phosphate buffered saline (PBS, 43.5 mM ionic strength) was respectively measured using a Beckman DU640 UV-Visible spectrophotometer (Fullerton, CA).[51] Briefly, 2.0 mL of the nanoparticle dispersion (1.0 mg/mL) was prepared in a UV cuvette, and covered with a lid to keep water from evaporation during the experiments. The cuvette was placed in a water bath equipped with a temperature controller and incubated for one minute after the predetermined temperature was reached. The transmittance of the dispersion at various temperature points was recorded at 550 nm.

2.2.6 Viscosity test

The viscosity of the nanoparticle dispersions as a function of temperature was measured using an HR-2 Discovery Hybrid Rheometer (TA Instruments).[33,52] Two flat parallel plates (25

cm in diameter) were used, and the distance between two plates was adjusted to 0.6 mm. During the experiments, a constant stress of 2 Pa and a frequency of 0.1 Hz was applied. To measure viscosity, 0.6 mL of nanoparticle dispersions (60 mg/mL in PBS) was loaded on the plate, viscosity of the samples was recorded with temperature increasing at a rate of 2 °C/min from 15 to 40 °C.

2.2.7 Water loss

The water retention of the hydrogels was determined using an established method.[53] Briefly, 1.0 mL of the nanoparticle dispersion (60 mg/mL in PBS) was added to an Eppendorf tube, total mass (W_o) of the tube and the sample was recorded. The tube was then transferred into a water bath and incubated at 37 °C for 4 hours. The lost water from the hydrogels during the incubation was discarded carefully from the top, and total mass (W_i) of tube and hydrogel was weighted. The weight percentage of lost water was defined as: $(W_o\text{-}W_i)/W_o\times100$ %. To observe pore structures of the hydrogels, at the end of water loss experiments, the thermally gelling hydrogels were quickly frozen in liquid nitrogen and dried in vacuo. The cross sections of the hydrogels were observed under an SEM as described above.

2.2.8 *In vitro* release of protein

Bovine serum albumin (BSA) and erythropoietin (Epo) was used as a model protein drug and labelled with Cy®5 dye (Lumiprobe Co., Hunt Valley, MD) following the manufacturer's protocol. The release kinetics of Cy®5-labeled BSA/Epo was then determined as described previously.[33] Briefly, 1.0 mL of nanoparticle dispersion (60 mg/mL in PBS) was mixed with 1.0

mg of Cy®5-labeled BSA/Epo at room temperature and the mixture was heated to 37 °C to allow for gelation. Then, 2.0 mL of pre-heated PBS media (37 °C) was added onto the top of the hydrogel. The sample was quickly put into an incubator at 37 °C under gentle shaking. At different time intervals, 150 μL of the supernatants were taken and added into wells of a 96-wells plate. Fluorescence intensities were recorded using a microplate reader (Spectra Max Gemini EM XPS, Molecular Devices, San Jose, CA) at an excitation of 640 nm and an emission of 700 nm.

2.2.9 *In vitro* cell cytotoxicity

Cytotoxicity of the thermally-gelling hydrogels to cells was conducted according to the publication.[54] Briefly, 0.54 mL of DMEM was added into the thermally-gelling hydrogels and incubated at 37 ◦C in a cell culture incubator. After culture for 3 days, 0.06 mL was taken out as the conditioned media for the cell viability assay. NIH 3T3 fibroblasts were plated at a density of 25,000 cells per well in a 48-well plate and cultured in DMEM media containing 20 % of the above-collected conditioned media. Cell viability was then characterized using a modified Alamar Blue dye assay.[55]

2.2.10 *In vivo* biocompatibility and cancer cell trap

Animal subcutaneous implantation model was used to determine the tissue compatibility of thermally-gelling hydrogel as described previously.[56] In brief, a 100 μL of the pre-gel nanoparticle dispersion (60mg/ml) and saline as control was subcutaneously injected in dorsally in a Balb/C mouse (25 g body weight) obtained from The Jackson Laboratory (Bar Harbor, ME).

After implantation for 24 hours, the mouse was sacrificed and the implants and the surrounding tissues were isolated, and then sectioned for H&E staining. Additionally, a subcutaneously implanted cancer trap mouse model was used to assess the ability of chemokine-releasing thermal gelling hydrogel for recruiting prostate cancer cells.[57] 2.0 μL of Epo (10 units in PBS) was mixed with 50 μL of the thermally-gelling nanoparticle dispersion (80 mg/mL in PBS), and then was injected into both sides of the back of mice via 18-gauge needle. After 12 hours, intravascular injection of prostate cancer cells (DAB2IP-knockdown PC3 cells, gift from Dr. Jer-Tsong Hsieh at the University of Texas Southwestern Medical Center at Dallas) was administered into mice. The cells were labelled with Vybrant™ DiD Cell-Labeling Solution (Thermo Fisher Scientific, Waltham, MA) according to the manufacturer's protocol before injection. *In vivo* cell recruitment to the sites of hydrogel implants was monitored using Kodak In-Vivo Imaging System FX Pro (Carestream Health Inc., New Haven, CT, USA) as described previously.[57] At the end of the study, implants and surrounding tissues were frozen sectioned and analyzed using H&E and immunohistochemistry as previously described.[58] Images were taken utilizing a Leica fluorescence microscope (Leica Microsystem GmbH, Wetzlar, Germany) combined with a Retiga-EXi CCD camera (QImaging, Surrey, BC, Canada). Cell number was calibrated using ImageJ software. All animal experiment protocols were approved by Animal Care and Use Committee of the University of Texas at Arlington.

2.2.11 Statistical analysis

All data were evaluated using a two-tailed Student t-test and presented as mean ± standard deviation. Statistical analyses of all data were performed by a Student t-test. The results

showed significance when p value < 0.05. All tests were conducted in triplicate for statistical analysis.

2.3 Results & Discussion

2.3.1 Synthesis and characterization of hydrogel nanoparticles

Three of hydrogel nanoparticles with various AAc contents were synthesized via free radical polymerization (**Table 2.1**). All three as-prepared particles are highly mono-dispersed. The polydispersity index of the PMOA3 nanoparticles is 0.005 with narrow size distribution of the nanoparticles at room temperature (**Figure 2.2A**). The finding is in line with the observation of SEM (**Figure 2.2B**). Slight reduction of the particle size in SEM images is due to the particle dehydration during SEM sample preparation. From **Figure 2.2C**, one can observe the dependence of size on temperature for all three nanoparticles. The average diameter for the PMOA0 is 211.4 nm at 24 °C but reduces to 163.3 nm at 37 °C. Similar observation has been obtained on the other two samples. The average diameter is 237.9 nm and 271.8 nm at 24 °C while it is 169.2 nm, and 179.2 nm at 37 °C for PMOA1 and PMOA3, respectively. Furthermore, the average size of the hydrogel nanoparticles increases from 211.4 to 237.9 and 271.8 nm at room temperature with increasing of AAc from 0 to 1 and 3 %, respectively. This is because more AAc introduces more charged density into the hydrogel nanoparticles, resulting in greater swelling of the particles. Conductivity titration study reveals that the content of carboxyl groups for PMOA1 and PMOA3 are 9.628 and 23.1 nmole/mg, respectively. The observation can be

further confirmed by zeta potential of the hydrogel nanoparticles (**Figure 2.2D**). The zeta potential of the PMOA0, PMOA1 and PMOA3 is -5.69 mV, -16.8mV to -23.57 mV, respectively. These observations are in good agreement with early publications.[59,60]

Table 2.1 Monomer composition in feed (moles). Where the total moles of three monomers are 0.026 moles, SDS is as a detergent and APS is as an initiator.

Samples	**MEO_2MA (mol)**	**$OEGMA_{300}$ (mol)**	**AAc (mol)**	**EGDMA (mol)**	**SDS (mol)**	**APS (mol)**
PMOA0	0.02314	0.0026	0	0.00026	0.000139	0.000438
PMOA1	0.02288	0.0026	0.00026	0.00026	0.000139	0.000438
PMOA3	0.02236	0.0026	0.00078	0.00026	0.000139	0.000438

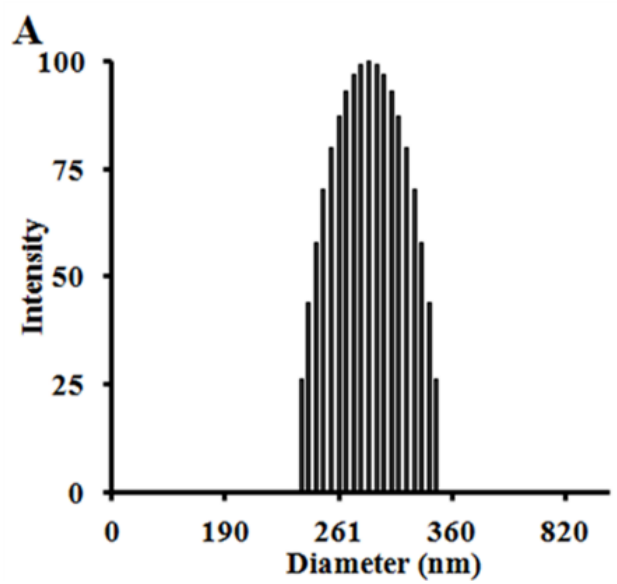
A
100
75
50
25
0
Intensity
0
190
261
360
820
Diameter (nm)

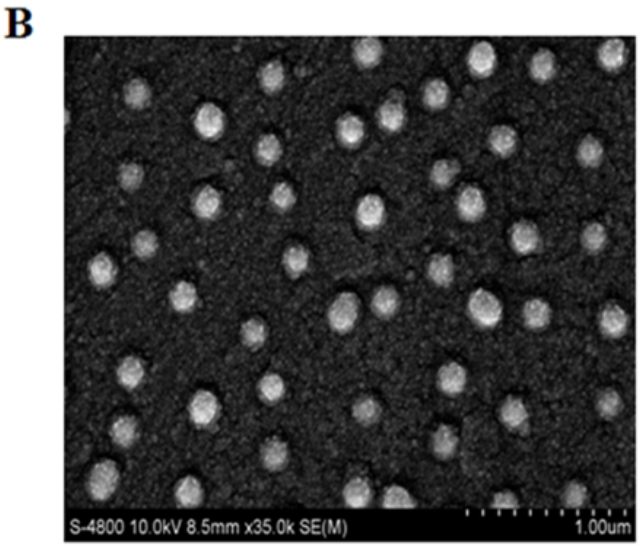
B
S-4800 10.0kV 8.5mm x35.0k SE(M)
1.00um

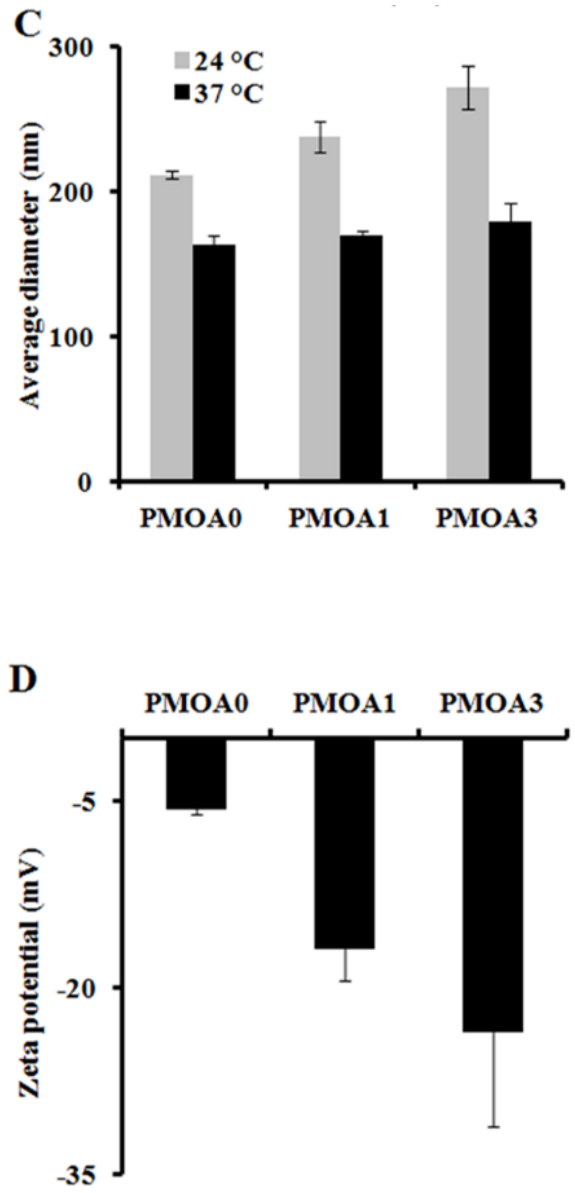

Figure 2.2 A) Dynamic Light Scattering (DLS) measurements demonstrating polydispersity of PMOA3 nanoparticle at 24°C. **B)** Scanning Electron Microscope (SEM) image illustrating that the particles are in spherical shape. **C)** DLS measurement at both 24 °C and 37 °C demonstrating an increase in particle size with the increase of acrylic acid content. **D)** DLS measurement demonstrating a decrease in zeta potential with the increase of acrylic acid.

2.3.2 Turbidity test and thermally-triggered gelation

To determine phase transition temperature of the hydrogel nanoparticles, turbidity of the diluted hydrogel nanoparticles (1.0 mg/mL in DI water and PBS) at different temperatures was determined using a UV-Visible spectrophotometer. The results show that all three nanoparticles exhibit temperature-sensitive property (**Figure 2.3A**). For PMOA0 and PMOA1, transmittance of the dispersions decreases gradually with increasing temperature. There is a sharp drop in the transmittance when heated to 28°C and 30°C (defined as phase transition temperature), respectively.[61] On the other hand, onset of the phase transition temperature for PMOA3 cannot be reached even when the temperature is raised up to 40 °C. The increase in the phase transition temperature with increasing AAc contents can be explained as follows. More AAc contributes to high ionic strength (as confirmed in **Figure 2.2D**). In addition, the repulsive force between these negatively charged carboxyl groups keeps the polymer chains from aggregation.[59] Similar observations are also documented in several recent publications.[59,60]

The phase transition temperatures of these nanoparticles at physiological media (PBS, pH: 7.4 and ionic strength: 43.5 mM) were also investigated (**Figure 2.3A**). One can observe that the phase transition temperature of all three hydrogel nanoparticles shifts to a lower temperature. Furthermore, the presence of salts initiates the nanoparticle's flocculation when temperature is heated above the phase transition temperature. This phenomenon occurs because the ions in PBS can disturb the closest hydration shells between water and particles, leading to aggregation of the hydrogel particles when heating. On the contrary, all three nanoparticles are highly colloidally stable in DI water at the studied temperature range. Interestingly, all nanoparticles with concentration of 60 mg/mL exhibit a thermogelling property in PBS media. At room temperature (24 °C), the nanoparticle dispersions can flow freely. However, the dispersions become

physically gelled and cannot escape from the inverted tube when temperature reaches to 37 °C (**Figure 2.3B**). This thermally-triggered gelation may be explained as follow: poly[oligo(ethylene glycol) methacrylate] segments of the nanoparticles turns from hydrophilic into hydrophobic beyond the phase transition temperature, leading to the hydrophobic interaction among the particles to form a physical network in presence of salt as shown in recent studies.[39,40] The thermosensitive hydrogels, PMOA0, PMOA 1 and PMOA3, can revert to sol state by cooling down. This temperature-dependent phase change can be carried out indefinitely at least *in vitro*. Furthermore, the viscosities of the dispersions were measured with increasing temperature. In concurrence with an earlier study, we find a sharp increase in viscosity when the dispersion is heated above the gelation temperature, and the gelation temperature increases with increasing AAc contents (**Figure 2.3C**).[40]

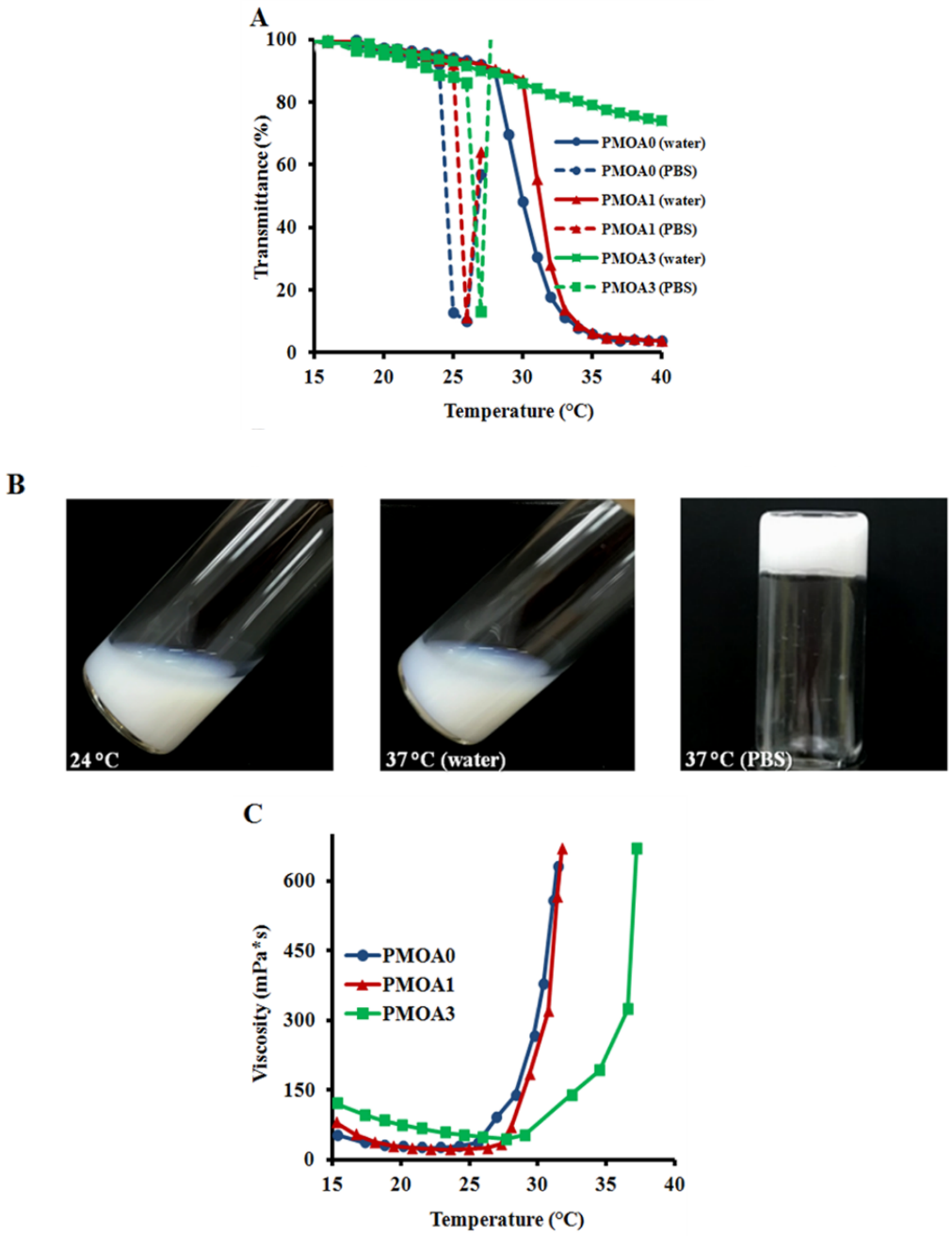

Figure 2.3 A) Turbidity measurement of thermogelling nanoparticles (1.0 mg/mL in deionized water) demonstrating an increase in transition temperature with the increase of acrylic acid. Hydrogel nanoparticles dispersed in PBS (ionic strength: 43.5 mM) have lower transition temperatures than with deionized water. **B)** Inversed particle sample (PMOA3) in a test tube illustrating that the hydrogel nanoparticles (60 mg/mL) form gel at physiological temperature. **C)** Rheometry measurement of thermogelling nanoparticles (60 mg/mL) demonstrating the viscosity as a function of temperature.

2.3.3 Water loss and microstructure of the hydrogel

Since the syneresis of hydrogels has adverse effects for applications of the injectable hydrogel scaffold in tissue engineering and drug delivery,[62] the water loss of the thermogelling macroscopic hydrogels were carried out, and the results are presented in **Figure 2.4A**. Without AAc (PMOA0), approximately 48.4 wt% of water is expelled from the hydrogel after incubated at 37 °C for 4 hours. As expected, addition of AAc has significant impact on water loss. Water loss for PMOA1 (1 % AAc) and PMOA3 (3 % AAc) were measured to be 32.4 and 7.6 wt%, respectively. The phenomena is in good agreement with recent observations that associate improved hydrogel charges with increased AAc content which in turn, attributes to enlarged pore size, reduced hydrogel shrinkage and augmented water retention of the hydrogel.[36] SEM was further used to investigate microstructure of these hydrogels (**Figure 2.4B to D**). An interconnected porous structure can be observed in all three hydrogels. This structure is very critical for hydrogel scaffolds because it allows cells to migrate, and nutrients and waste products to exchange between the scaffolds and surrounding media.[63] The presence of AAc makes the pore size of PMOA1 and PMOA3 larger than that of PMOA0 (5.5, 12.3, and 32.1 μm for PMOA0, PMOA1 and PMOA3, respectively). These results are consistent with those of water loss investigation.

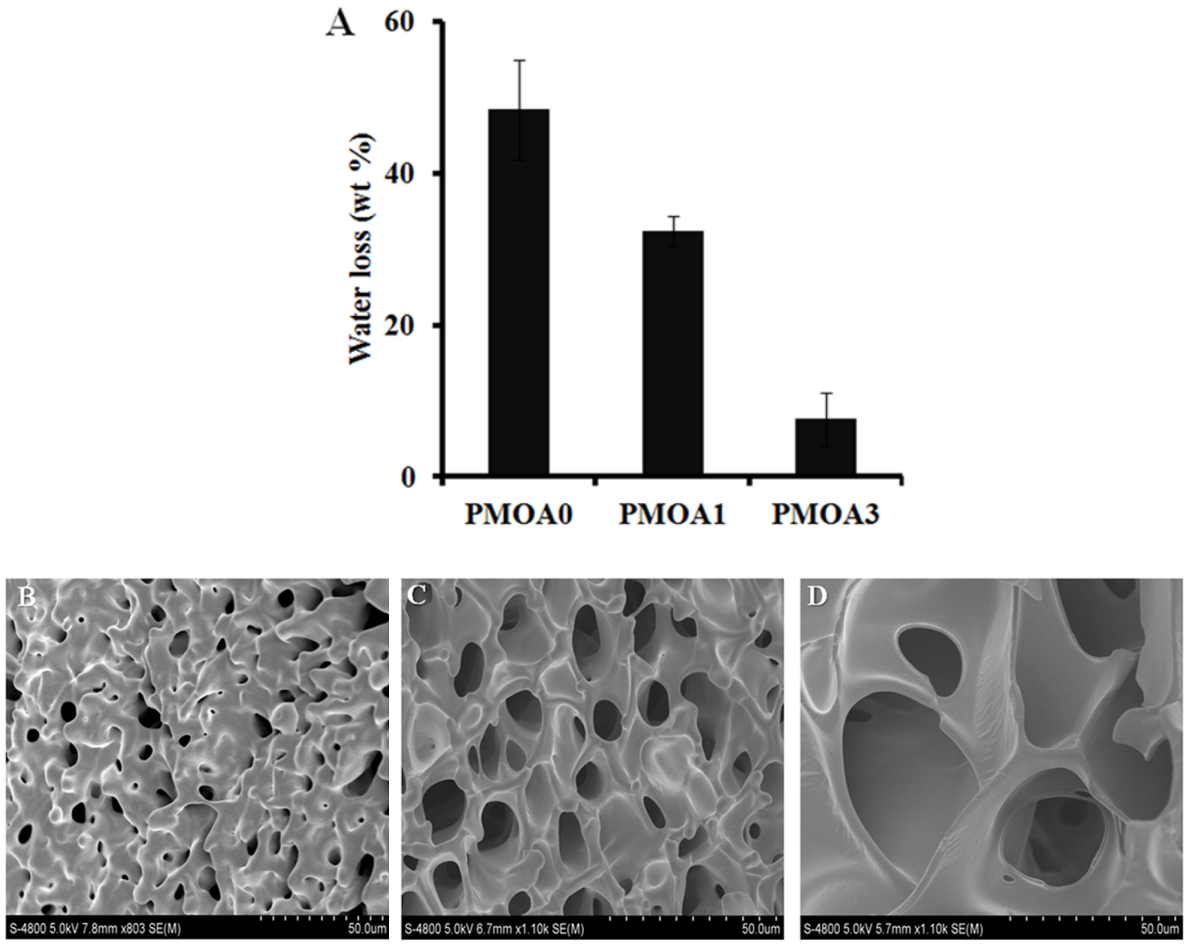

Figure 2.4 A) Measurement of water loss demonstrating a decrease in water loss with the increase of acrylic acid. 1.0 mL of hydrogel nanoparticles (60 mg/mL) were incubated at 37 °C for 4 hours, and then the released water was collected from the top of the gels and measured the weight of the lost water. SEM Images illustrating porosity of PMOA0 **(B)**, PMOA1 **(C)**, and PMOA3 **(D)** nanoparticles matrix.

2.3.4 *In vitro* release of protein

The slow release properties of hydrogels were first characterized using Cy®5-labeled BSA. We find that all three hydrogels show a burst release at first 1 hour but BSA released from PMOA0 (~43 %) is faster than that of PMOA1(~39 %) and PMOA3 (~31 %). The burst release may create the chemokine gradient for initiating cell migration, while subsequent slow release of BSA maintains the gradient for maximal and accumulative recruitment of the cells. After that, BSA gradually released out from the matrix of these hydrogels. PMOA0 released 50% BSA in 11 hours. On the other hand, the release of 50 % BSA from PMOA1 and PMOA3 took longer duration for 17 and 23 hours, respectively (**Figure 2.5A**). With regard to the release of Cy®5-labeled Epo, a similar release profile can be observed (**Figure 2.5B**) although Cy®5-labeled Epo shows a faster release than BSA. The faster release of Epo than BSA may be caused by their size difference. Molecular weights of Epo and BSA are 30 and 66.5 kD, respectively. It is well established that smaller size of protein has faster release rate.[64] The surface charge of protein has also been shown to influence protein release from hydrogel nanoparticles.[65] However, surface charge of proteins play insignificant role in our findings, since both proteins have a similar isoelectric point (around 4.5).

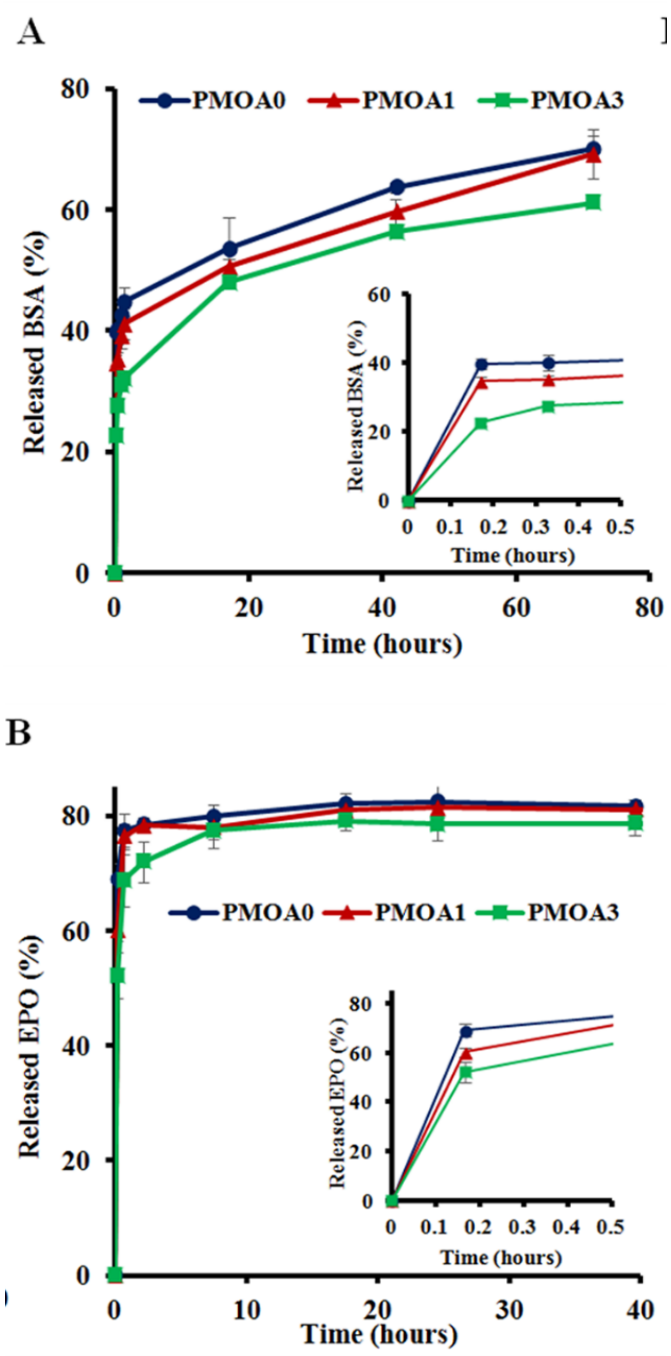

Figure 2.5 *In vitro* release tests of proteins. **A)** Release profiles of Cy®5-labeled BSA and **B)** release profiles of Cy®5-labeled Epo.

2.3.5 Hydrogel's responses to cell *in vitro* and tissue *in vivo*

To evaluate toxicity of the hydrogels to cell *in vitro*, the conditioned media of the hydrogels were collected at the defined time points, and the toxicity of them to 3T3 fibroblast cells was estimated using an Alamar Blue assay (**Figure 2.6A**). After 3 days, PMOA3 exhibits the least toxic response among these hydrogels although all three hydrogels exhibit minimum toxicity to 3T3 fibroblasts. Combining the results with the protein release *in vitro*, PMOA3 was chosen as a protein delivery scaffold *in vivo*. However, prior to doing that, response of the PMOA3 hydrogel to tissue needs to be further evaluated *in vivo*. Here a mouse subcutaneous implant model was employed, and the poly(lactic-co-acid) (PLGA) particle served as a control.[56] As expected, PLGA implant triggers more foreign body reactions in the surrounding area of the implant than the PMOA3 gel (**Figure 2.6B**). Quantitative analysis further shows that PMOA3 hydrogel triggers significant lesser inflammatory cell accumulation (~4X) than the PLGA implants (**Figure 2.6B**). The histological evidence supports that PMOA3 hydrogels possess good tissue compatibility. These results are in consistent with previous finding that poly(oligo(ethylene glycol)) nanoparticles and their derived products have similar tissue responses as the FDA-approved poly(ethylene glycol) polymer.[33]

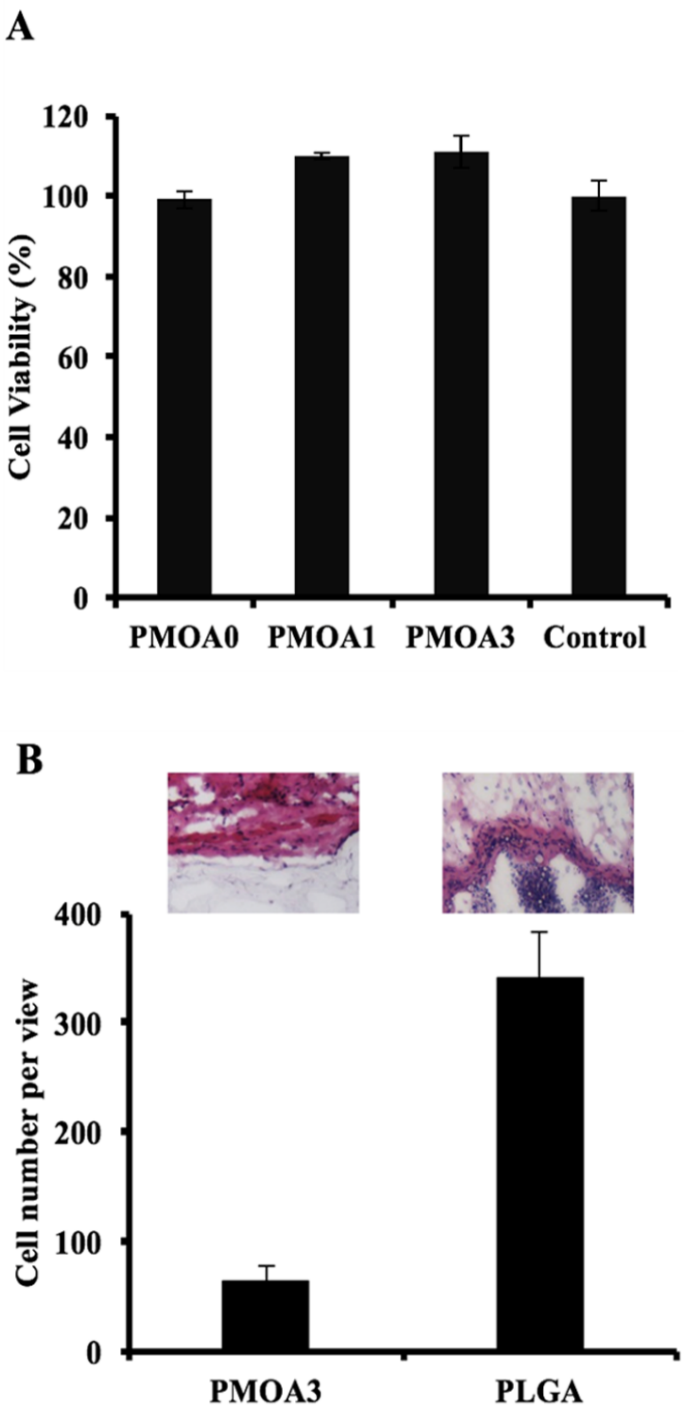

Figure 2.6 In vitro analysis of hydrogel-associated cell and tissue toxicity. **A)** *In vitro* toxicity of the thermogelling gels to cells. **B)** H&E staining and cell quantification of tissue surrounding PMOA3 and PLGA implants.

2.3.6 *In vivo* cancer cell trap

To investigate the capability of thermally induced gelling system as a cancer trap implant, Epo-loaded PMOA3 nanoparticles or Epo alone were implanted in the subcutaneous cavity via 18-gauge needle. After 12 hours, mice were administered IV injection of DiD-labeled prostate cancer cells (PC3-KD cells). After cancer cell implantation, migration of the cancer cells were imaged after 2 days and 4 days, respectively. Based on NIR imaging, the Epo-loaded PMOA3 implant recruited significantly more PC3-KD cells than Epo alone (**Figure 2.7A**). Total intensity of PC3-KD cells from the implanted site was $3.14x10^6$ at Day 2 and $3.66x10^6$ at Day 4 (**Figure 2.7B**). Previous studies have demonstrated that Epo receptor is highly expressed in many different cancer cells such as breast, head-and-neck tumors, colon, lung, prostate and melanoma, and Epo-releasing scaffolds prompts more melanoma cell migration.[57,66–68] In addition, our previous study has demonstrated that similar hydrogel has controlled protein release properties. Equally important, using an *in vivo* cancer cell trapping mouse model, Epo-releasing PMOA hydrogel is able to recruit cancer cells to the implant site effectively. This injectable, thermogelling PMOA hydrogel may be used to create Epo gradient for recruiting and trapping circulating cancer cells to reduce or delay cancer metastasis.

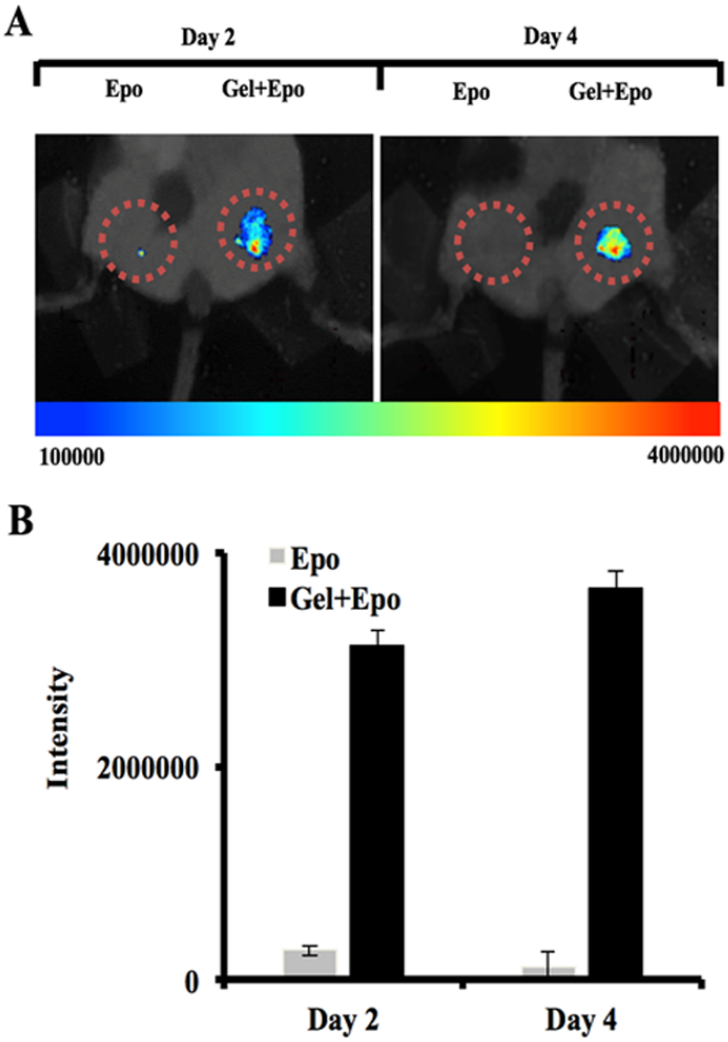

Figure 2.7 The ability of chemokine-releasing thermogelling nanoparticles to recruit prostate cancer cells in mice. **A)** Whole body imaging and **B)** fluorescent intensity measurement of NIR-labeled prostate cancer cells at the implant site of Epo and Epo-releasing thermogelling nanoparticles in animals.

2.4 Conclusions

In short, an injectable, thermogelling poly(oligo(ethylene glycol))-based nanoparticles were successfully prepared.[69] Both *in vitro* and *in vivo* testing confirm that the PMOA hydrogels made of these nanoparticles, induce minimal toxicity to cells and tissue responses. By simply mixing the protein with the hydrogel nanoparticle at room temperature, the mixture can easily be injected into the body and turn into the physical hydrogel at the body temperature, serving as a depot for controlled release of proteins. *In vivo* cancer cell migration experiment show a dramatic reduction of metastasis by tuning the release of Epo. In general, this study suggests that this PMOA hydrogel nanoparticle has a great potential in protein therapy and drug delivery.

CHAPTER 3

Pre-targeting Platform for Imaging and Enhancing Drug Delivery

3.1 Introduction

Development of drug delivery platforms has been accelerated based on the idea of combining targeting ligands and imaging/therapeutic agents into a single platform.[1–4] While some advancements have been made thus far in the area of cancer diagnosis and treatment,[2,3,5] little progress has been made of developing theranostic platforms for inflammatory diseases which was the goal of this investigation.

A larger number of pre-targeting platforms for theranostic cancer treatment have been reported in the literature thus far.[6,7,9,10] Two-step processes were typically employed for this strategy. Briefly, the first step was to direct accumulation of an imaging/pre-targeting agent at the disease site. Then, the second step was to deliver the therapeutic agent to the diseased tissue by interacting with the pre-targeting agent.[11–13] For instance, radiolabeled monoclonal antibodies (mAbs) and radioimmunoconjugates had been developed as a radioimmunodetection (RID) agent and radioimmunotherapeutic (RIT) agent, respectively.[7,14] The studies have shown that the pre-

targeting strategy has much higher tumor specificity (tumour/non-tumour (T/NT) ratio) than the conventional approach. In addition, pre-targeting platforms are beneficial for diagnostics and therapy due to minimal exposure of normal tissues to therapeutic agents and limited hematological toxicity.[15] Although significant progresses have been made on tumor detection/treatment using the pre-targeting platforms, such approach has not been investigated for detecting and treating inflammatory diseases.

Non-covalent affinity interactions are the most common pre-targeting strategy.[16,17] Amongst non-covalent binding systems, avidin/biotin system has been widely studied due to the multiple binding sites of avidin as well as the protein has the strongest non-covalent interaction with biotin (dissociation constant:10^{-15} M).[16,18] In fact, the avidin/biotin system has been extensively utilized in biochemical assay and affinity purification due to its unique advantages including signal amplification, high specificity and robust stability.[19] However, avidin/biotin system has limited *in vivo* application due to the following deficiencies. First, avidin may cross-react with endogenous biotin or to lectin. Second, biotinylated molecule can bind to endogenous biotin-binding proteins such as eggs or bacteria.[20] To overcome these limitations, streptavidin with an isoelectric point (pI) of 5~6, an avidin analogue derived from *Streptomyces avidinii*, has been exploited as a pre-targeting platform. Although streptavidin/biotin system has excellent binding affinity with significantly low non-specific binding,[21,22] such system has limited *in vivo* utility due to the facts that streptavidin has high affinity to fibronectin and kidney tissue.[23,24] In recent years, neutravidin is emerging as an alternative to avidin or streptavidin in avidin/biotin system-based pre-targeting platforms.[25] Neutravidin is a deglycosylated derivative of avidin with pI of ~6.3. The lack of the carbohydrate moieties and thus the nearly neutral pI reduces its nonspecific binding to surface of cells while preserving the high binding affinity with biotin.[25]

Many inflammatory cells-targeting imaging methods have been developed for the diagnosis of inflammatory diseases.[26–28] In many of those studies, since inflammation involves infiltration and activation of macrophages, the activated macrophage has been used as a biomarker for targeting and imaging.[1,29,30,32,70] In more detail, activated macrophages over-express folate receptors (FR) and those cells play a role of pathogenesis of inflammatory diseases by downregulations of producing a plethora of pro-inflammatory mediators. These macrophages' products, including IL-1, TNF-α, reactive oxygen species, and other potent chemokines or cytokines,[33] would eventually enhance the progressions of inflammatory diseases.[34] Since inflammatory macrophages express high level of folate receptor (FR), FR has been extensively employed as the targeting site for inflammation diagnosis and treatment.[33,35,36]

In the present work, we proposed a pre-targeting "sandwich" platform to amplify inflammation theragnosis via neutravidin-biotin system (as schematically illustrated in Figure 1.2). Specifically, a biotinylated- and folate-conjugated optical imaging nanoparticle was prepared and it is targeting macrophages first and accumulating in the inflammation site via folate/FR interactions. Secondly, we then assess the capability of the pre-targeting "sandwich" platform to reduce inflammatory responses both *in vitro* and *in vivo*. Overall, our results support that the innovative theranostic platform can, not only eliminate the unnecessary treatment, but also enhance delivery of anti-inflammatory drugs to the inflamed cells/tissues.

3.2 Materials and methods

3.2.1 Materials

Amino-terminalized poly(ethylene glycol-b-caprolactone) (NH_2-PEG-PCL) (M_w:2200-b-7000) was purchased from Polymer Source Inc.(Dorval, Canada). D-Biotin, neutravidin, DiD dye were obtained from Thermo Fisher Scientific (Waltham, MA). Dimethylformamide (DMF), dimethyl sulfoxide (DMSO), DMSO-d^6, trimethylamine (TEA), tetrahydrofuran (THF), N-hydroxysuccinimide (NHS), N,N'-dicyclohexylcarbodiimide (DCC), folate binding protein (FBP), dexamethasone (Dex), fluorescein (FITC), and Nile Red (NR) were received from Sigma-Aldrich (St. Louis, MO). Lipopolysaccharide, LPS, was received from *Escherichia coli*, Sigma, St Louis MO. The murine macrophage Raw 264.7 cell line was obtained from the American Type Culture Collection (Rockville, MD, USA). Milli-Q grade deionized water was used through all experiments.

3.2.2 Synthesis and characterization of folate- or biotin-conjugated copolymers

An amphiphilic copolymer, poly(ethylene glycol-b-ε-caprolactone) (abbreviated as PEG–PCL) was used to form drug encapsulated micelle with an average diameter 100-150 nm. To synthesize folate-conjugated PEG-PCL (abbreviated as F-PEG-PCL), carboxyl group of folate was initially activated according to a published paper[71]. Briefly, a 191.9 mg of folate was completely dissolved in 15.0 ml of DMF and incubated in the presence of a 100.0 mg of NHS and a 179.3 mg of DCC overnight at room temperature. After filtering out the byproduct, dicyclohexylurea (DCU), using a gravity filtration with filter papers, the activated folate solution was mixed with a 200.0 mg of NH_2-PEG2.2k-PCL7k dissolved in 2.5 ml dimethyl siloxane

followed by adding a 4.5 µl of triethylamine. The mixture was stirred overnight at room temperature, and then dialyzed against DI water for 24 hours (molecular weight cut-off, MWCO: 2 kD). The crude F-PEG-PCL copolymers were collected after the lyophilization. The dried powders were then re-dissolved in THF and the insoluble free folate was then removed by filter papers. The filtrate was dialyzed against DI water again for 5 days to completely remove THF and unreactive free folate. The purified F-PEG-PCL was lyophilized to collect the final dried powders. The structure of the folate-conjugates was determined by ^{1}H NMR. Briefly, the conjugate was prepared in DMSO-d^{6} at the concentration of 7.0 mg/ml in a 5.0 mm NMR tube at room temperature. NMR spectra were recorded on a Varian Gemini 2000 spectrometer working at 300 MHz for protons.

To synthesize biotin-conjugated PEG-PCL (B-PEG-PCL), carboxyl group of biotin was activated as described above. Briefly, a 106.2 mg of biotin was dissolved in 5.0 ml of DMF completely, and then a 100.0 mg of NHS and a 179.3 mg of DCC were added. The activation reaction preceded overnight at room temperature. Following the filtration of the precipitate with the filter papers, a 200.0 mg of NH_2-PEG2.2k-PCL7k dissolved in 2.5 ml DMSO with a 4.5 µl of triethylamine. The mixture was incubated overnight at room temperature, and then following progress is the same as described above. Free biotin was removed by gravity filtration with ice-cold ethanol.

3.2.3 Preparation of fluorophore loaded folate-, biotin- or biotinylated folate-conjugated micelles

For *in vitro* targeting studies, FITC labeled F-PEG-PCL micelles (denoted as FMC-FITC) and B-PEG-PCL micelles (denoted as BMC-FITC) were prepared followed by an

emulsion/solvent evaporation method as described previously [72]. Briefly, both a 10.0 mg of F-PEG-PCL (or B-PEG-PCL) and a 40.0 μg of FITC were dissolved in 2.0 ml of DMF, and then the solution was added dropwise to 20.0 mL of DI water while sonicating at speed 5 for one minute. After evaporating DMF under gentle stirring for 12 hours, the FMC-FITC (or BMC-FITC) was purified with dialysis against DI water for 12 hours. Then the FMC-FITC (or BMC-FITC) solution was filtrated using a 0.22 μm filter with a syringe and then concentrated via ultrafiltration at 5,000 *g* (MWCO: 3 kD) for 15 minutes. Additionally, biotinylated folate-conjugated micelles with either FITC or Nile Red fluorophore (denoted as BFMC-FITC or BFMC-NR) were also prepared. Briefly, a 5.0 mg of F-PEG-PCL and a 5.0 mg of B-PEG-PCL, as well as a 40.0 μg of FITC (or Nile Red) were dissolved in 2.0 ml of DMF and the following progress is the same as described above. The BFMC-NR was used for pretargeting/imaging step in the proposed "sandwich" platform. For *ex vivo* studies, DiD loaded FMC or BMC (FMC-DiD or BMC-DiD) were prepared via the same procedure except that a 200 μg of DiD was used. The FMC-DiD was used for a traditional direct targeting approach and the BMC-DiD was used in drug delivery step of the "sandwich" pre-targeting strategy. The mean particle size and polydispersity index (PDI) of the above-prepared micelles in ddH_2O (pH 7.4) were obtained using a dynamic light scattering, Malvern Zeta Sizer (Malvern, NanoZS, UK), and their morphologies were observed by High-resolution Transmission Electron Microscopy, (H-9500, Hitachi, Japan).

3.2.4 Preparation and Characterization of an anti-inflammatory drug loaded micelles

Dexamethasone (Dex), an anti-inflammatory drug, loaded micelles (FMC-Dex or BMC-Dex) were prepared using published method.[39] Briefly, a 0.5 mg of Dex, along with a 10.0 mg of

either F-PEG-PCL or B-PEG-PCL were co-dissolved in 2.0 ml of DMF. The mixtures were then dropped into the 20.0 ml of DI water while sonicating for one minute and magnetically stirred for 12 hours followed by filtration using 0.22 μm filter with syringe. Finally, the purified micelles solutions were condensed via ultrafiltration (MWCO: 100 kD, Millipore, Massachusetts, USA) at 5,000 rpm for further use. The filtrates were collected for measuring unencapsulated Dex. The unencapsulated Dex in the substrate was calculated by absorbance at 242 nm using UV-Vis spectrophotometer (Agilent Technologies, 89090A) so that the initial amounts of entrapped Dex in FMC-Dex and BMC-Dex were calculated. Encapsulation efficiency (EE%) (**Equation 1**) and drug loading (DL%) (**Equation 2**) were calculated using the formulas. Stability of those micelles were monitored by measuring their sizes and polydispersities at 4 and 23 °C degree for up to 7 days.

$$Encapsulation\ Efficiency\ (\%) = \frac{Weight\ of\ Dex\ \ in\ micelles}{Weight\ of\ total\ feeding\ Dex} \times 100\% \quad (\mathbf{1})$$

$$Drug\ Loading\ (\%) = \frac{Weight\ of\ encapsulated\ Dex\ in\ micelles}{Weight\ of\ total\ micelles} \times 100\% \quad (\mathbf{2})$$

3.2.5 *In vitro* drug release study

For *in vitro* Dex release study, a dialysis method was employed as described before.[40] Briefly, 1 ml of the prepared FMC-Dex and BMC-Dex as well as free Dex were placed into different dialysis tubes (MWCO: 3.5-5 kD) and incubated within 50 ml tube with 5.0 ml of PBS (pH 7.4) as physiological media at 37 °C while shaking at 50 rpm in an incubator/shaker. At set

time points (10, 20, 40 min, 1, 2, 4, 6, 12, 24, 48, 72 and 80 h), an aliquot 300 µl of the dialysate was collected from each test tube and the same volume of fresh PBS (pH 7.4) was refilled. Absorbance of all the collected dialysates were measured at wavelength 242 nm using a UV-Vis spectrophotometer (Agilent Technologies, 89090A). The absorbance of free micelles, FMC and BMC, were subtracted out from the Dex loaded micelles (FMC-Dex and BMC-Dex) in order to measure absorbance of only Dex. The release experiment was carried out in triplicate.

3.2.6 *In vitro* targeting study of FMC, BMC and BFMC to Folate Binding Protein or neutravidin

To test targeting abilities of the micelles, Folate binding protein (FBP)-coated PFTE disks were prepared as described before.[41] Briefly, PFTE septum disks with diameter of 15 mm were rinsed with PBS solution and then dried in air. Then, a 10.0 µl of FBP in PBS (0.24 µg/ml) was dropped on the PFTE disk and allowed it for drying completely at room temperature. 10.0 µl of the prepared micelles (FMC-FITC, BMC-FITC and BFMC-FITC) were dropped on the top of the FBPs, and incubated for 30 minutes at room temperature. Fluorescent images were captured under a fluorescence microscope, and intensity was processed via ImageJ software. To investigate the role of folate on micelle targeting, FBPs were blocked with a 10.0 µl of folate solution (concentration 30 or 3 µg/ml) prior to the addition of the micelle's dispersions (FMC-FITC and BFMC-FITC).

Binding abilities of the micelles to neutravidin had been studies as well. Briefly, a neutravidin-coated 96 well Nunc plate (Thermo Fisher Scientific) was first washed 3X with a PBS solution containing 0.05% of Tween 20. Then a 200µl of FITC labelled FMC, BMC and BFMC in different concentrations were dropped on the top of the each well. After incubated for

30 minutes at room temperature, wells were washed triplicate with PBS media containing 0.05% of Tween 20 in order to remove the unbound micelles prior to fluorescent intensity measurement. Furthermore, a set of competition experiments were carried out to investigate the biotin's role. For that, prior to the addition of the micelles, the free biotin with different concentrations were incubated for 30 minutes. Fluorescent signals were recorded using a Tecan Infinite® 200 PRO microplate reader (Männedorf, Switzerland) with excitation at 470nm and emission at 520 nm, respectively.

3.2.7 *In vitro* pre-targeting study of the nanoplatform to activated macrophages

Mouse macrophage RAW264.7 cells (MΦs) were cultured in Dulbecco's modified Eagle's medium supplemented with 10% fetal calf serum (Invitrogen, Carlsbad, CA) and 100 U/ml penicillin as well as 100 μg/ml streptomycin at 37°C in a humidified 5% CO_2 incubator. MΦs were activated by culturing in the presence of lipopolysaccharide (LPS, from *Escherichia coli*, Sigma, St Louis MO) (1 μg/ml) overnight following a previous publication.[42] For the pre-targeting approach, the activated MΦs were first incubated with BFMC-NR (0.1 mg/ml) for 30 min, and then cultured after addition a 100.0 μg/ml neutravidin for 30 min, followed by incubation in the presence of BMC-FITC (0.1 mg/ml) for another 30 min. After each step, the MΦs were washed with PBS three times. For the "traditional" direct targeting method without applying neutravidin-biotin system was also performed under the same condition. Briefly, the same amount of activated MΦs were incubated with FMC-FITC (0.1 mg/ml) for traditional group for 30 min and washed on the same way. Additionally, four different control groups were prepared in the same concentrations; one control group for the "traditional" approach and three groups for the "sandwich" approach. Control 1) BFMC-FITC followed direct-targeting

approach; Control 2) skip the pre-targeting step; Control 3) skip the neutravidin as a bridge; Control 4) skip both the pre-targeting step and the neutravidin. Fluorescence imaging of the cells was recorded using a fluorescent microscopy. Additionally, suspended activated MΦs were also prepared for performing targeting study and quantifying the data using a Tecan Infinite® 200 PRO microplate reader (Männedorf, Switzerland). The suspended MΦs targeting study were performed with the same protocols above.

3.2.8 *Anti-inflammation of the* pre-targeting nanoplatform in vivo

The therapeutic efficacy of the pre-targeting nanoplatform to inflammation was evaluated using an implant-associated animal model as described in the previous publication.[42] All animal experiment protocols were approved by Animal Care and Use Committee of the University of Texas at Arlington. In brief, 100.0 µl of the PLGA micron dispersions (60mg/ml) and saline as control was subcutaneously injected in the dorsal of Balb/C mouse (25 g body weight) obtained from The Jackson Laboratory (Bar Harbor, ME). At step 1, after implantation for 24 hours, the pre-targeting agent- BFMC-DiD was intraperitoneally administrated into mice. At step 2 and 12 hours after step 1, neutravidin protein, served as an amplifying bridge, was administered intraperitoneally. Finally, at step 3 and 12 hours after step 2, Dex loaded-micelles were intravenously injected in animals. The effect of new "sandwich" nanosystem to target inflammatory site was monitored using Kodak In-Vivo Imaging System FX Pro (Carestream Health Inc., New Haven, CT, USA). At the end of the study, implants and surrounding tissues were isolated and frozen sectioned. The tissue sections were H&E and immunohistochemistry stained. The histology images were taken utilizing a Leica fluorescence microscope (Leica

Microsystem GmbH, Wetzlar, Germany) combined with a Retiga-EXi CCD camera (QImaging, Surrey, BC, Canada). Cell number was calibrated and quantified using ImageJ software.

3.2.9 Statistical analysis

All the data were evaluated using two-tailed student t-test and presented as mean ± standard deviation. Statistical analyses of all data were performed by a Student t-test. The results showed significant when a p value < 0.05 on a 2-tailed test. At least triplicate tests were conducted for statistical analysis.

3.3 Results

3.3.1 Preparation and characterization of the polymeric micelles

To prepare the polymeric micelles, we first synthesized F-PEG-PCL and B-PEG-PCL polymers using a carbodiimide coupling chemistry respectively. **Figure 3.1C** showed ^{1}H NMR spectra of NH_2-PEG2.2k-PCL7k polymer in DMSO-d_6. For biotin-conjugated polymer, B-PEG-PCL, biotin group was identified through two characteristic peaks of biotin group which can be identified through the methane protons (b_1 and b_2) at 4.2 and 4.3 ppm and the urea protons (a_1 and a_2) at 6.3 and 6.4 ppm (**Figure 3.1B**).[43] For folate-conjugated polymer, F-PEG-PCL, ^{1}H NMR measurement showed the characteristic resonances of folate at 4.28, 4.51, 6.68, 7.66 and 8.64 ppm (**Figure 3.1A**) and the expanded peaks indicate the successful conjugation of folate into the PEG-PCL polymer. The results support that biotin was successfully conjugated into PEG-PCL polymer. Meanwhile, the characteristic peaks of PEG blocks (methane group at 3.65

ppm) and PCL blocks (methane group at 2.25 ppm) can be observed for both F-PEG-PCL and B-PEG-PCL polymers.[37]

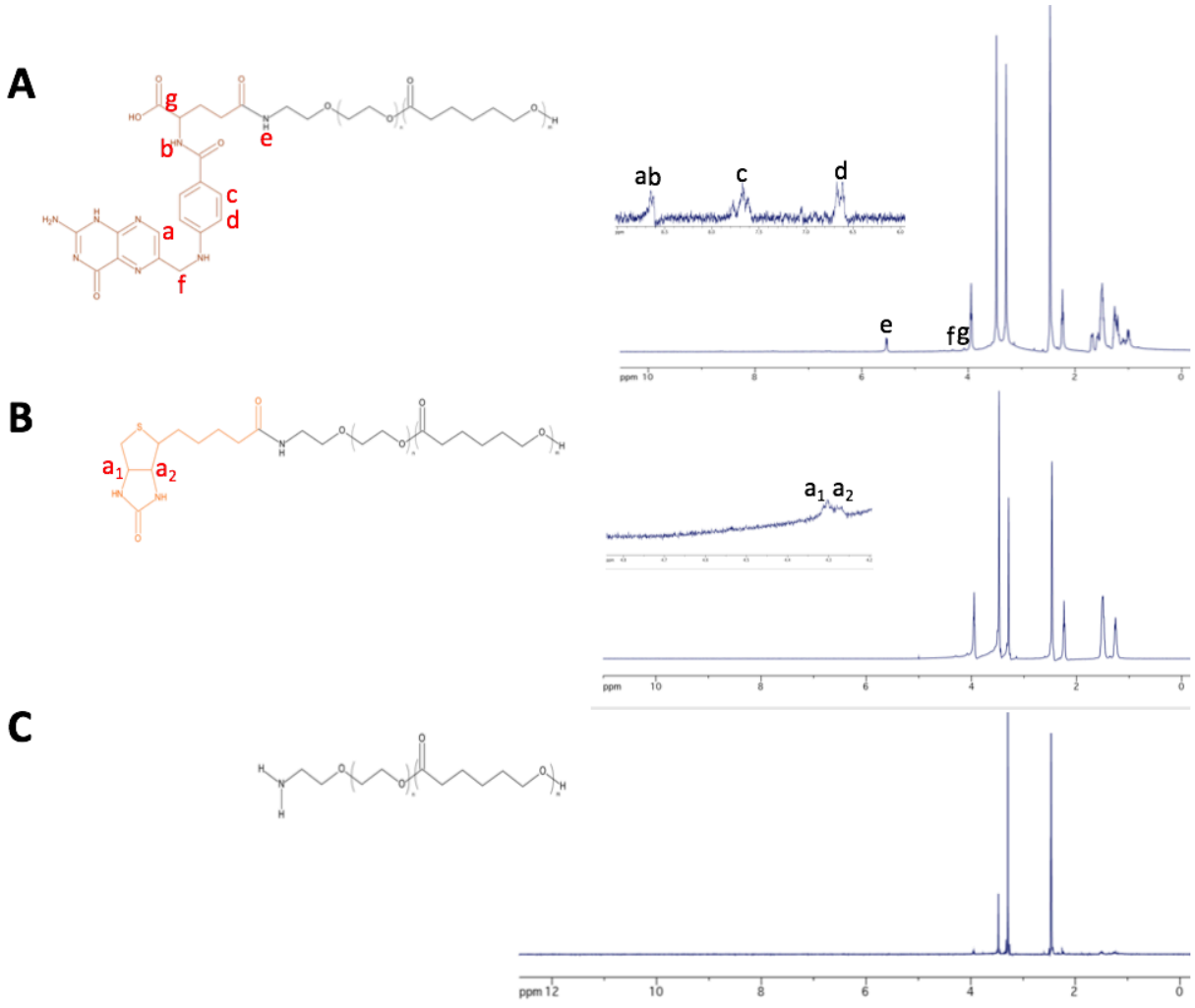

Figure 3.1 ^{1}H NMR spectra of **A)** F-PEG2.2k-PCL7k, **B)** B-PEG2.2k-PCL7k and **C)** NH_2-PEG2.2k-PCL7k in DMSO-d_6. The expanded peaks "a" to "g" indicate the successful synthesis of block co-polymers.

The conjugated polymers were then self-assembled into the micelles as diagnostic agent/drug carriers. To investigate their ability to target folate receptors, fluorophores loaded folate-conjugated (FMC), biotin-conjugated (BMC) as well as both folate- and biotin-conjugated (BFMC) micelles were prepared by the self-assembly method (**Figure 3.2A**). High-resolution transmission electron microscopy (HRTEM) images confirm homogeneous and round-shaped morphology of the micelles in spite of slight reduction of particle size due to dehydration during the process of sample preparation (**Figure 3.2A & B**). Further, dynamic light scattering (DLS) measurement showed that the average sizes of each micelle in diameters are 109.0, 153.8 and 156.1 nm for BMC-FITC, BFMC-FITC and FMC-FITC, respectively (**Figure 3.2C**), and the as-prepared micelles are relatively monodispersed (**Figure 3.2D**). These prepared micelles were employed for next binding studies.

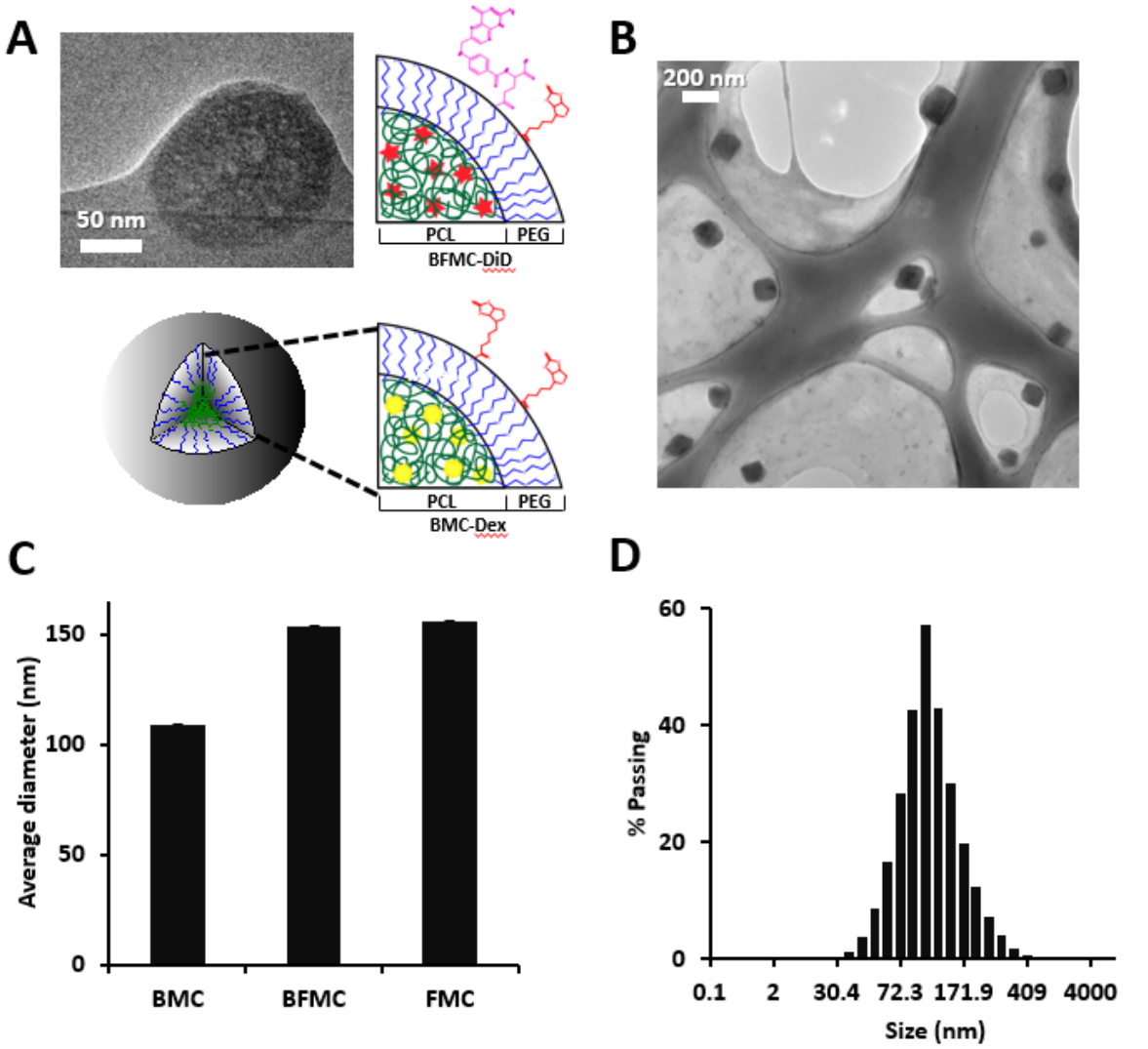

Figure 3.2 Fluorescence dye labelled polymeric micelles were characterized their physical properties. **A)** A Graphical presentation shows the structure of a fluorophore or a drug-loaded ligand conjugated polymeric micelle. **B)** High-resolution Transmission Electron Microscope images illustrates that BFMC-FITC micelle forms a spherical shape. **C)** Dynamic Light Scattering (DLS) measurement determines the particle sizes of BMC-FITC (labeled as BMC), BFMC-FITC (BFMC), and FMC-FITC (FMC) micelles at room temperature and **D)** polydispersity of the BMC-FITC.

3.3.2 *In vitro* binding study of the prepared micelles to folate binding protein

The binding affinity of these micelles to folate binding protein (FBP) was determined after 30 minutes incubation at room temperature. When using FITC loaded FMC and BFMC, bright green color was observed on FBP-coated disks, indicating the strong interaction of those two micelles with FBP (**Figure 3.3A**). However, when using BMC-FITC, we find no detectable fluorescent signal. These results suggest that biotin-conjugated micelles have little or no affinity to FBP-coated disks. Quantification analysis showed that compared to BMC, there were approximate 8- and 6-fold fluorescent intensities for FMC and BFMC, respectively. In addition, one could observe that incorporation of biotin group into BFMC only had slight interference to binding ability to FBP (~ 27% reduction compared to FMC). To further confirm the role of folate ligands on the interaction of the micelles with FBP, a set of competition experiments was conducted in which the FBP-coated films were incubated with the free folate prior to addition of the micelles. The results indicated that, as the amount of free folate increased, the intensity of the fluorescent signal decreased (**Figure 3.3B**). These results support that the binding of the micelles to FMC is folate specific and folate concentration dependent.

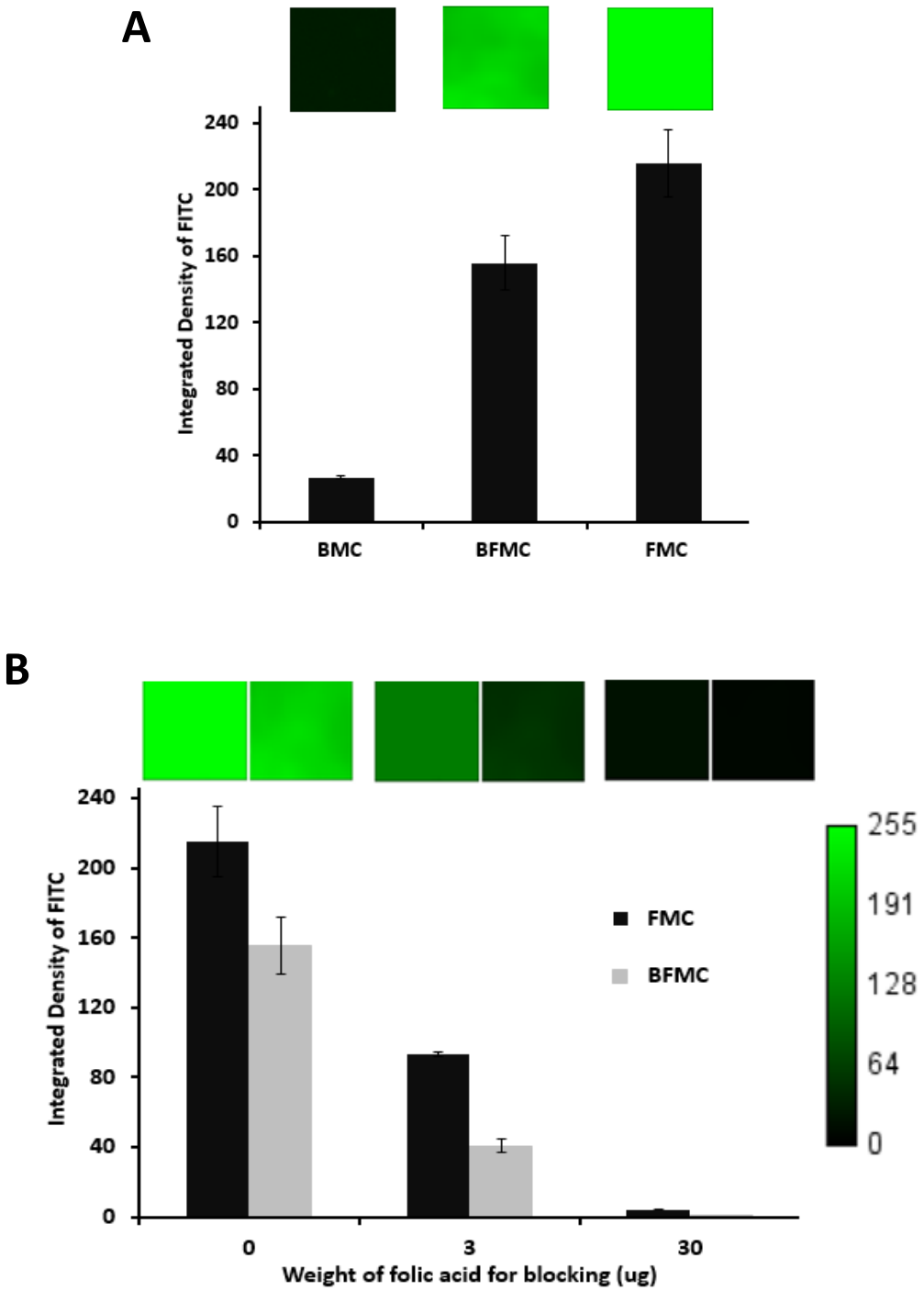

Figure 3.3 *In vitro* binding affinity of micelles to folate binding protein was determined. **A)** Folate conjugated micelles (FMC) and biotin-conjugated folate conjugated micelles (BFMC) bind 8- and 6- fold more to folate binding protein (FBP) than biotinylated micelle (BMC), respectively. **B)** Blocking study was performed with free folate in different concentrations.

3.3.3 *In vitro* binding study of the prepared micelles to neutravidin

Using neutravidin-coated well plates, we investigated the ability of the biotinylated micelle to interact with neutravidin by reading of fluorescence intensities with a microplate reader.[44] As shown in **Figure 3.4A**, there were strong fluorescent signals from wells treated with BMC and BFMC while there was very weak signal associated with FMC-treated wells. Compared to FMC treatment, there were approximate 9-fold and 3-fold increases in fluorescent intensity for BMC and BFMC treatment, respectively. These results support a strong interaction of biotin presenting in micelles with neutravidin. To validate the binding specificity between biotinylated micelles and neutravidin plate, a competition experiments was conducted in which different concentrations of free biotin were added into the culture media (**Figure 3.4B**). It showed that, as the amount of free biotin increased, fluorescent intensities decreased gradually. These results support the indispensable role of the biotin in binding of the micelles to neutravidin.

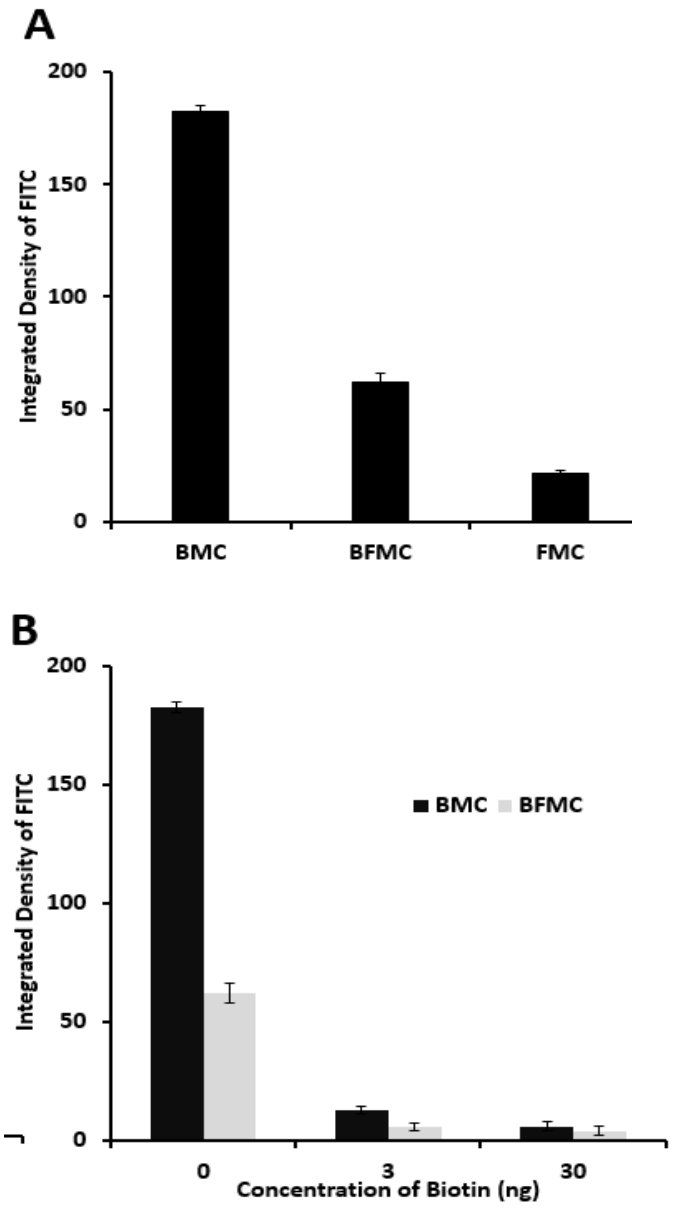

Figure 3.4 *In vitro* study was carried out to determine the binding affinity of micelles to neutravidin. **A)** *In vitro* binding study between ligand conjugated micelles and neutravidin concludes that biotin conjugated micelle (BMC) and biotin-conjugated folate conjugated micelles (BFMC) binds 9- and 3- fold more to neutravidin than folate-conjugated micelle (FMC), respectively. **B)** Study shows that free biotin reduces micelle accumulation on neutravidin coated surface in a dose dependent fashion.

3.3.4 *In vitro* pretargeting study of the new pretargeting nanoplatform to macrophages *in vitro*

To further evaluate effect of the nanoplatform for the enhanced macrophages (MΦs) targeting, two different fluorophores-loaded micelles were used; the first fluorophore is Nile Red (BFMC-NR) for the pre-targeting step and another is FITC (BMC-FITC) for following the amplifying step. In **Figure 3.5A & B**, the sandwich approach significantly increases the accumulation of BMC on activated MΦs (strong FITC signal). On the other hand, one can observe that without step 1 BFMC-NR (control 1) or without step 2 neutravidin and step 3 BFMC-NR (control 3) treatment, accumulation of BMC on the activated MΦs significantly reduce (very weak FITC signal). Meanwhile, without step 2 -neutravidin treatment (control 2), the strong signal (in red color) can be found with control 2 treatment, indicating that BFMC is able to binding to the activated MΦs via interactions between folate of BFMC and folate receptor on MΦs, however, lack of neutravidin treatment prevents BMC from accumulating on macrophages. These results confirmed that the effective biorecognition between folate and its receptor on activated MΦs, as well as the biotin and neutravidin interaction, played an important role on achievement and enhancement of the fluorescent signals.

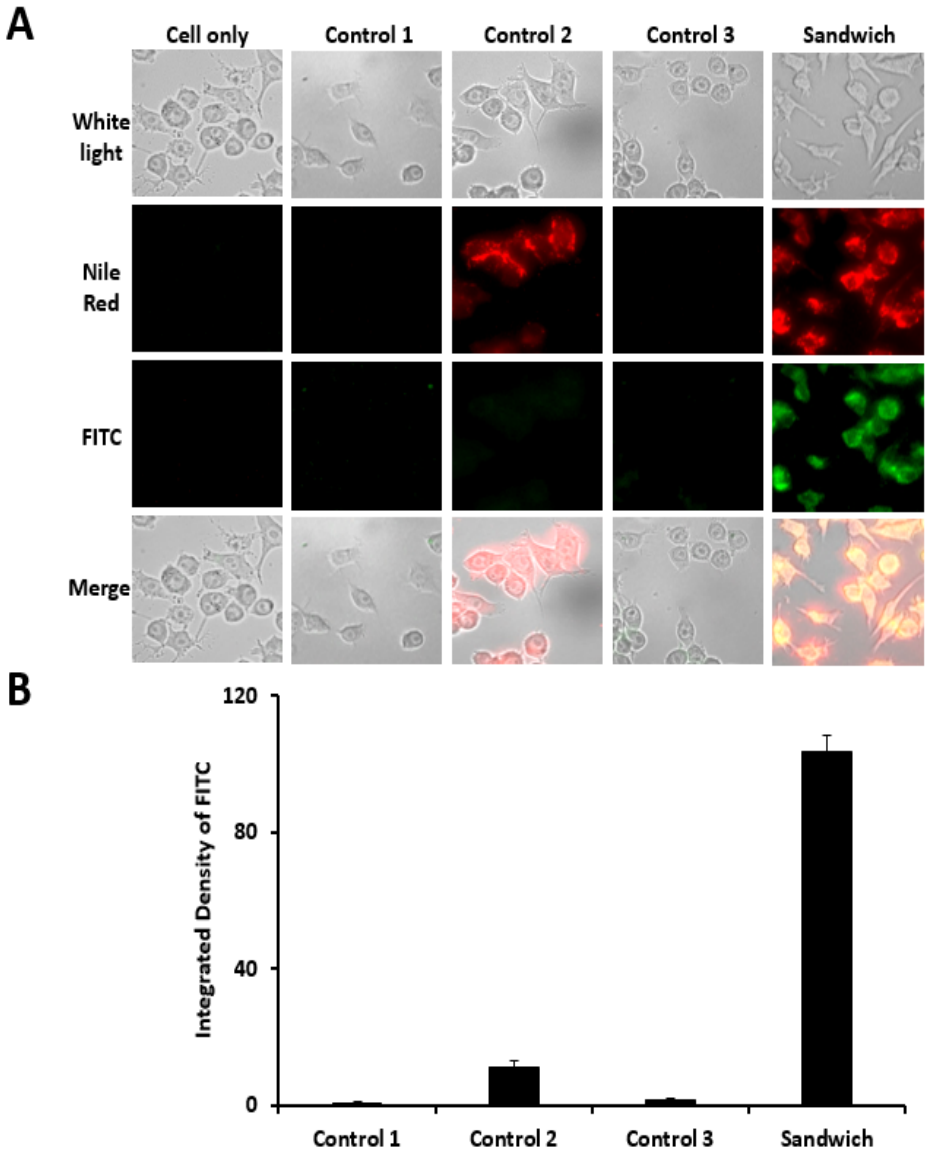

Figure 3.5 *In vitro* macrophages targeting study with the pre-targeting (Sandwich) strategy and three control groups was performed. respectively. **A)** Activated macrophages were cultured, treated with four different groups and then fluorescent imaging was captured under a fluorescent microscope. For the Sandwich approach, the macrophages were treated sequentially with BFMC-NR (step 1), neutravidin (step 2) and BMC-FITC (step 3). Control 1: neutravidin+BMC-FITC (no step 1); Control 2: BFMC-NR + BMC-FITC (no step 2) and Control 3: BMC-FITC (no step 1 and 2). **B)** The quantitative data from **(A)** was calculated based on the microscope images using ImageJ software.

The amplifying signal of the pre-targeting nanoplatform was then compared with the direct targeting method (**Figure 3.6A & B**). Fluorescent signals can be observed in both FITC-loaded BFMC and FITC-loaded FMC (the direct targeting method) although the slightly weak signal for FITC-loaded BFMC treatment is slightly weaker than the one for FITC-loaded FMC treatment. However, once macrophages treated with the pre-targeting strategy, fluorescent signal was obviously amplified. Quantitative analysis also showed an approximate 17-fold and 3.5-fold increase in fluorescent intensity compared to FITC-loaded BFMC and FITC-loaded FMC, respectively. This *in vitro* MΦs targeting studies had confirmed that the new "sandwich" nanoplatform allowed more micelles to accumulate on the activated MΦs than the direct targeting approach via folate/folate receptor and biotin/neutravidin interactions, therefore, the strategy may be used to improve the efficiency of drug delivery.

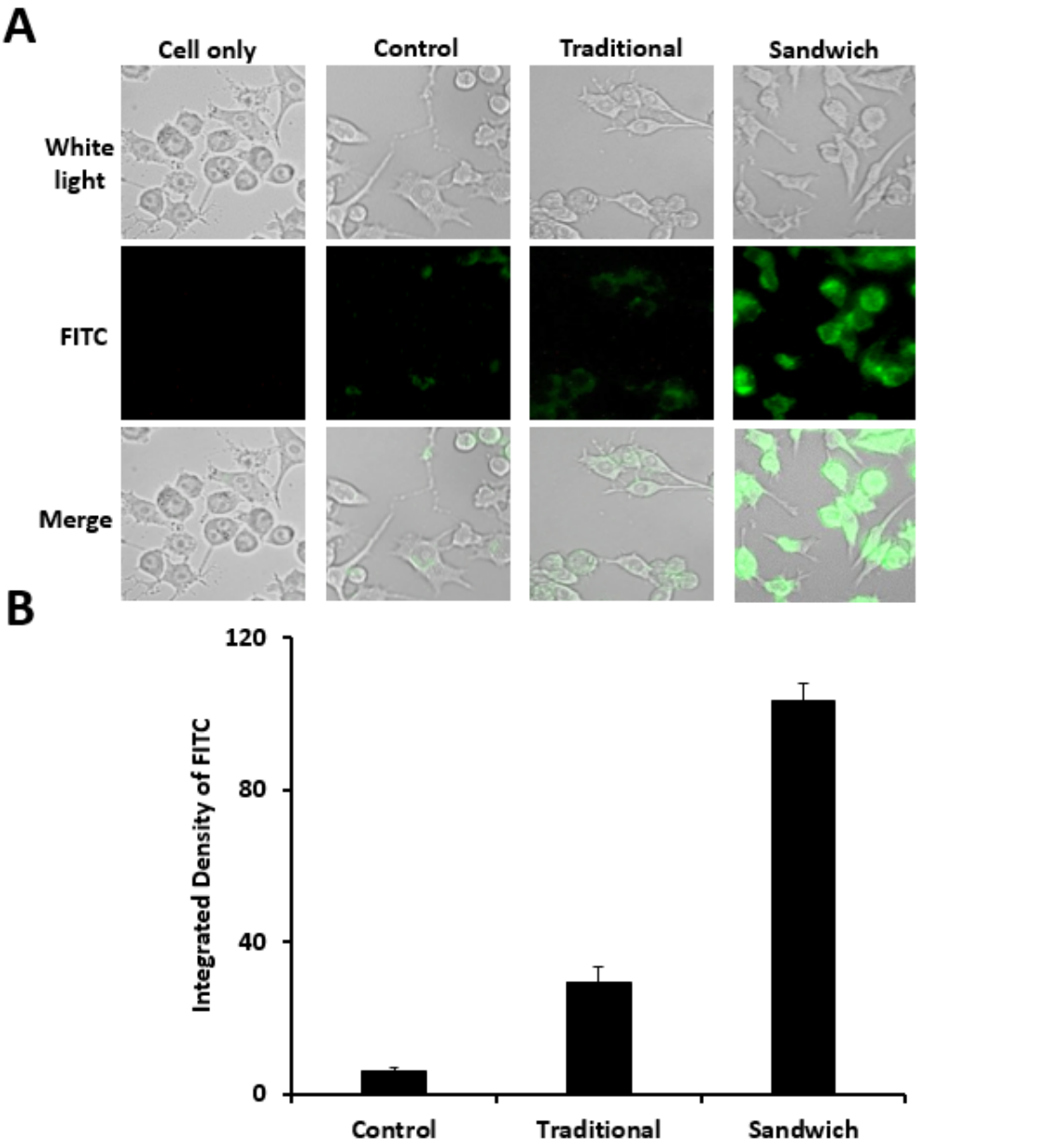

Figure 3.6 *In vitro* activated macrophages targeting study with both the direct targeting (Traditional) and the pre-targeting (Sandwich) strategies. Here three series of macrophage-targeting experiments were carried out. FITC-loaded BFMC, FITC-loaded FMC (direct targeting) and FMC+ neutravidin + FITC-loaded BMC (pre-targeting strategy). **A)** Fluorescent microscope imaging for macrophages treated by the above three groups. **B)** The quantitative data was calculated based on the microscope images using ImageJ software.

3.3.5 Dexamethasone release from micelles *in vitro*

Before loading dexamethasone (Dex) into the micelles, cytotoxicity of the micelles to the cell was performed using 3T3 fibroblast and Alamar Blue assay. The results (**Figure 3.7A**) showed that these micelles prompted minimal cytotoxicity in the tested concentration range. Next, Dex was loaded into BMC and FMC micelles. *In vitro* release showed that free Dex was released really fast with up to 90 % release over the first 3 hours (**Figure 3.7B**). On the other hand, only approximately 55 and 57 % of Dex were released from BMC and FMC micelles in 3 hours, respectively. Our results are similar to those of the previous study, suggesting that the Dex loaded micelles can slow down the release of Dex at a physiological environment.

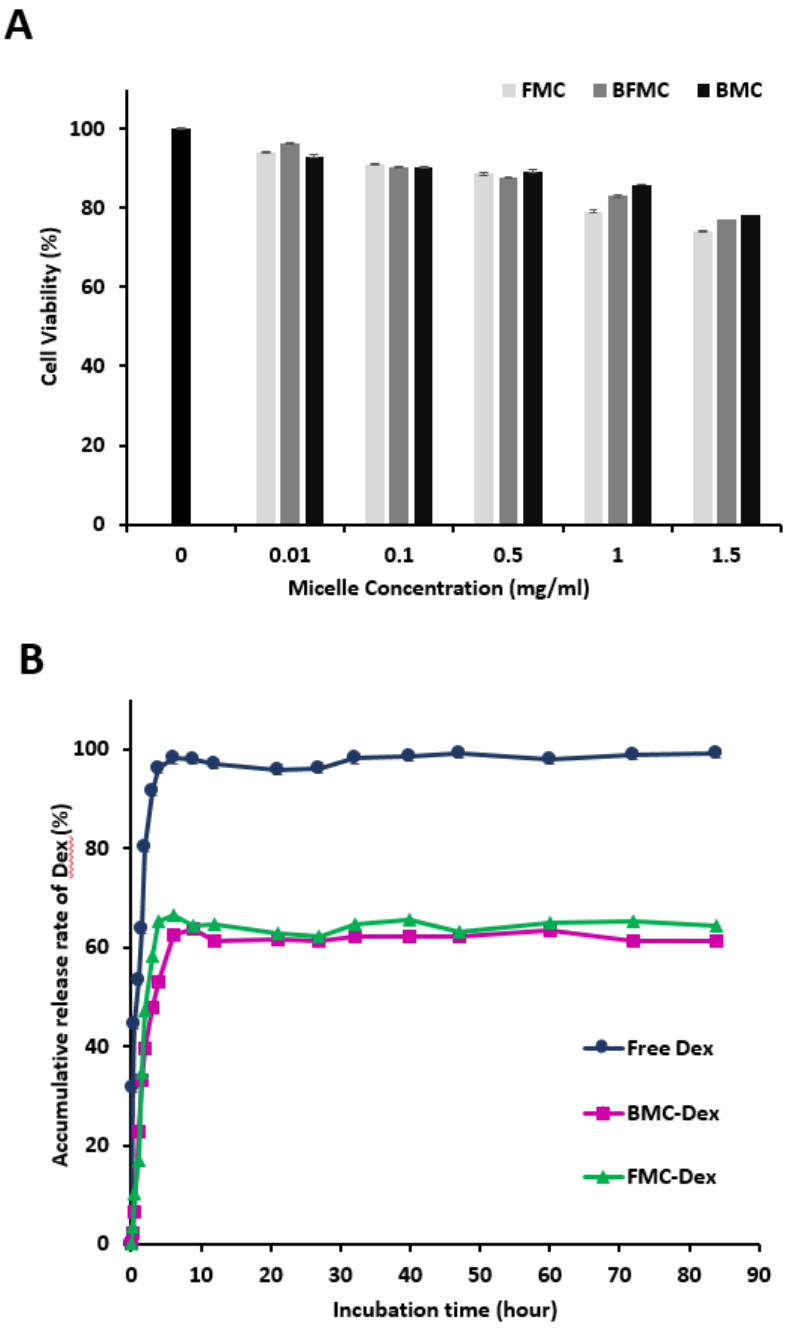

Figure 3.7 Cell toxicity and drug release properties of variously prepared micelles. **A)** Cytotoxicity of the micelles in different concentrations (0.01, 0.1, 0.5, 1, and 1.5 mg/ml) to cells (3T3 fibroblast cell). Test samples include BMC-FITC (labeled as BMC), BFMC-FITC (BFMC), and FMC-FITC (FMC) micelles. **B)** *In vitro* release profiles of Dex-loaded the micelles.

3.3.6. Evaluate efficacy of the pre-targeting nanoplatform on treating inflammation *in vivo*.

Finally, the efficiency of the pre-targeting nanoplatform to reduce inflammatory responses was assessed using mice subcutaneous inflammatory response model. For that, subcutaneous and localized inflammatory responses were induced by the implantation of poly-l-lactic acid particles. After implantation for 24 hours which is the optimal time to trigger the accumulation of inflammatory cells at the implantation site, animals were treated with or without Dex-loaded micelles via either traditional or sandwich approach by following the time line as depicted in **Figure 3.8A**. By analyzing the fluorescent intensities at the implant site, we find that, as anticipated, pre-targeting approach delivered the highest number of Dex-loaded micelles to the inflamed tissue site (**Figure 3.8B**). It is estimated that the amounts of Dex-loaded micelles delivered by the pre-targeting approach are 8 Folds of those by the traditional approach (**Figure3.8C**). The enhanced delivery of Dex-loaded micelles was confirmed by histological analyses. Finally, histology analyses on the extent of inflammatory responses at the implant sites also revealed that the pre-targeting approach has led to signification reduction of CD11b+ inflammatory cells. The overall results support that the pre-targeting approach significantly improved targeted drug delivery and thus amplified the anti-inflammatory efficacy of Dex-loaded micelles.

A

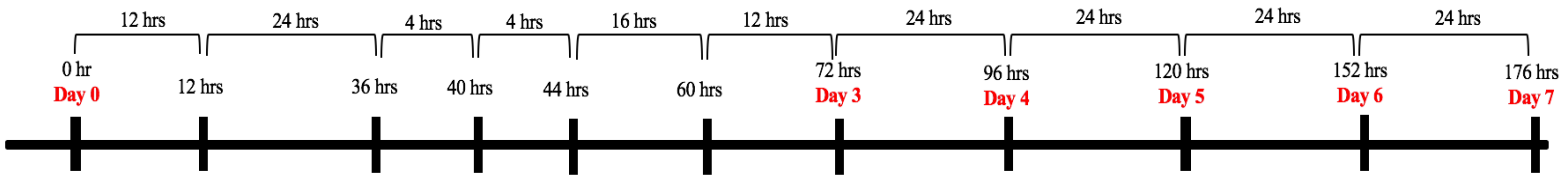

Saline	10% PLGA s.c. implantation	Blocking Avidin	saline	saline	Image 1 saline/DiD	Image 2	Image 3	Image 4	Image 5	Image 6	Image 7
Free Dex	10% PLGA s.c. implantation	Blocking Avidin	saline	saline	Image 1 Free Dex/DiD	Image 2	Image 3	Image 4	Image 5	Image 6	Image 7
Traditional Approach	10% PLGA s.c. implantation	Blocking Avidin	saline	saline	Image 1 FMC/Dex FMC/DiD	Image 2	Image 3	Image 4	Image 5	Image 6	Image 7
Sandwich Approach	10% PLGA s.c. implantation	Blocking Avidin	BFMC	Neutravidin	Image 1 BMC/Dex BMC/DiD	Image 2	Image 3	Image 4	Image 5	Image 6	Image 7

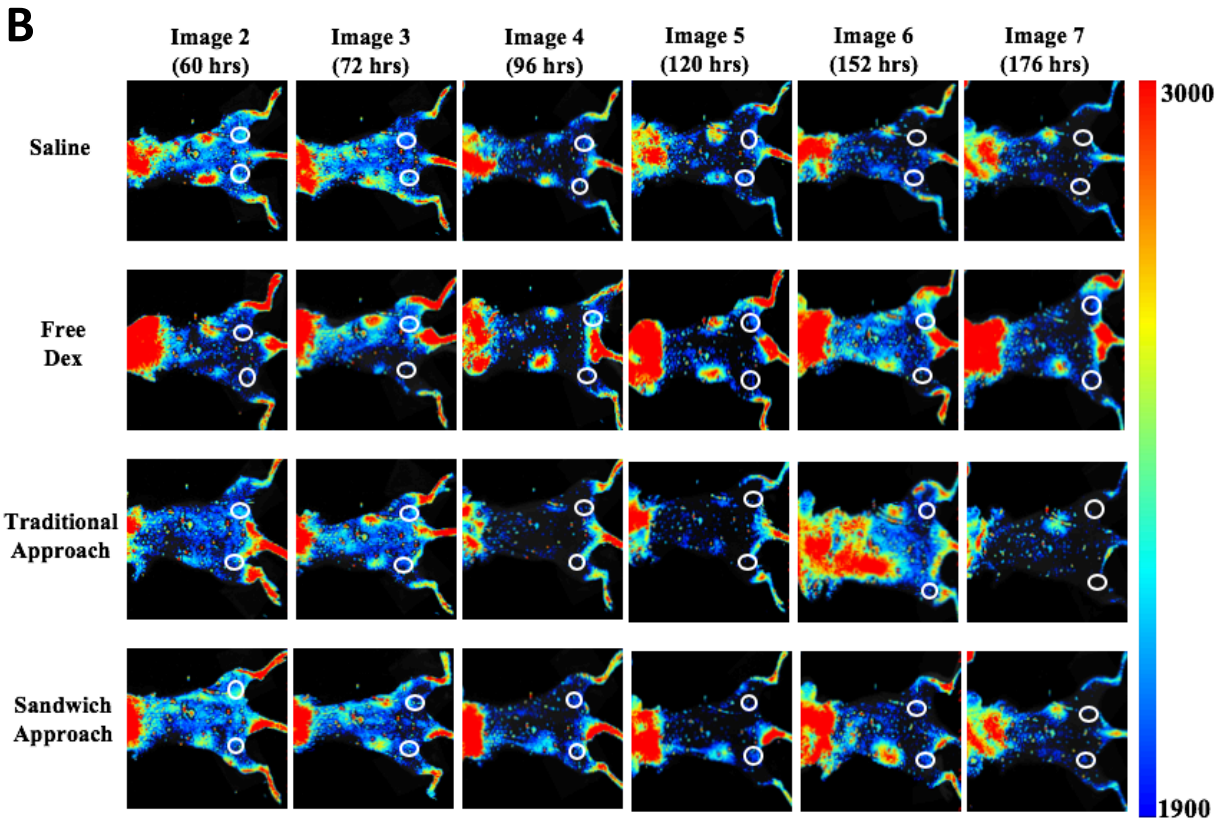
B
Image 2 (60 hrs)
Image 3 (72 hrs)
Image 4 (96 hrs)
Image 5 (120 hrs)
Image 6 (152 hrs)
Image 7 (176 hrs)
Saline
Free Dex
Traditional Approach
Sandwich Approach
3000
1900

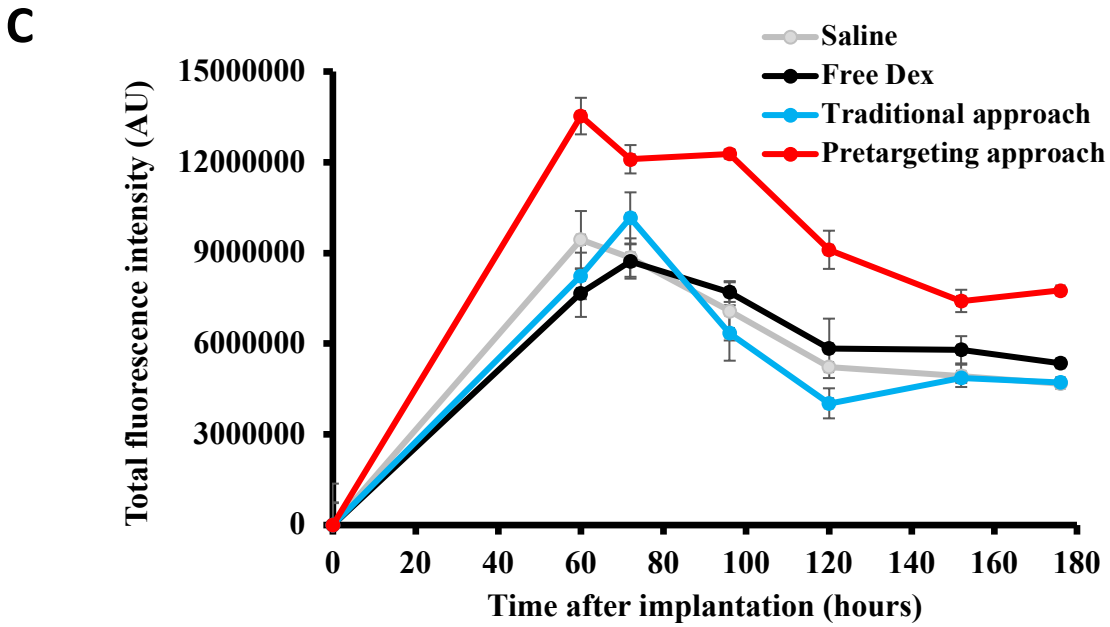
C
Saline
Free Dex
Traditional approach
Pretargeting approach
Total fluorescence intensity (AU)
15000000
12000000
9000000
6000000
3000000
0
0
20
40
60
80
100
120
140
160
180
Time after implantation (hours)

Figure 3.8 Animal study was carried out to evaluate the anti-inflammatory potential of the nanoplatform. Here we show **A)** a designed timeline for pre-targeting study *in vivo,* **B)** fluorescence images of variously treated animals at different time points (62 hours to 176 hours), and **C)** quantitative analyses of the fluorescence intensities at the inflamed tissue sites. The results support that pre-targeting strategy has amplified the delivery of Dex-loaded particles to the sites of inflammatory responses.

3.4 Discussion and Conclusions

Although avidin/biotin system has been widely investigated as a pretargeting platforms for tumor theragnosis,[44,45] little effort has been made to explore the potential of using the same strategy to treat inflammatory diseases. To find the answer, a novel pretargeting nanoplatform via neutravidin/biotin system was designed to target the activated macrophages recruited to the inflammatory site for theranostic purposes. Neutravidin is used here because the absence of the carbohydrate moieties makes it slightly acidic (pI: ~6.3), enabling prevention of its nonspecific binding to cell surfaces and proteins. The temporarily separated three-steps strategy were designed with two different surface-engineered micelles and a bridging molecule. Briefly, Step 1: Folate conjugated and biotinylated polymeric micelles are designed to target folate receptor which are highly expressed on activated MΦs. Step 2: Neutravidin protein binds to surface bio, which possess 4 avidin binding sites, is employed as the bridging molecules which provide for amplifying accumulation of drug-loaded cargos. Step 3: Biotinylated micelles, which caged an anti-inflammatory drug, Dex, were enhanced accumulated at the inflammatory sites by attaching to neutravidin protein.

To test the hypothesis, PEG-PCL polymers were employed to prepare micelles due to its controlled biodegradability and high biocompatibility[73]. Folate- or biotin-conjugated polymers (F-PEG-PCL or B-PEG-PCL) were successfully synthesized. Polymers are an attractive material for drug delivery because they are extraordinarily malleable and moldable for particles' sizes and shapes. Moreover, it can amplify encapsulation of outputs such as drugs,[46] as well as they are biocompatible and biodegradable into carbon dioxide and water. Based on diverse modality of polymers, polymeric nanoparticles as nanomedicines had been broadly used not only for increasing drugs loading efficiency and tuning the releasing rate but also for prolonged circulation half-life of nanoplatform in circulation system.[26,47]

We find that the folate-targeting neutravidin/biotin nanoplatform is an anti-inflammatory drug delivery system for treating activated macrophages and inflammatory responses. It is well documented that the activated macrophage is a biomarker of inflammation, and folate receptors are upregulated on surfaces of these activated macrophages.[33,48,49] Activated macrophages (up-regulating folate receptor) pretargeting experiments show that compared to the traditional direct targeting method, our drug delivery system can significantly improve the micelles homing to the activated macrophages. Since occurrence of inflammatory lesion triggers macrophage infiltration and activation, the activated macrophages can be used as a target for delivery of imaging reporter/drug. The folate ligand on the pretargeting micelles can be replaced with various cell or tissue-specific ligands such as amino-terminal peptide encompassing amino acids 2–26 (Ac2-26) so that the micelles can target Collagen IV which is a major component of the vascular membrane that is exposed at sites of vascular injury and inflammation.[50,51]

In short, neutravidin/biotin integrated pretargeting nanoplatform were successfully prepared. Both *in vitro* and *ex vivo* testing confirmed that the theranostic nanoplatform can

effectively detect inflamed tissue via fluorescent imaging first, and then amplify the delivery of anti-inflammatory drug, dexamethasone, at an inflammatory site. To further improve the drug delivery efficiency, BMC micelles may be prepared with larger molecular weight of polymer such as PCL. Additionally, micelles can be replaced by nanoparticles to improve their *in vivo* stability. Finally, the "sandwich" pretargeting nanoplatform may be further developed so that it becomes spatiotemporal control platform for intractable diseases with right moment, right place and right dose for personalized inflammatory diseases treatment.

CHAPTER 4

Tetrazine and Trans-cyclooctene Application for Development of Cell Therapy of Atherosclerosis

4.1 Introduction

Atherosclerosis begins with damages to the endothelium because of high blood pressure or high cholesterol level and eventually leads a cause of death. Initial damages on arterial wall, because of inflamed or activated endothelial cells (aECs) and promote platelet adhesion, can lead to thrombosis in late stage which underlies coronary artery disease.[74] The platelet-EC adhesion is caused by the binding of a protein, platelet glycoprotein 1b (GP1b), to von Willebrand Factors (vWF) expressed on the surface of inflamed EC membrane or subendothelium.[17] Cardiovascular interventions, such as angioplasty, are often developed in order to open the blocked blood vessels. However, those may even damage more the walls and cause thrombosis, inflammation, and re-narrowing of an artery again.[18] Unfortunately, there is no optimal treatment option for such conditions.

Nanomedicine for treatment of different cardiovascular diseases have been developed in recent years.[19] Active delivery nanosystems to the injured arterial sites via targeting agents has

been shown to develop therapeutic efficacy for cardiovascular diseases.[20–22] However, recent analysis of delivery nanosystem shows that less than 1% of injected nanosystem can actually target to the arterial sites.[75] Thus, there is an urgent demand in the atherosclerosis theragnosis.

To overcome the previous limitations, bioorthogonal click chemistry (especially tetrazine (Tz)/trans-cyclooctene (TCO)) was recently introduced to improve cell adhesion to cell/tissue.[75,76] The covalent bonds between them are very stable and fast. Several previous studies showed that cell surface modified with Tz/TCO click chemistry did not affect cell viability and allowed cell to stably attach in a microfluidic flow channel at a shear stress of 20 dyn/cm^2.[75,76] These results suggest that via *ex vivo* expansion and then engineering surface of endothelial cells (ECs) with TCO, coverage and retention of ECs in the damaged site may be significantly improved. The TCO-modified ECs can be characterized and optimized to maximize their migration, proliferation, differentiation and coverage as well as retention's abilities.

In this study, I developed an optimized novel multifunctional engineered nanoparticles (NPs) which specifically cover onto the injured arterial wall to serve as a temporary barrier that prevents platelet adhesion in order to achieve maximal cell functionalities, including cell recruitment and endothelial proliferation. Poly(L-lactic-co-glycolic acid) (PLGA), a FDA-approved biodegradable polymer was used to fabricate these NPs. The multi-ligand PLGA NPs showed a significantly greater targeting rate on to von Willebrand Factor, than the unmodified NPs, and recruited endothelial cells *in vitro* under both static and flow conditions. In addition, *ex vivo* engineered ECs by modifying EPC's surface with TCO to improve accumulation and retention rate of EPCs in the damaged vessel wall while keeping their abilities to viability, migration and proliferation as well as differentiation into endothelialization. This high impact

nanotechnology is expected further significant improvements in the treatment of cardiovascular diseases *in vivo*, especially the management of coronary artery diseases.

4.2 Experimental section

4.2.1 Materials

Dichloromethane (DCM) and Poly (lactic-co-glycolic acid) (PLGA, L/G 50:50, Mw: 25,000-35,000 Da) were obtained from EMD (Millipore Corporation) and Akina Inc (West Lafayette, IN), respectively. Polyvinyl alcohol (PVA, Mw: 13,000 Da, 85-89% hydrolyzed), coumarin 6, 1-Ethyl-3-(3-dimethylaminopropyl)carbodiimide (EDC), N-Hydroxysuccinimide (NHS), 2-(N-morpholino)ethanesulfonic acid (MES), Dulbecco's Phosphate-Buffered Saline (DPBS), and dimethyl sulfoxide (DMSO) were purchased from Sigma (St. Louis, MO). Tz-PEG_4-NHS, TCO-PEG_4-NHS, Tz-Cy5 and Tz-Cy3 were obtained from Click Chemistry Tools (Scottsdale, AZ). Human GP1b alpha protein and von Willebrand factor (vWF) were obtained from Sino Biological (Wayne, PA). CellTracker™ Red CMTPX were purchased from ThermoFisher Scientific (Waltham, MA). Lipophilic tracers-DiD was obtained from Molecular Probes (Eugene, OR). All chemicals were used without further purification. Milli-Q grade deionized water was used through all experiments.

4.2.2 Methods

4.2.2.1 Fabrication of coumarin 6-loaded PLGA nanoparticles (C6NPs)

Coumarin 6-loaded PLGA nanoparticles (C6NPs) were fabricated following the previous study.[77,78] Briefly, PLGA (100 mg) and coumarin 6 (0.5 mg) were dissolved in 3 mL of chloroform to form the organic (oil) phase. This solution was then added dropwise to 20 mL of poly vinyl alcohol (PVA) 5% (w/v) solution (water phase) and sonicated at 40 W for 10 mins on ice. The particle suspension was then stirred overnight at room temperature to ensure complete organic solvent evaporation. C6NPs were recovered by centrifugation at 15,000 rpm for 30 mins at 25ºC. All NPs were lyophilized and stored in powder form at -20ºC for further use.

4.2.2.2 Conjugation and characterizations of Tz-GP1b-conjugated C6NPs (Tz-GP1b-C6NPs)

A 1.0 mg of the C6NPs was activated with a 12.0 mg of EDC and a 18.0 mg of NHS in a 5.0 ml of MES buffer (0.1 M, pH 4.75) by gentle shaking at room temperature for 2 hours. The activated C6NPs were then centrifuged at 5000 rpm for 5 minutes. The collected pellets were washed with fresh PBS buffer and then resuspended well in PBS (pH 7.4). Meanwhile, Tz-conjugated GPIb (Tz-GP1b) was prepared. Briefly, a 50.0 μg of GP1bα powder was completely dissolved in PBS (1.0 mg/ml) in a small Eppendorf tubes, and then Tz-PEG_4-NHS (100 times excess at molar ratio) in a 2.0 μl DMSO was added. The mixture was shaken gently at room temperature for 1 hour. Tz--GP1b was purified by using a sterilized centrifuging column (MWCO 300,000) at 5000 rpm for 5 min. The conjugation degree of Tz was determined by TCO-Cy5. Finally, the activated C6NPs were added into Tz-GPIb PBS media (2.0 mg/ml). The mixture was incubated at 4.0 ºC for overnight. The degree of Tz-GPIb conjugated into C6NPs was evaluated via absorbance of GPIb protein using an UV/Vis spectrophotometer. Tz-GP1b-C6NPs were collected by the centrifuge. GPIb-C6NPs were also prepared as control group.

The hydrodynamic diameter of the particles were measured by Dynamic Light Scattering (DLS). NPs' hydrodynamic diameters were reported as the mean of the diameter distribution. High-resolution transmission electron microscopy (HRTEM) images was used to confirm homogeneous and round-shaped morphology of the samples. Each solution was placed on a CF400-CU TEM grid (Electron Microscopy Sciences, Hatfield, PA) and imaged with a Tecnai T12 HRTEM microscope (FEI, Hillsboro, OR). *In vitro* cell cytotoxicity test for the Tz-GPIb-C6NPs was performed as described before. In brief, EC cells were prepared onto a 96-well plate at the seeding cell density of 0.01×10^6 cells/well and the cells were treated with different concentrations of Tz-GPIbA-NPs for 24 hours; 0.0, 0.1, 0.5, 1.0, 1.5 and 2.0 mg/ml. The treated cells were then tested for cell viability by incubating them with Alamar blue (10.0 µl in each well) and incubated for 4 hours at 37°C in a cell culture incubator without exposure to direct light. The absorbance was measured at 570 nm, using 600 nm as a reference wavelength (normalized to the 600 nm value) and Fluorescence at 550 nm (emission wavelength 600 nm) and 560 nm (emission wavelength 610 nm). The study was performed in triplicates.

4.2.2.3 Modification and characterizations of TCO-labeled HUVEC cells

4.2.2.3.A Modification of HUVEC cells membrane

To improve the homing ability of HUVEC cells on to Tz-GP1bα NPs bound vWF surface, membrane of the cells were modified with TCO-PEG_4-NHS. Briefly, TCO-PEG_4-NHS with different concentrations (0.0, 1.0, 5.0, 10.0 and 25.0 µM) were treated with 50,000 cells suspended in 1 mL of DPBS for 30min at room temperature. The amount of TCO labeled on the membrane of each HUVEC cell was measured by further treatment with 40µM of Tz-Cy3 for 30

min. After the treatment, TCO-labeled cells were washed with fresh media and fluorescence intensities of Cy3 were measured using a UV/vis spectrophotometer (Infinite M200 plate reader, Tecan, Durham, NC). Further TCO labeled ECs co-stained with Tz-Cy3 and NucBlue (Thermofisher Scientific, Waltham, MA) and imaged using Leica Fluorescent microscope under 20X magnification.

4.2.2.3.B Stability of TCO labeling on HUVEC cells

In order to check the TCO availability on HUVEC cell membrane, TCO stability was measured against time.[79] HUVECs were seeded onto a 96-well plate at the cell density of 1×10^4 cells/well and cultured for one day. After one day, a 150.0 µl of cultured media were replaced with 10.0 µM of TCO-PEG_4-NHS media and incubated at 37 ºC for 30 min. Non-labeled TCO was washed with a 150.0 µl of fresh media twice. After that, the fresh media in wells designated as "Day 0" were replaced with a 10.0 µM of a Tz-fluorophore (Tz-Cy5) containing culture media. The fluorescence intensity was measured after 30 min incubation using a microplate fluorescence reader. The other wells were performed the same way at different time points (day 2, 4, and 6.) Additionally, cells were prepared for qualitative optical imaging in order to confirm the remained available TCO on the cell surface after 2 days. A 10.0 µM of Tz-Cy5 was treated at day 0 for all the wells and another a 10.0 µM of Tz-Cy3 was followed at day 2.

4.2.2.3.C HUVEC cells functional studies

The viability of HUVECs post TCO modification was evaluated based on the cell metabolic activity. In brief, HUVECs tagged with various concentrations of TCO (1, 2, 5,

10,25uM) were seeded into 96 well plate at density of 2.5 X 10^4 cells/cm^2 and cultured for 24 hours. The metabolic status of the cells was determined using MTS assay following manufacturer's instructions (CellTiter 96® AQueous One Solution Cell Proliferation Assay, Promega, Madison, WI) and compared with unmodified HUVECs.

Further, the functional performance of TCO tagged HUVECs was evaluated in terms of NO production and LDL uptake. HUVECs were prepared in 96 well plate for these studies as formerly described. Following the 24 hour culture of ECs post tagging, intercellular NO production by cells were determined using Intracellular Nitric Oxide Fluorometric Assay kit (Cell Biolabs, Inc., San Diego, CA). In brief, NO fluorometric probe (provided with the kit) was incubated with HUVECs at 37ºC for 2 hours. As the NO fluorometric probe enters the cells, it would be deacetylated by intracellular esterases to a non-fluorescent intermediate which is rapidly oxidized by nitric oxide into a fluorescent triazolo-fluorescein analog. After 2 hrs of incubation, cells were lysed using 1X cell lysis buffer (provided with the kit) for 30min and fluorescence for NO production was measured at a wavelength of 480nm (excitation)/530nm (emission) using UV/vis spectrophotometer (Infinite M200 plate reader, Tecan, Durham, NC). Protein content present in cell lysate for each treatment group was also determined using standard BCA assay (ThermoFisher, Waltham, MA). Cells grown on TCPS without any treatment and those treated with NOS (nitric oxide synthase) inhibitor L-NNA (N5-[imino(nitroamino)methyl]-L-ornithine) at 50 µM served as a positive and negative control respectively. To evaluate the cells ability to uptake LDL, TCO tagged HUVECs were incubated with Dil-Ac-LDL (ThermoFisher, Waltham, MA) at the concentration of 10µg/ml for 6 hours at 37ºC. Fluorescence imaging of Dil-Ac-LDL internalized within HUVECs was captured using Leica fluorescence microscope and quantified using ImageJ software.

4.2.2.4 Click chemistry confirmation between Tz-NPs and TCO-HUVECs

HUVEC cells were seeded onto a 24-well plate at the cell density of 0.05×10^6 cells/well in a 1.0 ml of cultured media. In order to confirm the TCO-Tz click chemistry between NPs and cells, seven different groups were designed to perform; 1) C6NP + HUVECs, 2) GPIb-C6NP + HUVECs, 3) Tz-GPIb-C6NP + HUVECs, 4) C6NP + TCO-HUVECs, 5) GPIb-C6NP + TCO-HUVECs, 6) Tz-GPIb-C6NP + TCO-HUVECs and 7) a blocking group (Tz-Cy5 + Tz-GPIb-C6NP + TCO-HUVECs). Four groups out of seven were replaced their cultured media with fresh media containing 10.0 μM TCO-PEG_4-NHS and incubated for 30 min while the remaining three groups were replaced with fresh media without TCO-PEG_4-NHS. For blocking study, the blocking group was treated with a 10.0 μM of Tz-Cy5 in media for 20 min while other groups were treated with fresh media. Finally, all seven groups were treated with 1.0 mg/ml of C6NPs at 37 ºC for 20 min.

4.2.2.5 *In vitro* binding study under a static condition

In vitro binding studies between vWF and Tz-GPIb-C6NPs as well as TCO-HUVEC cells under a static condition were performed. First, the vWF protein (a 15.0 μM concentration in PBS) was prepared on a hydrophobic surface and dried. To evaluate the binding between the vWF and GPIb proteins, C6NP, GPIb-C6NP and Tz-GPIb-C6NP suspensions(1.0 mg/ml) were then treated on the top of the vWF protein at 37 ºC for 30 minutes. After washing with fresh PBS twice, fluorescence imaging was captured using a fluorescence macroscope under a green channel. To determine if TCO-conjugated cells can bind to the NPs, NucBlue and Cell tracker™

Red CMPTX were used to label TCO-HUVECs and HUVECs following the manufacturer's protocols. The HUVECs were incubated on the top of the C6NP-treated slides as described above at 37 ºC for 30 minutes. After non-binded cells to NPs were washed with fresh PBS twice, the slides were subjected to the fluorescence imaging. The results were analyzed with ImageJ software.

4.2.2.6 *In vitro* binding study under flow conditions

The previous *in vitro* binding study were also performed under various flow conditions. For this, collagen coated Ibidi µSlides$^{0.4}$ (Ibidiwas immobilized with 30µg/ml of vWF for 1 hour at 37ºC. After coating, 1 mg of either unconjugated C6NPs, Gp1bα-C6NPs or Tz-Gp1bα C6NPs was perfused through the channels of the flow slide using a syringe pump (Harvard Apparatus Infuse/Withdraw Syringe Pump) that was set to withdraw solution at 0.17125 mL/min to give a corresponding shear stress of 0.25 dyn/cm^2 according to manufacturer's specifications. Following the NPs attachment, 10^5 of NucBlue and Cell tracker^{TM} Red CMPTX -labeled, TCO modified HUVECs was perfused at 0.25 dyn/cm^2 for 6 min. Upon the completion of flow, the microslides were imaged using Leica fluorescent microscope at FITC channel to observe NP attachment and at DAPI or Cy3 channel to visualize the captured cells.

4.2.2.7 Statistical analysis

All the data were evaluated using two-tailed student t-test and presented as mean ± standard deviation. Statistical analyses of all data were performed by a Student t-test. The results

showed significant when p value < 0.05. At least triplicate tests were conducted for statistical analysis.

4.3 Results

4.3.1 Characterizations of Tz-GPIb-C6NPs

DLS measurements showed that the fabricated C6NPs have an average diameter of 101 nm (polydispersities 0.005) while the other two conjugates, GPIb-C6NPs and Tz-GPIb-C6NPs have 110nm (0.01) and 107 nm (0.004), respectively, which has slightly larger diameters than C6NPs. The HRTEM images (**Figure 4.1A**) show that the C6NPs has a spherical morphology before and after the conjugations with either GPIbA or Tz-GPIb. To evaluate toxicity of the Tz-GPIb-C6NPs to HUVEC cells *in vitro*, Alamar Blue assay was performed in various concentrations of NPs. The results show that this particles trigger minimal toxicity to the cells (approximately 10.0 % reduction on the cell viability when treated with the particles at concentration of 2.0 mg/ml). (**Figure 4.1B**)

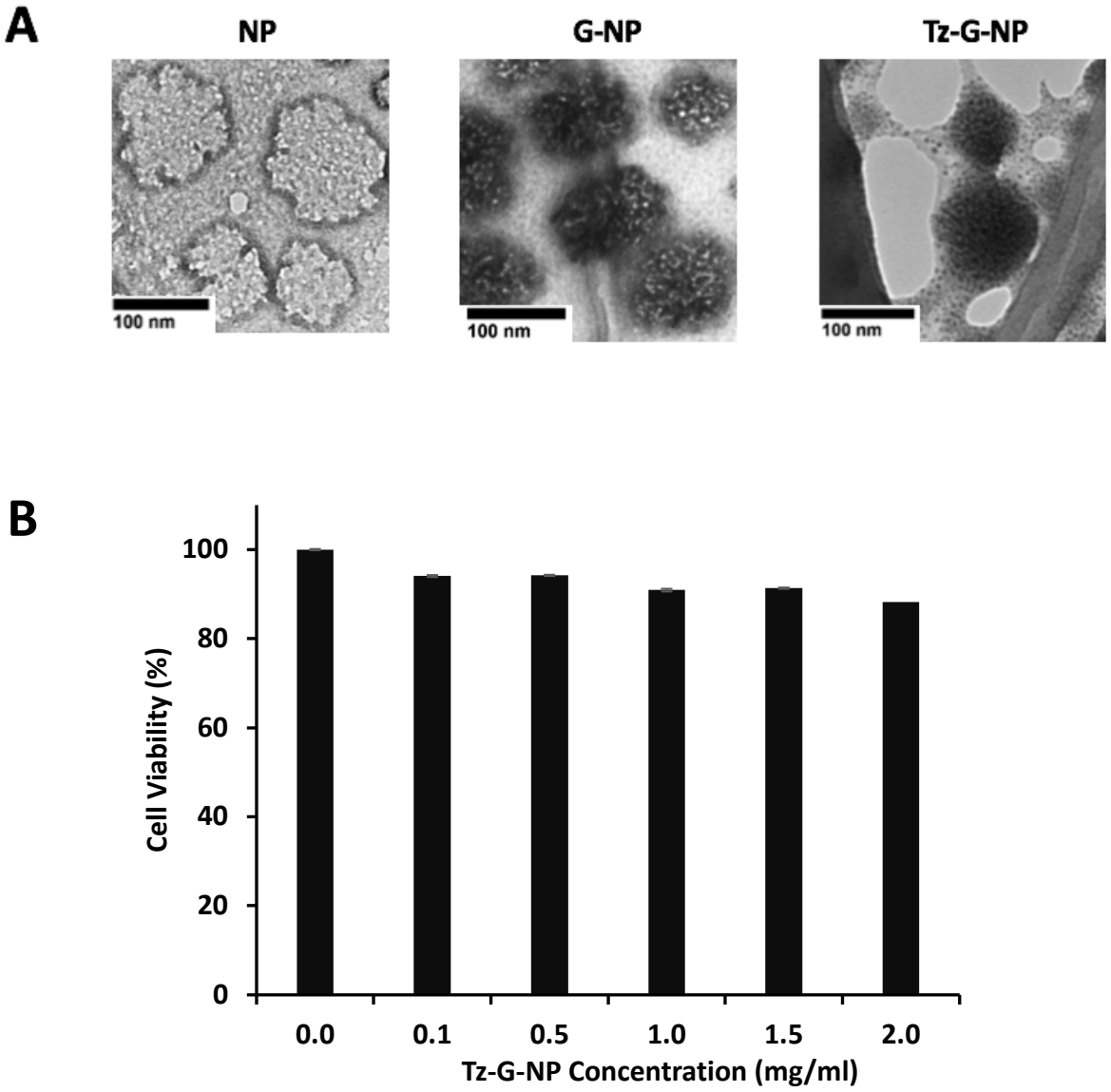

Figure 4.1 Characterization of GPIb or Tz-GPIb conjugated PLGA nanoparticles. **A)** High-resolution Transmission Electron Microscope (HRTEM) images illustrating PLGA and conjugated PLGA nanoparticles form spherical shapes; PLGA only, GPIb-C6NPs and Tz-GPIb-C6NPs. **B)** *In vitro* analysis of cell cytotoxicity demonstrating *in vitro* toxicity of the Tz-GPIb-C6NPs to HUVEC cells.

4.3.2 Characterizations of TCO-HUVECs

4.3.2.A Development of TCO modified HUVECs

HUVECs were modified using TCO-PEG_4-NHS targeted to free amines that were present on extracellular cell membrane proteins. We have observed the successful engineering of cell membrane with TCO moieties based on its reaction with Cy3 labeled Tz. Further, the amount of TCO incorporated on the cell surface significantly enhanced with increasing concentration of TCO-PEG_4-NHS and ~7% of initial amount of Tz-Cy3 that was added to the cell's suspension reacted with cell surface post modified with 40μM of TCO.

Long term stability of the TCO groups on HUVEC surfaces is essential for development of targeting rate of cells to the Tz groups on NPs. The 1×10^4 TCO-HUVECs were incubated with a 150.0 μl of culture media containing a 10.0 μM of a Tz-Cy5 for 30 min at each time point (day 0, 2, 4 and 6). The results show that a gradual reduction of the Cy5 signals from the HUVECs surface over time. However, more than 30.0 % of the signals were still detectable from the HUVECs 6 days after the initial TCO-labeling. Additionally, to evaluate the TCO groups remaining on the cell surface, Tz-Cy3 was treated at day 2, day 4 and day 6, respectively. Fluorescent images of Cy3 were captured following the Cy3 treatment. One can observe from **Figure 4.2** that Cy3 signals (in green color) are still detectable up to day 6, suggesting that some TCO still remains on cell surfaces and can effectively react with Tz.

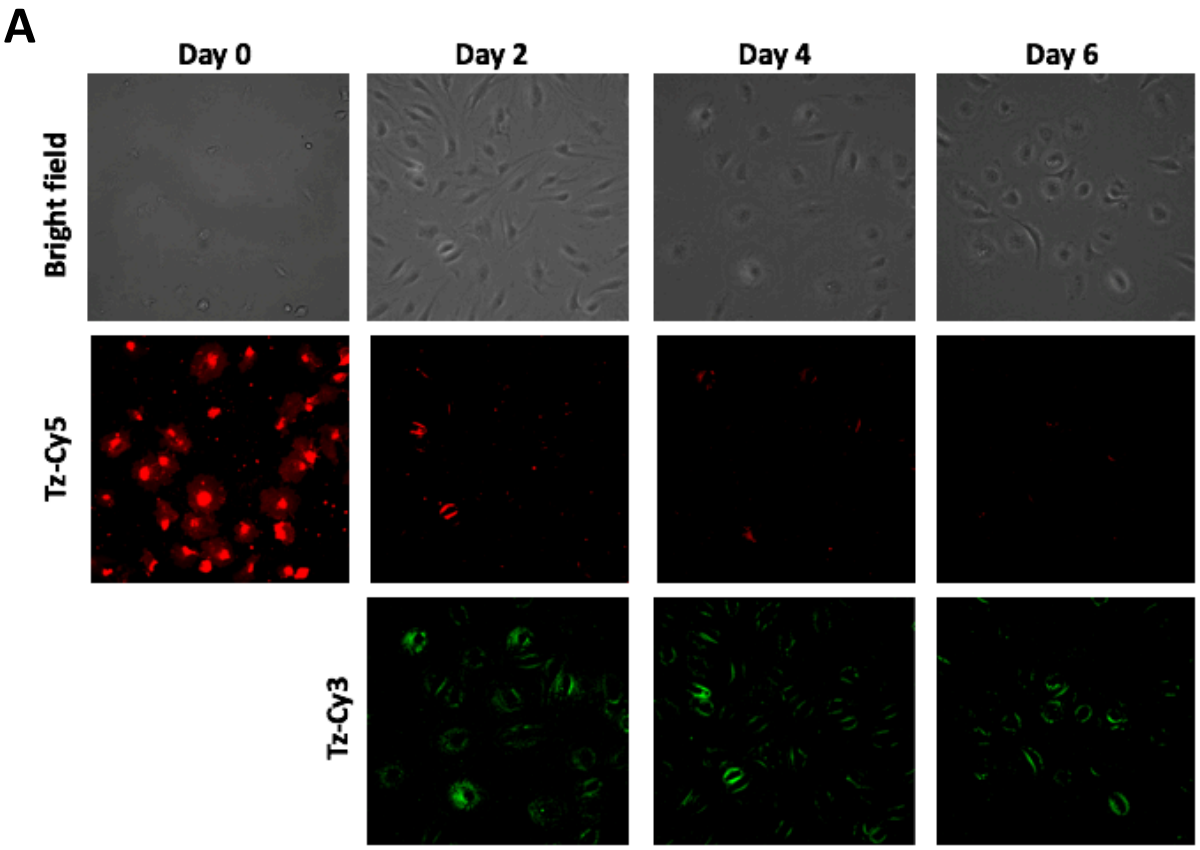
A
Day 0
Day 2
Day 4
Day 6
Bright field
Tz-Cy5
Tz-Cy3

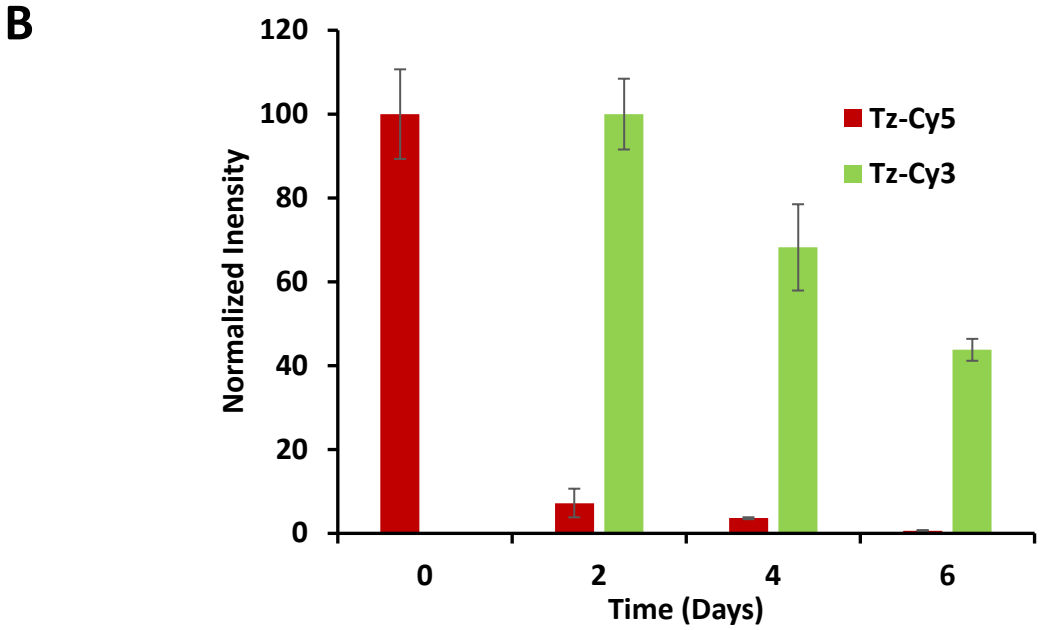
B
120
100
80
60
40
20
0
Normalized Inensity
Tz-Cy5
Tz-Cy3
0
2
4
6
Time (Days)

Figure 4.2 Characterization of TCO modified HIVEC cells. **A)** Images show that Tz-Cy5 and Tz-Cy3 were clicked on TCO modified HUVEC cells. **B)** Qualitative imaging demonstrate the stability of TCO on the cell surface using treatments with 10 uM of Tz-Cy5 at day 0 and 10 uM of Tz-Cy3 at day 2.

4.3.2.B Functional studies of TCO-HUVECs

After conjugation with various amounts of TCO on the cell surface, their effect on cellular viability and functionality were determined. It was observed that more than 90% of TCO modified cells were viable when cell surface was modified with TCO-PEG_4-NHS of concentrations ranging from 1-10μM (**Figure 4.3A**). However, at high concentrations of TCO (>10μM) induced cellular toxicity and reduced the cell viability to 65% with respect to the unmodified cells.

The maintenance of HUVEC functionality after TCO conjugation was studied based on their NO production and ability to internalize LDL particles post tagging. We found that increasing amount of TCO on HUVECs surface from 1μM to 10μM upregulates NO production in HUVECs, however, at 25μM the NO production was significantly reduced and have similar response to those treated with L-NNA, an inhibitor known to decrease NO production within the cells (**Figure 4.3A & B**). On other hand, we didn't observe any negative effect of TCO modification on the ECs' natural capability to internalize LDL particles. At all concentrations of TCO-PEG4-NHS, HUVECs have similar rate of uptake with respect to unmodified cells (**Figure 4.3C**).

A

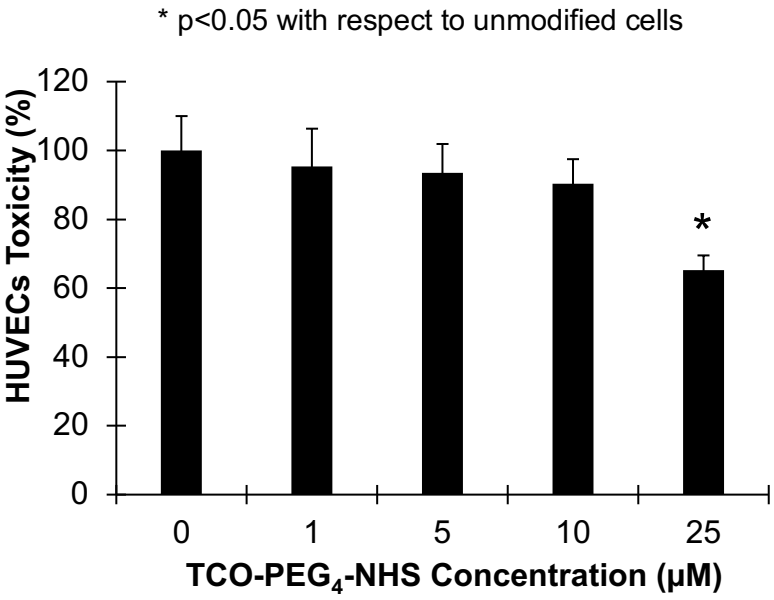
* p<0.05 with respect to unmodified cells
HUVECs Toxicity (%)
120
100
80
60
40
20
0
*
0
1
5
10
25
TCO-PEG4-NHS Concentration (µM)

B

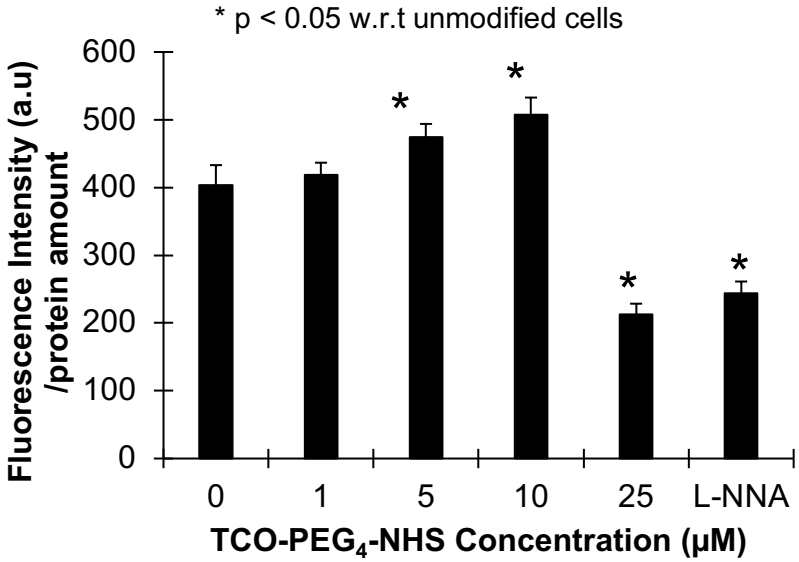
* p < 0.05 w.r.t unmodified cells
Fluorescence Intensity (a.u) /protein amount
600
500
400
300
200
100
0
*
*
*
*
0
1
5
10
25
L-NNA
TCO-PEG4-NHS Concentration (µM)

C

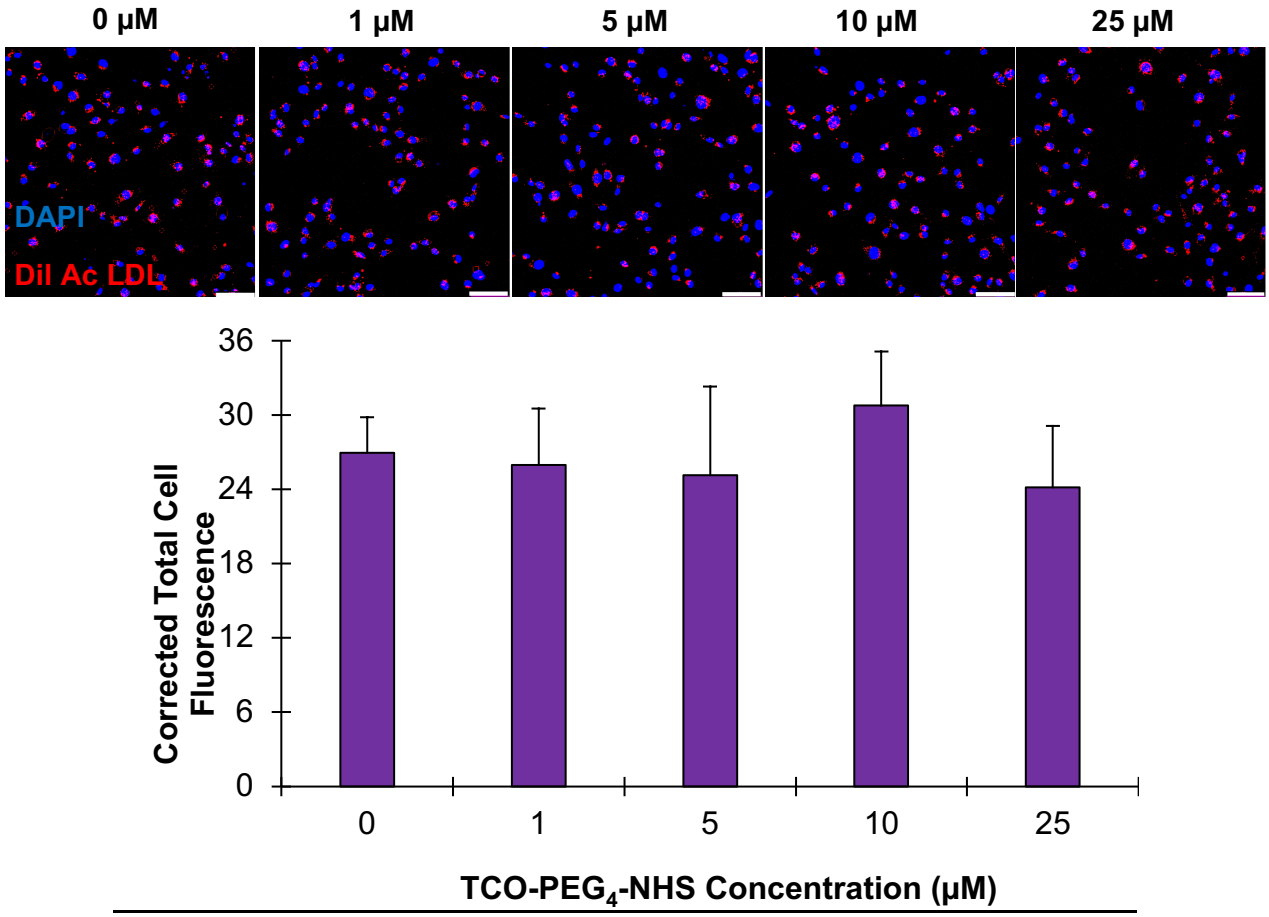

Figure 4.3 A) Cell cytotoxicity against different TCO concentrations. The maintenance of HUVEC functionality after TCO conjugation was studied based on their **B)** NO production and **C)** ability to internalize LDL particles post tagging.

4.3.3 Click chemistry confirmation between Tz-NPs and TCO-cells

To evaluate the click chemistry between Tz-NPs and TCO-cells, seven different groups were designed for *in vitro* binding studies. For this study, HUVECs and TCO-HUVECs were prepared separately and seeded on a 24-well plate. C6NP, GPIb-C6NP and Tz-GPIb-C6NP were then treated on the top of the HUVECs. As expected, the bright green color (**Figure 4.4A & B**) can be observed only in the treatment of Tz-GPIb-C6NP + TCO-HUVECs. To further determine the role of Tz/TCO click chemistry, TCO-HUVECs were treated with Tz-Cy5 prior to the treatment of Tz-GPIb-C6NP. One can observe strong fluorescent signals (red color) from Cy5 signals were obtained on the surface of HUVECs (red). (**Figure 4.4A**) The results suggest that the binding force between the cells and NPs is mainly due to the click chemistry reaction between Tz and TCO.

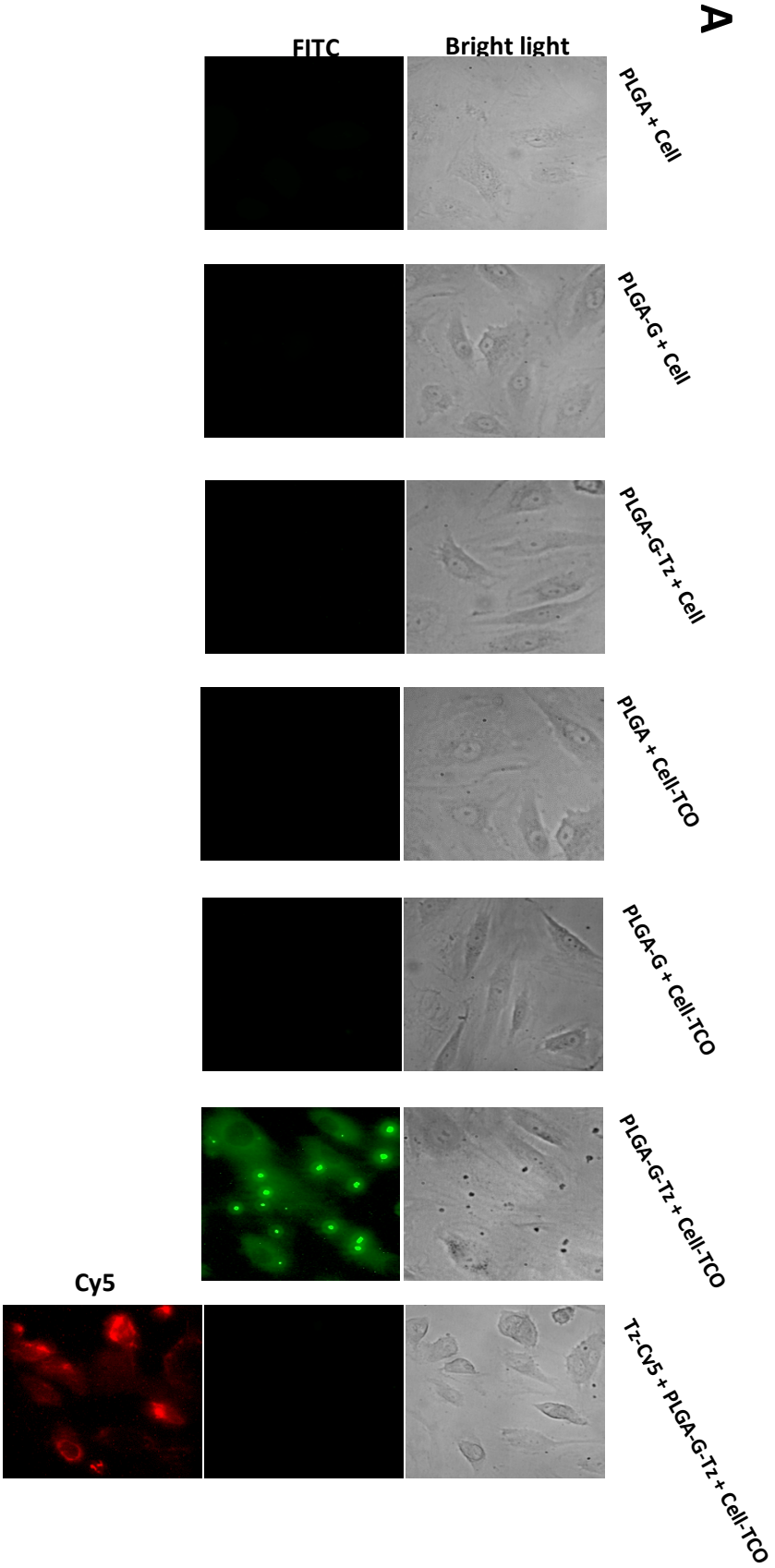
A
FITC
Bright light
PLGA + Cell
PLGA-G + Cell
PLGA-G-Tz + Cell
PLGA + Cell-TCO
PLGA-G + Cell-TCO
PLGA-G-Tz + Cell-TCO
Cy5
Tz-Cy5 + PLGA-G-Tz + Cell-TCO

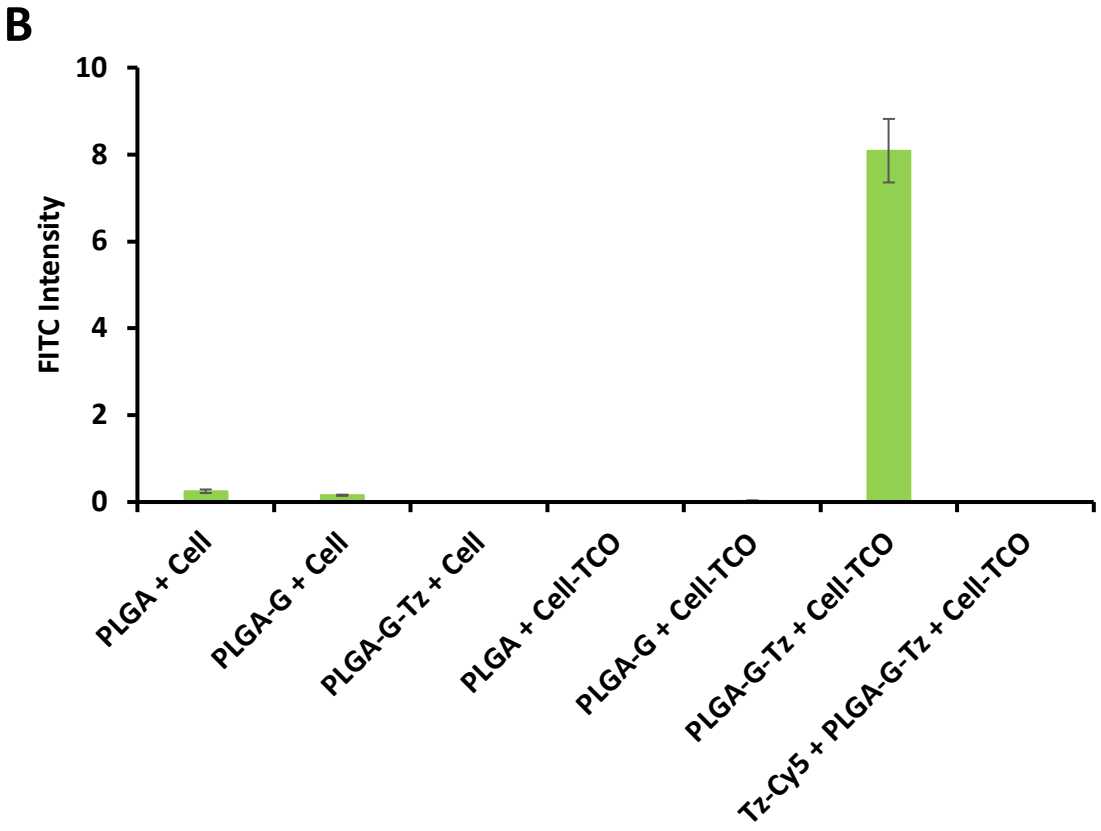

Figure 4.4 A) The click chemistry between TCO and Tz. **B)**Qualitative imaging demonstrate the binding between the cells and particles *in vitro*.

4.3.4 *In vitro* binding study under static / flow condition

To evaluate the GPIb proteins targeting rate to the vWF, all three samples, C6NPs, GPIb-C6NPs and Tz-GPIb-C6NPs, were incubated on the top of the vWF-coated slides under a static condition at 37 ºC for 30 minutes. The results are shown in **Figure 4.5A & B**. The GPIb-C6NPs group bound to vWF protein the most. Modification of GPIb has minimal impact on Tz-GPIb-c6NPs binding to vWF (10.0 % less binding rate compared to the GPIb-C6NP group (**Figure 4.5C**). To evaluate the binding between the Tz-NPs and TCO-HUVECs, the free HUVECs and TCO-HUVECs were incubated on the top of the previous three groups and the results show in **Figure 4.5D**. Only treatment of the Tz-GPIb-C6NPs group shows strong cell targeting signals. The binding study was further evaluated under a flow condition. It is found that the result under flow condition was similar to the static condition data. (**Figure 4.6**)

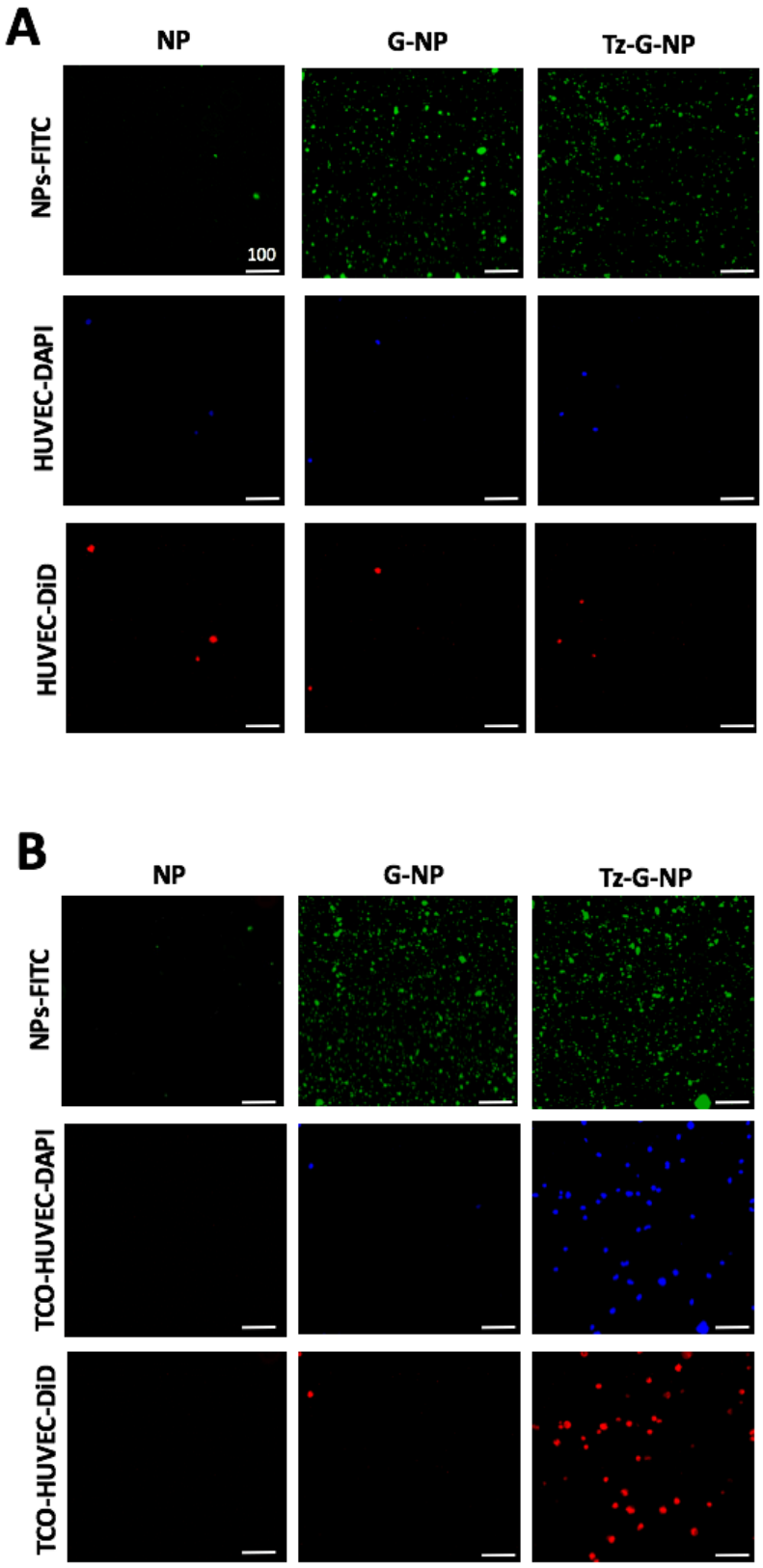
A
NP
G-NP
Tz-G-NP
NPs-FITC
100
HUVEC-DAPI
HUVEC-DiD
B
NP
G-NP
Tz-G-NP
NPs-FITC
TCO-HUVEC-DAPI
TCO-HUVEC-DiD

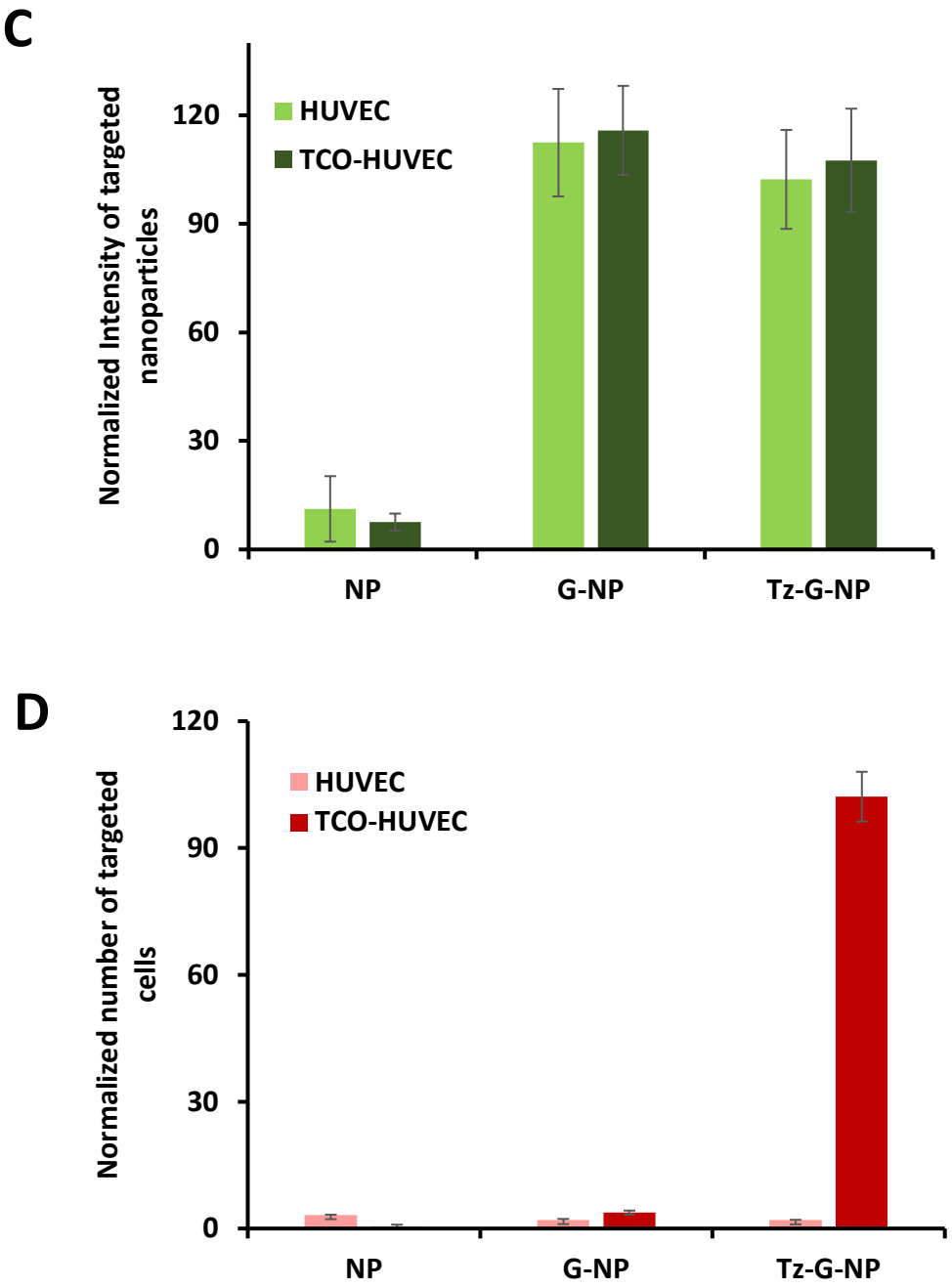

Figure 4.5 *In vitro* binding study between vWF and PLGA-GP1BA-Tz NPs as well as TCO tagged HUVEC cells. The vWF protein was coated on the surface and then incubated the prepared NPs for 30 minutes. Finally, TCO-tagged HUVEC cells were added into the culture for 30 minutes. **A) and B)** Flurescent imags of NPs and cells at different steps. **C)** Quantitative data demonstrate the targeted NPs to vWF proteins and **D)** the number of the recruited HUVEC cells to the NPs**.**

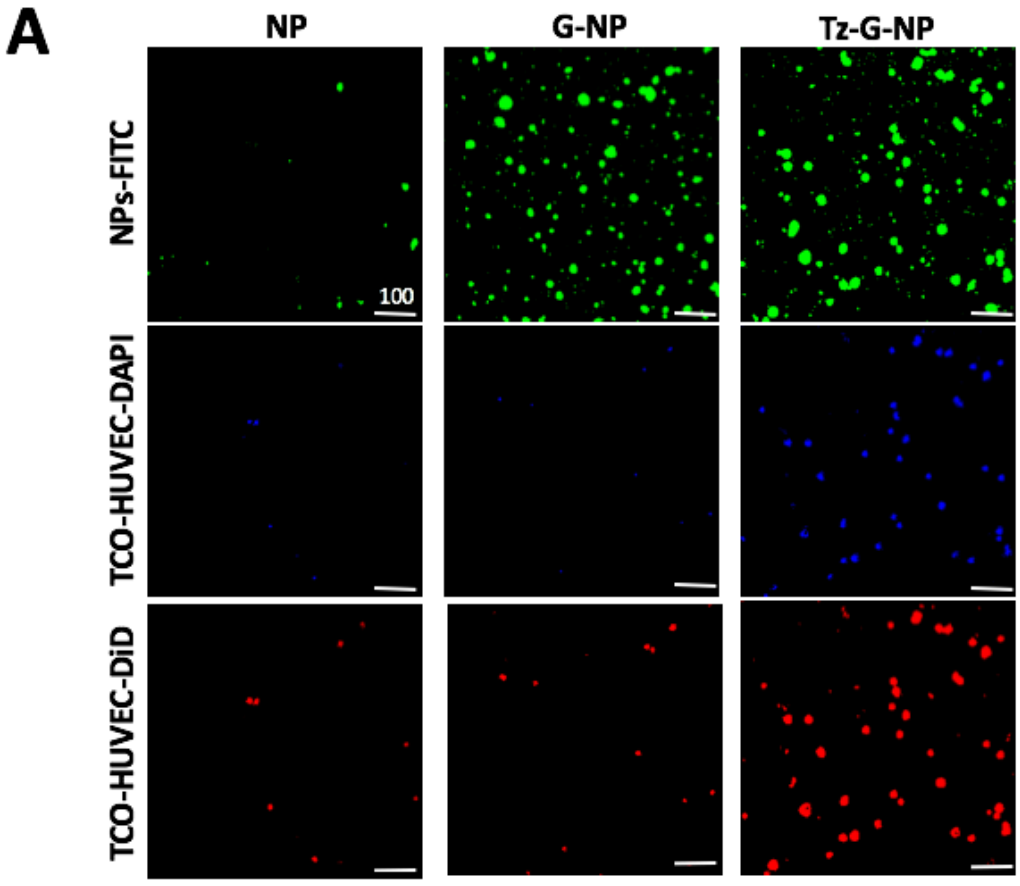
A
NP
G-NP
Tz-G-NP
NPs-FITC
TCO-HUVEC-DAPI
TCO-HUVEC-DiD
100

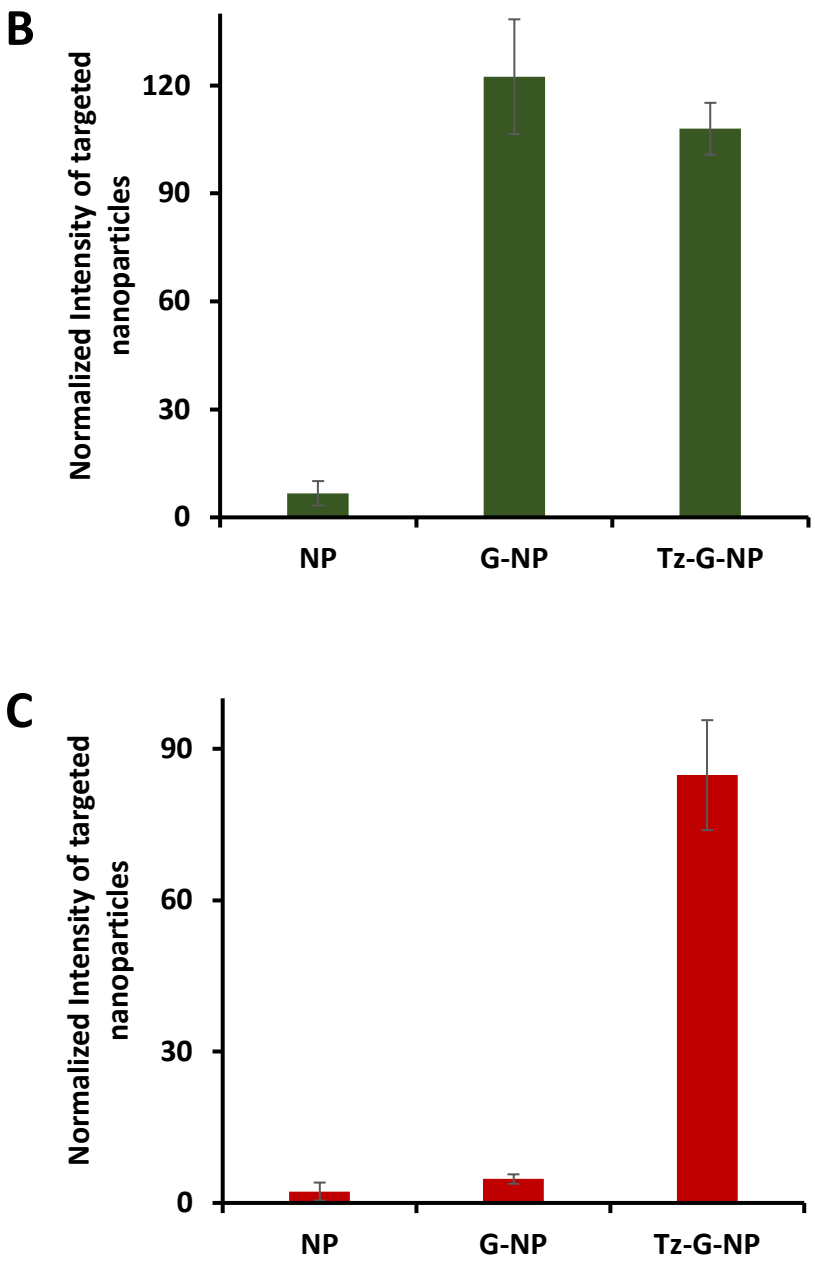

Figure 4.6 *In vitro* binding study under flow condition. **A)** vWF proteins were prepared on the surface of the flow chamber and PLGA-GP1BA-Tz nanoparticles was flowed prior to TCO tagged HUVEC cells. Qualitative imaging demonstrate that NPs were evenly binded to vWF protein on the serface and the following HUVEC cells were recruited to the NPs. Quantitative data of the targeted NPs to vWF proteins **(B)** and cells **(C)**.

4.4 Discussion

Cell therapies based on their restoration of tissue hemostasis offer healing of injured arterial wall. But one of the remained challenges is the low rate of cell recruitment at target sites. As a result, the therapeutic benefits on the injured sites show poor clinical outcomes. To overcome this issue, researches have engineered the surface of cells to improve cell homing at the targeted sites.[80–82] Among different methods for engineering the cell surface, a biorthogonal click chemistry based on tetrazine (Tz)/trans-cyclooctene (TCO) reaction has recently received attention.[76,83–85]

In this work, I focused on a two-step approach utilizing biorthogonal click chemistry to improve the cell delivery and homing to treat angioplasty induced vascular injury. To demonstrate our strategy, we formulated ~100nm sized PLGA nanoparticles conjugated with Tz-modified Gp1bα without losing Gp1bα ability to recognize injured vasculature. Then Tz tagged Gp1bα was conjugated on to PLGA nanoparticles to develop a multifunctional nanoparticle with targeting and cell capturing functionalities. These NPs mimics natural injury targeting power of platelet via Gp1bα interaction with vWF on subendothelial layer, resulting in particle accumulation specifically to the injured arterial wall exposing Tz linkers attached to Gp1b. Second, TCO tagged ECs were developed by modifying free amines on extracellular proteins and delivered to injured vasculature. Strong association of TCO on cells with Tz on NPs would allow ECs capture and homing on the treatment site to support *in situ* endothelial regeneration. I postulate that our two-step approach utilizing multifunctional nanoparticle and engineered cells to heal vascular injury offer several advantages: (1) injury specific delivery of nanoparticles as well as therapeutic cells for regeneration, (2) cell homing utilizing biorthogonal chemistry allow strong cell adhesion to tissue unlike conventional cell capturing methods based on antigen-

antibody reaction, (3) nanoparticle formulation allow us to incorporate growth factor molecules or therapeutic agents that may further assist in cell retention at diseases tissue, and (4) platelet mimicking property of nanoparticle reduces interaction of platelets and other inflammatory cells in circulation to injured arterial wall.

This study has shown that Gp1bα function to recognize vWF coated surfaces was affected with increasing amounts of Tz tagging to protein and thereby reducing the number of nanoparticles delivered to vWF coated surface by 50% when 100 molar excess of Tz tagged on to Gp1bα (molar ratio of Gp1bα :Tz is 1:100). Although the number of NPs delivered was reduced, 50% of Tz-Gp1bα PLGA NPs (1:100) bound to vWF surfaces was enough to show significant improvement in cell capturing compared to nanoparticles with Tz-Gp1bα PLGA NPs (1:25) and Gp1bα PLGA NPs. Therefore, we utilized Tz-Gp1bα PLGA NPs (1:100) for further studies reported.

In parallel, I developed TCO tagged endothelial cells (TCO-ECs) by immobilizing TCO-PEG_4-NHS on to free amine present on extracellular membrane proteins. With increasing amount of TCO-PEG_4-NHS, the amount of tagging on cells has significantly increased, however this also compromised cellular viability and resulted in only 65% cell viability post treatment with 25μM of TCO-PEG_4-NHS. Further, NO production by modified cells are dysregulated and significant decrease in their production was observed when cells tagged with 25μM of TCO-PEG4-NHS. On other hand, LDL uptake process by endothelial cells remain unaffected at all concentrations of TCO-PEG_4-NHS.

Although NPs can be easily taken up by HUVEC at static condition or low shear stress flow, they do not sufficiently arrest on ECs under high shear flow.[86] Hence, enhancing NPs adhesion and uptake by inflamed ECs under arterial flow conditions (>10 dyn/cm2) is critical for

their application in drug delivery. To overcome inadequate accumulation of HUVEC at the injured site, the cell surface was modified with bioorthogonal click chemistry. Inspired by the natural capability of platelet interaction with injured vascular endothelium, we have developed nanoscaffoldsual functional -EC adhesion during blood coagulation under physiological flow conditions, we developed a novel type of ligand and click chemistry conjugated-PLGA NPs for a targeted delivery of HUVEC on the arterial wall. We used PLGA to formulate these NPs because they have been approved by the FDA for drug delivery. PLGA NPs was synthesized with a 200-nm diameter because NPs with a diameter between 100 and 200 nm have a comparatively longer half-life in the circulation due to their sizes being large enough to avoid uptake in the liver, but small enough to avoid filtration in the spleen.[87]

The surface modification that we opted for has been widely used for optimizing the rate of NPs adhesion and retention. The ligands GP1bA and Tz were conjugated on the NPs surface to facilitate particle adhesion and internalization by inflamed ECs. GP1bA is the ligand binding subunit of the glycoprotein Ib-IX-V complex that is almost exclusively expressed on platelets. It binds vWF expressed on inflamed endothelial cells and sub-endothelium.[88] In comparison to adhesion molecules such as integrins that mediate cell adhesion primarily at low shear stress, GP1b can effectively interact with vWF at a high level of shear stress found in arterioles and small arteries.[89]

4.5 Conclusions

In the present study, I developed a novel Tz-GP1b-conjugated C6PLGA NPs for recruiting ECs to the injury site. Our data showed that: (1) Tz modified Gp1b-NPs were able to retain the similar adhesive and targeting property of unmodified Gp1bα towards vWF coated surfaces; (2) TCO decoration on ECs surface was effective and have minimal effect on the cellular viability and functionality; (3) TCO moieties were stably expressed for long term on the EC surface; and (4) Tz-Gp1b NPs effectively engaged with TCO engineered ECs via biorthogonal click chemistry and capture cells under both static and flow conditions. This NPs provides a new tool for treating cardiovascular diseases.

Chapter 5

Summary and Conclusions

Platform 1: Temperature sensitive injectable hydrogels have been used as drug/protein carriers for a variety of pharmaceutical applications. Oligo(ethylene glycol) methacrylate (OEGMA) monomers with varying chain lengths of ethylene oxide have been used for synthesis of *in situ* forming hydrogel. In this study, a new series of thermally induced gelling hydrogel nanoparticles (PMOA hydrogel nanoparticles) was developed by copolymerization with di(ethylene glycol) methyl ether methacrylate (MEO_2MA), poly(ethylene glycol) methyl ether methacrylate (300 g/mol, $OEGMA_{300}$), and acrylic acid (AAc). Effects of acrylic acid content on the physical, chemical, and biological properties of the nanoparticle-based hydrogels were investigated. Due to its high electrostatic property, addition of AAc increases LCST as well as gelation temperature. Further, using Cy5-labelled bovine serum albumin and erythropoietin (Epo) as model drugs, studies have shown that the thermogelling hydrogels have the ability to tune the release rate of these proteins *in vitro*. Finally, the ability of Epo releasing hydrogels to recruit prostate cancer cells was assessed *in vivo*. Overall, our results support that this new series of

thermally induced gelling system can be used as a protein control releasing vehicle and a cancer cell trap.

Platform 2: This work details the development of a "sandwich" platform via neutravidin-biotin system for the detection and treatment of inflammation. Specifically, biotinylated- and folate-conjugated optical imaging micelles were prepared to pretarget activated macrophages via folate/folate receptor interactions. Multivalent neutravidin proteins in optimal concentration were also prepared to accumulate on the biotinylated macrophages. Finally, biotinylated anti-inflammatory drug-loaded micelles were fabricated to delivery drugs at the inflammatory sites via the highly specific neutravidin-biotin affinity. Both *in vitro* and *ex vivo* studies have shown that the "sandwich" pretargeting platform was able to diagnose inflammation by targeting activated macrophages and also to improve the therapeutic efficacy by amplifying the drug delivery to the inflammatory tissue. The overall results support that the neutravidin-biotin pretargeting platform have the potential for inflammatory disease diagnosis and treatment.

Platform 3: Damage the arterial walls leads the development of late pathological conditions such as thrombosis (blood clot). Herein, we applied of a state-of-the-art nanotechnology, a bioorthogonal click chemistry, to improve endothelial healing and coverage of the injured arterial wall based on pretargeting PLGA nanoparticles and following recruited endothelial cells. Surfaces of PLGA nanoparticles and endothelial cell were modified with tetrazine and trans-cyclooctene respectively and this technology developed *in vitro* cell recruiting ability for effective treatment of atherosclerosis. In the nanoparticle preparation, the PLGA nanoparticles were successfully conjugated with tetrazine without losing the function of a biological ligand, GPIbA proteins to bind onto the damage site. In the endothelial cell preparation, the trans-cyclooctene was successfully conjugated on the cells membrane with an

optimal amount for development of a cell recruiting rate to the damage site. *In vitro* binding studies under both static and flow conditions confirmed that the developed conjugated nanoparticle has successfully pre-targeted on the damage site and effectively recruited endothelial cells. This study promises improved cell stability on advanced atherosclerosis lesions for cell therapy.

References

1. Kretlow, J. D., Klouda, L. & Mikos, A. G. Injectable matrices and scaffolds for drug delivery in tissue engineering. *Advanced Drug Delivery Reviews* (2007). doi:10.1016/j.addr.2007.03.013

2. Yang, J. A., Yeom, J., Hwang, B. W., Hoffman, A. S. & Hahn, S. K. In situ-forming injectable hydrogels for regenerative medicine. *Progress in Polymer Science* (2014). doi:10.1016/j.progpolymsci.2014.07.006

3. Choi, B. *et al.* Introduction to In Situ Forming Hydrogels for Biomedical Applications. in (2015). doi:10.1007/978-981-287-152-7_2

4. Hennink, W. E. & van Nostrum, C. F. Novel crosslinking methods to design hydrogels. *Advanced Drug Delivery Reviews* (2012). doi:10.1016/j.addr.2012.09.009

5. Yang, X., Zhang, G. & Zhang, D. Stimuli responsive gels based on low molecular weight gelators. *J. Mater. Chem.* (2012). doi:10.1039/c1jm13205a

6. Yan, J., Liu, K., Li, W., Shi, H. & Zhang, A. Thermoresponsive Dendronized Polypeptides Showing Switchable Recognition to Catechols. *Macromolecules* (2016). doi:10.1021/acs.macromol.5b02259

7. Vo, T. N. *et al.* Injectable dual-gelling cell-laden composite hydrogels for bone tissue engineering. *Biomaterials* (2016). doi:10.1016/j.biomaterials.2015.12.026

8. Khang, M. K., Zhou, J., Huang, Y., Hakamivala, A. & Tang, L. Preparation of a novel injectable in situ-gelling nanoparticle with applications in controlled protein release and cancer cell entrapment. *RSC Adv.* (2018). doi:10.1039/C8RA06589F

9. Patel, S. K. & Janjic, J. M. Macrophage targeted theranostics as personalized nanomedicine strategies for inflammatory diseases. *Theranostics* (2015). doi:10.7150/thno.9476

10. Ryu, J. H. *et al.* Theranostic nanoparticles for future personalized medicine. *Journal of Controlled Release* (2014). doi:10.1016/j.jconrel.2014.04.027

11. Luk, B. T. & Zhang, L. Current advances in polymer-based nanotheranostics for cancer treatment and diagnosis. *ACS Applied Materials and Interfaces* (2014). doi:10.1021/am5036225

12. Lim, E. K. *et al.* Nanomaterials for theranostics: Recent advances and future challenges. *Chemical Reviews* (2015). doi:10.1021/cr300213b

13. Jokerst, J. V. & Gambhir, S. S. Molecular imaging with theranostic nanoparticles. *Acc. Chem. Res.* (2011). doi:10.1021/ar200106e

14. Kumar, R. *et al.* Small conjugate-based theranostic agents: An encouraging approach for cancer therapy. *Chem. Soc. Rev.* (2015). doi:10.1039/c5cs00224a

15. Devaraj, N. K., Weissleder, R. & Hilderbrand, S. A. Tetrazine-based cycloadditions: Application to pretargeted live cell imaging. *Bioconjug. Chem.* (2008). doi:10.1021/bc8004446

16. Haun, J. B., Devaraj, N. K., Hilderbrand, S. A., Lee, H. & Weissleder, R. Bioorthogonal chemistry amplifies nanoparticle binding and enhances the sensitivity of cell detection. *Nat. Nanotechnol.* (2010). doi:10.1038/nnano.2010.148

17. Orford, J. L., Selwyn, A. P., Ganz, P., Popma, J. J. & Rogers, C. The comparative pathobiology of atherosclerosis and restenosis. *Am. J. Cardiol.* (2000). doi:10.1016/S0002-9149(00)01094-8

18. Löwenberg, E. C., Meijers, J. C. M. & Levi, M. Platelet-vessel wall interaction in health and disease. *Netherlands Journal of Medicine* (2010).

19. Rockley, M., Jetty, P., Wells, G., Rockley, K. & Fergusson, D. Prolonged versus brief balloon inflation during arterial angioplasty for de novo atherosclerotic disease: Protocol for a systematic review. *Systematic Reviews* (2019). doi:10.1186/s13643-019-0955-2

20. Wickline, S. A., Neubauer, A. M., Winter, P., Caruthers, S. & Lanza, G. Applications of nanotechnology to atherosclerosis, thrombosis, and vascular biology. *Arteriosclerosis, Thrombosis, and Vascular Biology* (2006). doi:10.1161/01.ATV.0000201069.47550.8b

21. Garnacho, C., Serrano, D. & Muro, S. A Fibrinogen-Derived Peptide Provides Intercellular Adhesion Molecule-1-Specific Targeting and Intraendothelial Transport of Polymer Nanocarriers in Human Cell Cultures and Mice. *J. Pharmacol. Exp. Ther.* (2012). doi:10.1124/jpet.111.185579

22. Rossin, R., Muro, S., Welch, M. J., Muzykantov, V. R. & Schuster, D. P. In Vivo Imaging of 64Cu-Labeled Polymer Nanoparticles Targeted to the Lung Endothelium. *J. Nucl. Med.* (2007). doi:10.2967/jnumed.107.045302

23. O'Brien, F. J. Biomaterials & scaffolds for tissue engineering. *Materials Today* (2011). doi:10.1016/S1369-7021(11)70058-X

24. Hou, Q., De Bank, P. A. & Shakesheff, K. M. Injectable scaffolds for tissue regeneration. *Journal of Materials Chemistry* (2004). doi:10.1039/b401791a

25. Liu, H. *et al.* Reversible thermo-sensitivity induced from varying the hydrogen bonding between the side residues of rationally designed polypeptides. *Chem. Commun.* (2015). doi:10.1039/c5cc03017j

26. Kim, E. J., Choi, J. S., Kim, J. S., Choi, Y. C. & Cho, Y. W. Injectable and

Thermosensitive Soluble Extracellular Matrix and Methylcellulose Hydrogels for Stem Cell Delivery in Skin Wounds. *Biomacromolecules* (2016). doi:10.1021/acs.biomac.5b01566

27. Cheng, Y. *et al.* Thermosensitive hydrogels based on polypeptides for localized and sustained delivery of anticancer drugs. *Biomaterials* (2013). doi:10.1016/j.biomaterials.2013.09.064

28. Moon, H. J., Ko, D. Y., Park, M. H., Joo, M. K. & Jeong, B. Temperature-responsive compounds as in situ gelling biomedical materials. *Chemical Society Reviews* (2012). doi:10.1039/c2cs35078e

29. Kang, E. Y., Moon, H. J., Joo, M. K. & Jeong, B. Thermogelling chitosan-g-(PAF-PEG) aqueous solution as an injectable scaffold. *Biomacromolecules* (2012). doi:10.1021/bm300085c

30. He, C., Kim, S. W. & Lee, D. S. In situ gelling stimuli-sensitive block copolymer hydrogels for drug delivery. *Journal of Controlled Release* (2008). doi:10.1016/j.jconrel.2008.01.005

31. Alexander, A., Khan, J., Saraf, S. & Saraf, S. Poly (ethylene glycol)–poly (lactic-co-glycolic acid) based thermosensitive injectable hydrogels for biomedical applications. *J. Control. Release* **172**, 715–729 (2013).

32. Zhou, J. *et al.* Viscoelastic behavior and in vivo release study of microgel dispersions with inverse thermoreversible gelation. *Biomacromolecules* (2008). doi:10.1021/bm700918d

33. Cai, T. *et al.* Novel thermogelling dispersions of polymer nanoparticles for controlled protein release. *Nanomedicine Nanotechnology, Biol. Med.* (2012). doi:10.1016/j.nano.2012.02.002

34. Wang, D., Cheng, D., Guan, Y. & Zhang, Y. Thermoreversible hydrogel for in situ generation and release of HepG2 spheroids. *Biomacromolecules* (2011). doi:10.1021/bm101187b

35. Shen, Z., Mellati, A., Bi, J., Zhang, H. & Dai, S. A thermally responsive cationic nanogel-based platform for three-dimensional cell culture and recovery. *RSC Adv.* (2014). doi:10.1039/c4ra02852j

36. Li, Y. *et al.* Formation of Multidomain Hydrogels via Thermally Induced Assembly of PISA-Generated Triblock Terpolymer Nanogels. *Macromolecules* (2016). doi:10.1021/acs.macromol.5b02538

37. Guan, Y. & Zhang, Y. PNIPAM microgels for biomedical applications: From dispersed particles to 3D assemblies. *Soft Matter* (2011). doi:10.1039/c0sm01541e

38. Gu, J., Zhao, Y., Guan, Y. & Zhang, Y. Effect of particle size in a colloidal hydrogel scaffold for 3D cell culture. *Colloids Surfaces B Biointerfaces* (2015). doi:10.1016/j.colsurfb.2015.11.021

39. Gan, T., Zhang, Y. & Guan, Y. In situ gelation of P(NIPAM-HEMA) microgel dispersion and its applications as injectable 3D cell scaffold. *Biomacromolecules* (2009).

doi:10.1021/bm900022m

40. Gan, T., Guan, Y. & Zhang, Y. Thermogelable PNIPAM microgel dispersion as 3D cell scaffold: Effect of syneresis. *J. Mater. Chem.* (2010). doi:10.1039/c0jm00338g

41. Burek, M. *et al.* Thermoresponsive microgels containing trehalose as soft matrices for 3D cell culture. *Biomater. Sci.* (2017). doi:10.1039/c6bm00624h

42. Madsen, J. & Armes, S. P. (Meth)acrylic stimulus-responsive block copolymer hydrogels. *Soft Matter* (2012). doi:10.1039/c1sm06035j

43. Ryu, J. H. *et al.* Self-cross-linked polymer nanogels: A versatile nanoscopic drug delivery platform. *J. Am. Chem. Soc.* (2010). doi:10.1021/ja1069932

44. Chambre, L., Degirmenci, A., Sanyal, R. & Sanyal, A. Multi-Functional Nanogels as Theranostic Platforms: Exploiting Reversible and Nonreversible Linkages for Targeting, Imaging, and Drug Delivery. *Bioconjug. Chem.* (2018). doi:10.1021/acs.bioconjchem.8b00085

45. Cai, T., Marquez, M. & Hu, Z. Monodisperse thermoresponsive microgels of poly(ethylene glycol) analogue-based biopolymers. *Langmuir* (2007). doi:10.1021/la700923r

46. Aktan, B., Chambre, L., Sanyal, R. & Sanyal, A. "Clickable" Nanogels via Thermally Driven Self-Assembly of Polymers: Facile Access to Targeted Imaging Platforms using Thiol-Maleimide Conjugation. *Biomacromolecules* (2017). doi:10.1021/acs.biomac.6b01576

47. Lutz, J. F., Weichenhan, K., Akdemir, Ö. & Hoth, A. About the phase transitions in aqueous solutions of thermoresponsive copolymers and hydrogels based on 2-(2-methoxyethoxy)ethyl methacrylate and oligo(ethylene glycol) methacrylate. *Macromolecules* (2007). doi:10.1021/ma062925q

48. Zhou, J., Tsai, Y. T., Weng, H., Baker, D. W. & Tang, L. Real time monitoring of biomaterial-mediated inflammatory responses via macrophage-targeting NIR nanoprobes. *Biomaterials* (2011). doi:10.1016/j.biomaterials.2011.08.064

49. An, S. Y. *et al.* Preparation of monodisperse and size-controlled poly(ethylene glycol) hydrogel nanoparticles using liposome templates. *J. Colloid Interface Sci.* (2009). doi:10.1016/j.jcis.2008.11.022

50. Liu, Z. L. *et al.* Preparation and characterization of polymer-coated core-shell structured magnetic microbeads. *J. Magn. Magn. Mater.* (2003). doi:10.1016/S0304-8853(03)00230-0

51. Good, M. M. *et al.* Thermosensitive hydrogels deliver bioactive protein to the vaginal wall. *PLoS One* (2017). doi:10.1371/journal.pone.0186268

52. Nojoomi, A., Tamjid, E., Simchi, A., Bonakdar, S. & Stroeve, P. Injectable polyethylene glycol-laponite composite hydrogels as articular cartilage scaffolds with superior mechanical and rheological properties. *Int. J. Polym. Mater. Polym. Biomater.* (2017). doi:10.1080/00914037.2016.1182914

53. Sen, M. & Güven, O. Dynamic deswelling studies of poly(N-vinyl-2-pyrrolidone/itaconic acid) hydrogels swollen in water and terbinafine hydrochloride solutions. *Eur. Polym. J.* (2002). doi:10.1016/S0014-3057(01)00240-3

54. Ozcelik, B. *et al.* Highly porous and mechanically robust polyester poly(ethylene glycol) sponges as implantable scaffolds. *Acta Biomater.* (2014). doi:10.1016/j.actbio.2014.02.019

55. Parboosing, R., Mzobe, G., Chonco, L. & Moodley, I. Cell-based Assays for Assessing Toxicity: A Basic Guide. *Med. Chem. (Los. Angeles).* (2017). doi:10.2174/1573406412666160229150803

56. Weng, H., Zhou, J., Tang, L. & Hu, Z. Tissue responses to thermally-responsive hydrogel nanoparticles. *J. Biomater. Sci. Polym. Ed.* (2004). doi:10.1163/1568562041753106

57. Ko, C. Y. *et al.* The use of chemokine-releasing tissue engineering scaffolds in a model of inflammatory response-mediated melanoma cancer metastasis. *Biomaterials* (2012). doi:10.1016/j.biomaterials.2011.10.002

58. Nair, A. *et al.* Biomaterial implants mediate autologous stem cell recruitment in mice. *Acta Biomater.* (2011). doi:10.1016/j.actbio.2011.06.050

59. Kratz, K., Hellweg, T. & Eimer, W. Influence of charge density on the swelling of colloidal poly(N-isopropylacrylamide-co-acrylic acid) microgels. *Colloids Surfaces A Physicochem. Eng. Asp.* (2000). doi:10.1016/S0927-7757(00)00490-8

60. Burmistrova, A., Richter, M., Eisele, M., Üzüm, C. & von Klitzing, R. The effect of co-monomer content on the swelling/shrinking and mechanical behaviour of individually adsorbed PNIPAM microgel particles. *Polymers (Basel).* (2011). doi:10.3390/polym3041575

61. Lanzalaco, S. & Armelin, E. Poly(N-isopropylacrylamide) and Copolymers: A Review on Recent Progresses in Biomedical Applications. *Gels* (2017). doi:10.3390/gels3040036

62. Ramin, M. A., Latxague, L., Sindhu, K. R., Chassande, O. & Barthélémy, P. Low molecular weight hydrogels derived from urea based-bolaamphiphiles as new injectable biomaterials. *Biomaterials* (2017). doi:10.1016/j.biomaterials.2017.08.034

63. Staruch, R. M. T., Glass, G. E., Rickard, R., Hettiaratchy, S. P. & Butler, P. E. M. Injectable Pore-Forming Hydrogel Scaffolds for Complex Wound Tissue Engineering: Designing and Controlling Their Porosity and Mechanical Properties. *Tissue Eng. Part B Rev.* (2017). doi:10.1089/ten.teb.2016.0305

64. Tong, X., Lee, S., Bararpour, L. & Yang, F. Long-Term Controlled Protein Release from Poly(Ethylene Glycol) Hydrogels by Modulating Mesh Size and Degradation. *Macromol. Biosci.* (2015). doi:10.1002/mabi.201500245

65. Branco, M. C., Pochan, D. J., Wagner, N. J. & Schneider, J. P. The effect of protein structure on their controlled release from an injectable peptide hydrogel. *Biomaterials* (2010). doi:10.1016/j.biomaterials.2010.08.047

66. Mirmohammadsadegh, A. *et al.* Role of erythropoietin receptor expression in malignant

melanoma. *J. Invest. Dermatol.* (2010). doi:10.1038/jid.2009.162

67. Henke, M. *et al.* Erythropoietin to treat head and neck cancer patients with anaemia undergoing radiotherapy: Randomised, double-blind, placebo-controlled trial. *Lancet* (2003). doi:10.1016/S0140-6736(03)14567-9

68. Arcasoy, M. O., Jiang, X. & Haroon, Z. A. Expression of erythropoietin receptor splice variants in human cancer. *Biochem. Biophys. Res. Commun.* (2003). doi:10.1016/S0006-291X(03)01303-2

69. Khang, M. K., Zhou, J., Huang, Y., Hakamivala, A. & Tang, L. Preparation of a novel injectable in situ-gelling nanoparticle with applications in controlled protein release and cancer cell entrapment. *RSC Adv.* **8**, 34625–34633 (2018).

70. Saraf, S., Alexander, A., Ajazuddin, Khan, J. & Saraf, S. Poly(ethylene glycol)-poly(lactic-co-glycolic acid) based thermosensitive injectable hydrogels for biomedical applications. *Journal of Controlled Release* (2013). doi:10.1016/j.jconrel.2013.10.006

71. Yang, X. *et al.* Folate-functionalized polymeric micelles for tumor targeted delivery of a potent multidrug-resistance modulator FG020326. *J. Biomed. Mater. Res. - Part A* (2008). doi:10.1002/jbm.a.31537

72. Gao, H. *et al.* Pretreatment with chemotherapeutics for enhanced nanoparticles accumulation in tumor: The potential role of G2 cycle retention effect. *Sci. Rep.* (2014). doi:10.1038/srep04492

73. Wang, Q. *et al.* Targeted delivery of low-dose dexamethasone using PCL-PEG micelles for effective treatment of rheumatoid arthritis. *J. Control. Release* **230**, 64–72 (2016).

74. Ross, R. Atherosclerosis—an inflammatory disease. *N. Engl. J. Med.* **340**, 115–126 (1999).

75. Wilhelm, S. *et al.* Analysis of nanoparticle delivery to tumours. *Nature Reviews Materials* (2016). doi:10.1038/natrevmats.2016.14

76. Koo, H., Hahn, S. K. & Yun, S. H. Controlled Detachment of Chemically Glued Cells. *Bioconjug. Chem.* (2016). doi:10.1021/acs.bioconjchem.6b00546

77. Xu, H. *et al.* Multi-ligand poly(l-lactic-co-glycolic acid) nanoparticles inhibit activation of endothelial cells. *J. Cardiovasc. Transl. Res.* (2013). doi:10.1007/s12265-013-9460-5

78. Iyer, R. *et al.* Nanoparticle eluting-angioplasty balloons to treat cardiovascular diseases. *Int. J. Pharm.* (2019). doi:10.1016/j.ijpharm.2018.11.011

79. Costa, C. *et al.* In vitro cytotoxicity of superparamagnetic iron oxide nanoparticles on neuronal and glial cells. Evaluation of nanoparticle interference with viability tests. *J. Appl. Toxicol.* (2016). doi:10.1002/jat.3213

80. Becker, A. De & Riet, I. Van. Homing and migration of mesenchymal stromal cells: How to improve the efficacy of cell therapy? *World J. Stem Cells* (2016). doi:10.4252/wjsc.v8.i3.73

81. Kuriakose, A. E. *et al.* Stem Cells as Drug Delivery Vehicles. (2018).

82. Sarkar, D. *et al.* Engineered cell homing. *Blood* **118**, e184–e191 (2011).

83. Csizmar, C. M., Petersburg, J. R. & Wagner, C. R. Programming cell-cell interactions through non-genetic membrane engineering. *Cell Chem. Biol.* **25**, 931–940 (2018).

84. Takayama, Y., Kusamori, K. & Nishikawa, M. Click Chemistry as a Tool for Cell Engineering and Drug Delivery. *Molecules* **24**, 172 (2019).

85. Koo, H. *et al.* Bioorthogonal Click Chemistry-Based Synthetic Cell Glue. *Small* (2015). doi:10.1002/smll.201502972

86. Meyer, J. P. *et al.* Bioorthogonal Masking of Circulating Antibody-TCO Groups Using Tetrazine-Functionalized Dextran Polymers. *Bioconjug. Chem.* (2018). doi:10.1021/acs.bioconjchem.8b00028

87. Layek, B., Sadhukha, T. & Prabha, S. Glycoengineered mesenchymal stem cells as an enabling platform for two-step targeting of solid tumors. *Biomaterials* (2016). doi:10.1016/j.biomaterials.2016.02.024

88. Dickerson, J. B., Blackwell, J. E., Ou, J. J., Shinde Patil, V. R. & Goetz, D. J. Limited adhesion of biodegradable microspheres to E- and P-selectin under flow. *Biotechnol. Bioeng.* (2001). doi:10.1002/bit.1085

89. Petros, R. A. & Desimone, J. M. Strategies in the design of nanoparticles for therapeutic applications. *Nature Reviews Drug Discovery* (2010). doi:10.1038/nrd2591